DOI: 10.14750/ME.2021.008

Ph.D. Dissertation

Investigation the effect of activation and exfoliation on carbon nanosheets properties

By

Kanokon Nuilek

Supervisors:

Dr. Peter Baumli, Associate Professor

Dr. Andrea Simon, Associate Professor

Head of the Doctoral School

Prof. Gacsi Zoltan

Antal Kerpely Doctoral School of

Materials Science & Technology

At the Faculty of Materials Science & Engineering

Miskolc,

Hungary 2020

DOI: 10.14750/ME.2021.008

CONTENTS

DOI: 10.14750/ME.2021.008

DOI: 10.14750/ME.2021.008

ABBREVIATIONS

2D	2 dimensions	NDF	Neutral detergent fibre content
A	Electrode area (cm^2)	NS	Nettle stem
AC	Activated carbon	NSCNs	Nettle stem-derived carbon nanosheets
ADF	Acid detergent fibre content	PS	Peanut shell
ADL	Acid detergent lignin content	PSCNs	Peanut shell-derived carbon nanosheets
BET	Brunauer, Emmett and Teller analysis	Q	The total charge obtained by integrating the positive and negative sweeps in a curve (C)
C	Concentration of the electroactive species (mol cm^{-3})	SSA	Specific surface area (m^2 g^{-1})
C_A	Surface capacitance (F m^2)	TEM	Transmission Electron Microscope
Cs	Specific capacitance (F g^{-1})	ν	Scan rate (V s^{-1})
CHNS	Carbon, Hydrogen, Nitrogen and Sulfur analysis	XRD	X-ray diffraction
CNs	Carbon nanosheets	Δt	The discharge time (s)
CNT	Carbon nanotubes	ΔV	The voltage change after a full charge or discharge (v)
CV	Cyclic voltammetry	$\Delta_f G$	Standard formation Gibbs energy (kJ mol^{-1})
D	Diffusion coefficient (cm^2 s^{-1})	$\Delta_f H$	Standard formation enthalpy (kJ mol^{-1})
EDLC	Electrolytic double-layer capacitor	$\Delta_f S$	Standard formation entropy (J mol^{-1} K^{-1})
EDS	Energy Dispersive Spectroscopy	φ	Lignin/(Cellulose+Lignin) ratio
EIS	Electrochemical Impedance Spectroscopy		
GCD	Galvanostatic charging/discharging		
I	The discharge current (A)		
Ip	Peak current (A)		
m	Mass of active material on electrode (g)		
n	Number of electrons involved in the reaction		

DOI: 10.14750/ME.2021.008

LIST OF TABLES

DOI: 10.14750/ME.2021.008

LIST OF FIGURES

DOI: 10.14750/ME.2021.008

LIST OF FIGURES

DOI: 10.14750/ME.2021.008

LIST OF FIGURES

DOI: 10.14750/ME.2021.008

LIST OF FIGURES

DOI: 10.14750/ME.2021.008

1 Introduction

2D carbon nanostructures – namely graphene and carbon nanosheets – are increasingly being researched as candidates for energy storage devices such as batteries or capacitors. Carbon nanotubes, nanofibers, and nanosheets have been well documented. Glass-like carbon is a vital type of the carbon family, typically referred to as glassy carbon or vitreous carbon. Glassy carbon, described as amorphous carbon, is non-graphitizing and contains mostly sp^2 sites. The properties of carbon are a combination of the properties of glass and ceramic materials which are characterized by low density, high thermal and chemical resistance. Chemical and thermal treatments are the main steps of the preparation of carbon nanostructures. Among all the chemical activation agents, alkaline hydroxides such as potassium hydroxide (KOH) or sodium hydroxide (NaOH) are reported to be highly interesting from the performance point of view, allowing activated carbons to be prepared from many kinds of carbonaceous precursors. Chemical acids are used as intercalating agents to obtain exfoliated graphite by different processes. This activated carbon can be obtained from various agricultural wastes. Since no research has presented the synthesis of carbon by using two processes: activation and exfoliation. So this is an exciting novelty to the study.

The preparation of nanostructured materials from wastes has drawn tremendous interest in recent years. Many researchers have demonstrated that carbon materials used as adsorbents or electronic materials can be synthesized from low-cost waste materials by using alkaline hydroxides. The structures of nettle and peanut shells consist of cellulose, hemicellulose and lignocellulose. These materials are the major contents of biowaste which can play the role of carbon precursors in producing highly ordered nanocarbons, and contribute to the porosity of biochar yield.

Energy storage and delivery are one of the most promising areas for the application of-activated carbon. Supercapacitors, also called electric double-layer electrodes, are highly efficient in energy storage and delivery characteristics compared to batteries. They can deliver high rates of energy by using a mechanism of simple charge separation at the interface between the electrode and electrolyte. As far as it concerns, no previous studies have reported on using nettle stem or peanut shell as raw materials for producing carbon nanosheets by chemical activation and exfoliation processes. The activated carbon produced in this way can be used as electrode material for supercapacitors.

DOI: 10.14750/ME.2021.008

In this work, I focused on answering the following key questions:

- Can I prepare carbon nanostructure from natural materials? What are the structures and properties?
- Which factors can affect the properties of carbon obtained from natural materials?
- Does the chemical treatment affect the surface properties of carbon?
- Does the chemical treatment affect the electrochemical properties of carbon?
- Are the electrochemical properties of the synthesized carbon suitable to be applied in energy storage applications?

The goal of this research is to systematically study and investigate the effect of different alkaline hydroxides activators and acid exfoliators on the properties of carbon nanosheets, prepared from natural materials with the following considerations:

- Use of different hydroxide activators and acid exfoliators to synthesis carbon nanostructure materials.
- To study the structure of carbon nanosheets synthesized from natural materials.
- The microstructure and the chemical composition of carbon nanosheets were characterized using different characterization methods, including Scanning Electron Microscope (SEM), Transmission Electron Microscope (TEM), X-ray Diffraction (XRD), Energy Dispersive Spectroscopy (EDS), CHNS analysis techniques, BET specific surface area (SSA), micropore volume and pore diameter.
- Development of novel carbonaceous materials for supercapacitors. This study is focused on the surface properties (pores, surface area) and on the electrochemical properties. The investigated materials are synthesized, characterized and used as supercapacitor electrode materials.
- Identification of the effect of activators and exfoliators on the electrochemical performance of carbon nanostructure which can be used in supercapacitors to maximize the specific capacitance and energy density.
- Evaluation of performance parameters, such as specific capacitance, energy density, power density, and stability of the synthesized materials.

DOI: 10.14750/ME.2021.008

2 Literature overviews

Environmental awareness has given rise to the idea of utilizing natural waste and other everyday waste materials to be beneficial and cost-effective. The production of activated carbon (AC) from waste materials is a hot topic these days as sources of activated carbon are abundant and increasing. Activated carbon is widely used as a sorbent due to its low cost, exceptionally high porosity, customizable pore size and high absorbency. The activation process normally develops the pore structure of activated carbon. Natural materials are used as precursors for the carbon production. Activated carbon is made up of carbon as the main component, and other elements such as oxygen, hydrogen, nitrogen, sulfur and others.

The type of activation method and carbon precursors have a significant effect on the final characteristics and the efficiency of the activated carbon obtained. Activated carbon has the advantages of superior physicochemical properties such as high surface area, physical and chemical stability. The substrate for activated carbon preparation is abundant, easy to prepare, inexpensive, and has low density. For commercial-grade carbon, the surface area typically varies between 500 to 1500 $m^2 g^{-1}$ or up to 3000 $m^2 g^{-1}$ [1].

2.1 The structure of carbon synthesized from natural materials

Carbon is an essential element, which comes in various forms, such as graphite, graphene, coal, activated carbon, diamond, and carbon black. Allotropes of different carbon are shown in Fig. 2.1. The physical or chemical processes can improve the properties of carbon. During the physical process, large amounts of internal carbon are removed to provide a well-developed carbon structure. On the other hand, in the process of chemical activation, a dehydrator is used which affects the pyrolytic degradation and results in the formation of tar that increases the carbon yield [2].

DOI: 10.14750/ME.2021.008

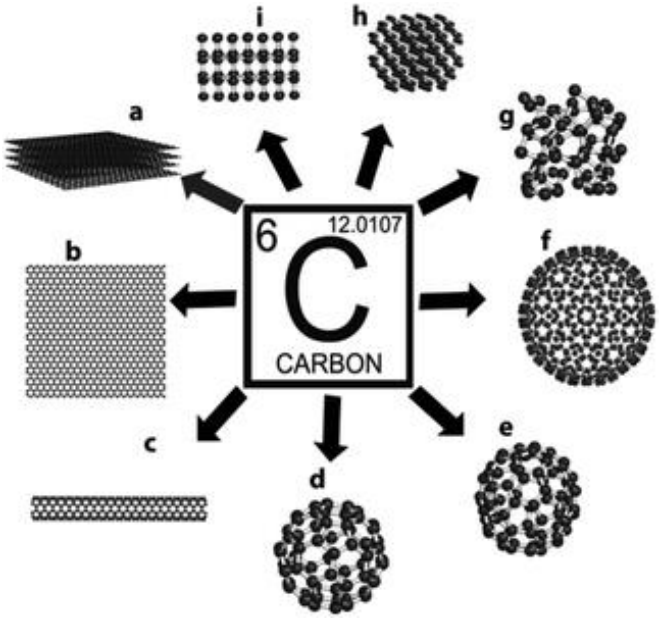

Figure 2.1 Different allotropes of carbon: (a) graphite, (b) graphene, (c) carbon nanotube, (d) C60, (e) C70, (f) C540, (g) amorphous carbon, (h) lonsdaleite, and (i) diamond [3].

Studies of nanostructures from waste materials have been of great interest [4]. Carbon nanomaterials obtained from natural waste materials reveal a wide range of properties, high efficiency, and wide range of applications. There are different methods for the synthesis of carbon materials. Therefore, using cheap and abundant natural waste materials in the production of carbon materials is very economical and attractive [5-9]. The use of waste or recycled materials is a breakthrough and a great opportunity as synthetic reinforcement can be economically produced. Carbon nanomaterials are important because of their good physical, mechanical properties, and high performance for composite materials [10-15].

Menendez-Diaz et al. [16] presented that carbons based on the allotropic form of graphite can be classified into graphitic carbons (which have a measurable crystallographic order in the direction irrespective of the presence of structural defects) and non-graphitic carbons (without any measurable crystallographic order in the c-direction apart from a more or less parallel stacking) carbons. Some of these microstructures are arranged in preferential directions, like synthetic graphite or graphitized carbon fibres, while disordered microstructures are characteristic of chars or activated carbons. Such a wide variety of possible structures gives rise to a large amount of different types of carbons. Figure 2.2 shows a schematic representation of some of these carbon structures.

DOI: 10.14750/ME.2021.008

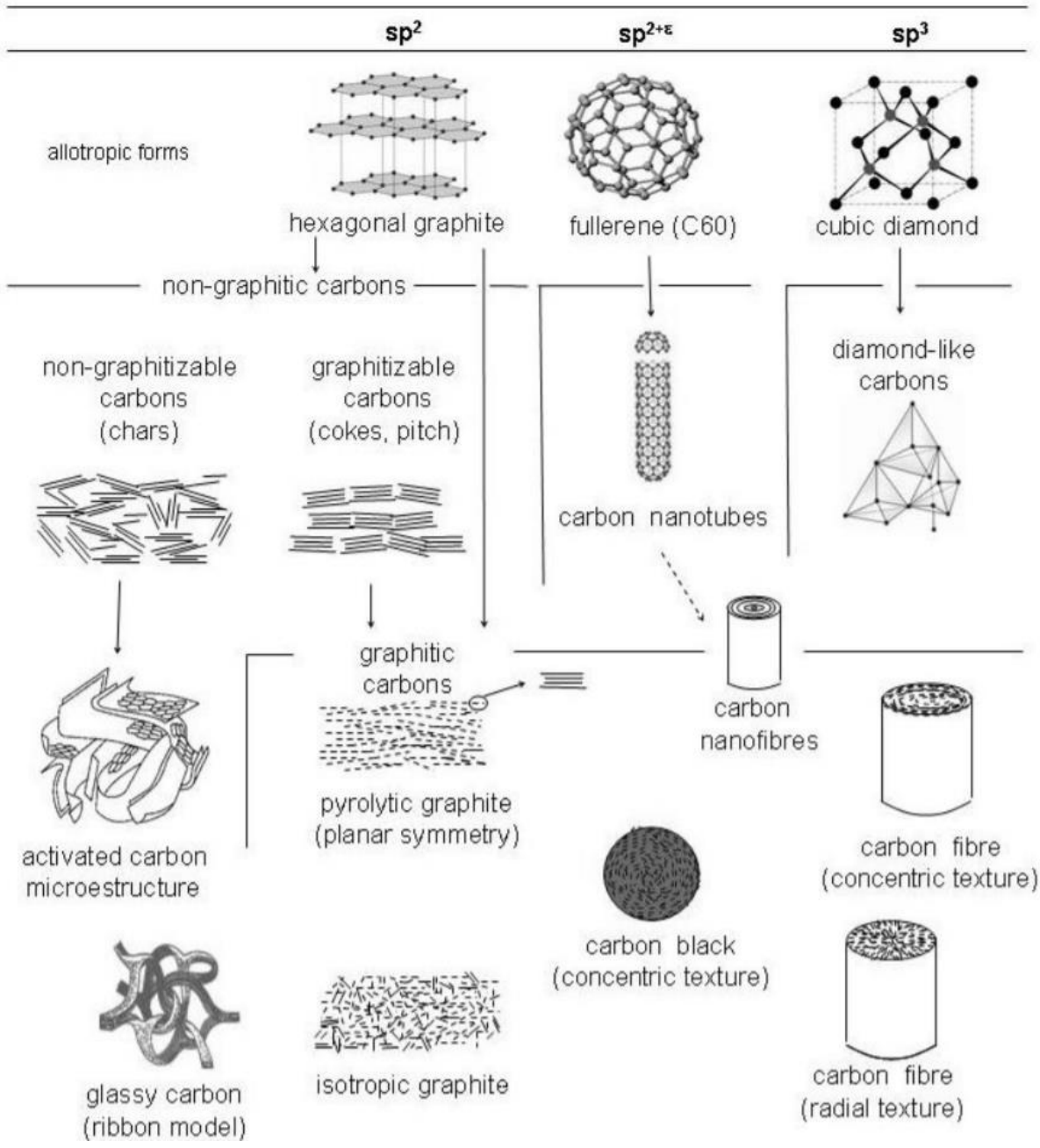

Figure 2.2 Major allotropic forms of carbon and a schematic representation of some of the carbon structures derived from these forms [16].

Graphite consists of carbon atom planes arranged in a hexagonal lattice with four atoms per unit cell. Strong covalent bonds exist between intraplaner atoms, while the interplaner bonding is of the weak Van der Waals type see Fig. 2.3 [17].

DOI: 10.14750/ME.2021.008

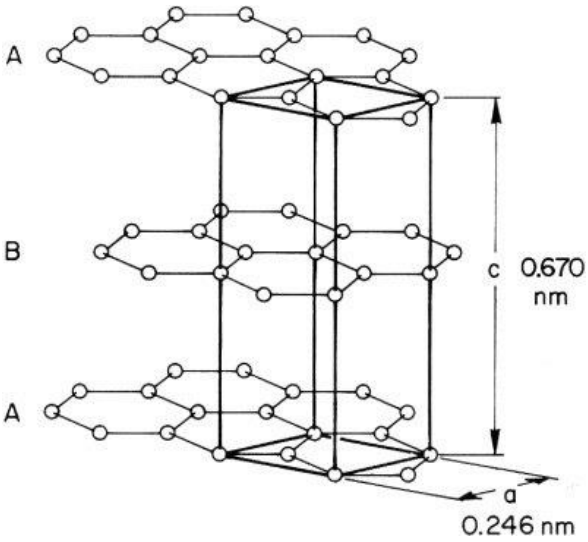

Figure 2.3 The crystal structure of graphite showing the hexagonal lattice [17].

The plant is a natural material that is abundant and interesting for research. The cell wall of the plant surrounds the cell membrane. It consists of several layers of cellulose, which are arranged in the primary and secondary walls. Cellulose is the most common organic compound in the world [18]. Hemicellulose can be used as a potential carbon material on account of its high carbon content, renewability, environmental sustainability, and special structure [19]. Lignin is an abundant biopolymer with high carbon content, high aromaticity, and an excellent precursor for the preparation of high-value carbon materials [20]. Stinging nettle (Urtica dioica) is a wild plant that grows in Europe, Asia, Northern Africa and Western North America, usually found in the countryside. Nettle plant has a very strong fibre and high carbon content. The applications of stinging nettle have been developed in textile products, medicine, cosmetics, food and bioenergy [21-24]. Peanut (Arachis hypogaea) is a major crop widely distributed throughout tropical and subtropical parts of Asia, Africa, Oceania, North and South America and Europe. Natural structures of peanut shell consisting of cellulose, hemicellulose and lignocellulose are the major contents of biowaste, which can play the role of carbon precursors in producing highly ordered nanocarbons [4, 9]. Waste peanut shells, generated in large volume annually, are considered lignocellulose biomass waste [25]. As cellulose has appreciable carbon content [26-29], it can be a suitable material for the preparation of activated carbon [30-31]. The carbon content in cellulose varies from 40 wt.% to 44 wt.%. However, this content may increase above 80 wt.% for carbonized samples and reach in the range of 95wt.% for activated carbon [22, 32].

DOI: 10.14750/ME.2021.008

Using various carbonisation and activation methods can convert biomass materials into carbon as shown in Fig. 2.4. Both physical and chemical methods are used to transfer biomass into value-added carbon materials. By controlling different parameters to obtain carbon with different properties [33].

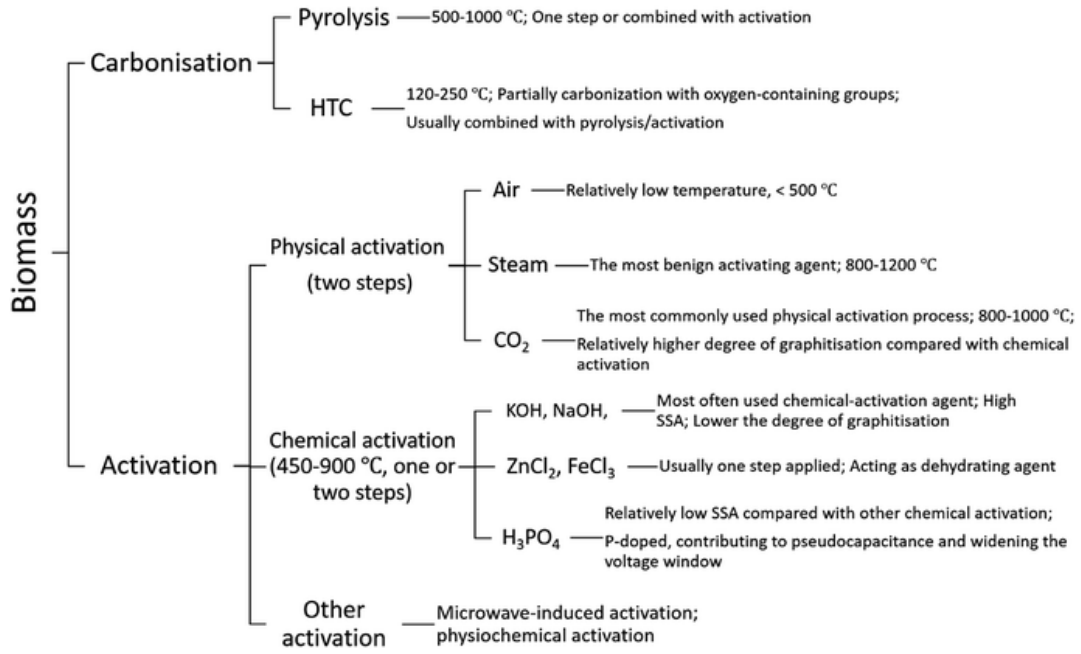

Figure 2.4 The methods for converting biomass to carbon materials [33].

2.2 Effect of organic components on carbon properties

Lignocellulosic waste materials are massively produced worldwide. Lignocellulose or lignocellulosic biomass is plant dry matter composed of carbohydrate polymers, namely cellulose and hemicellulose, and lignin (Fig 2.5, Table 2.1) [34]. Lignocellulosic materials are widely used as precursors and account for around 45% of the total raw materials used for the manufacture of activated carbon [35].

Cellulose [$(C_6H_{10}O_5)n$] builds up the main structure of the plant cell wall, which is a crystalline structure. Material with high cellulose content can be used for biofuel production [36]. Xue et al. [37] showed that the activated carbon from pure cellulose has 39.66 wt.% carbon content and the highest specific surface area (1,077.54 m^2 g^{-1}) after activating by the $ZnCl_2$ through microwave heating. They indicated that cellulose maintained the activated carbon porous structure and facilitated the formation of the mesoporous structure. Activated carbon was prepared with different contents of lignin and

DOI: 10.14750/ME.2021.008

cellulose exhibited differences in BET surface area, mesoporous volume, pore-volume, and average pore width. As the cellulose content was increased, the BET surface area was gradually increased, whereas the mesoporous volume initially increased and then decreased [37].

Table 2.1 Content of lignin, cellulose and hemicellulose of lignocellulosic materials.

Natural biomass	Lignin (%)	Cellulose (%)	Hemicellulose (%)	Ref.
Tomato leaves	24.86	10.91	8.13	[38]
Tomato stems	16.01	27.03	21.08	[38]
Waste tea	38.96	18.75	17.96	[38]
Almond shell	36.12	21.72	27.74	[38]
Coconut shell	30.1	19.8	68.7	[39]
Palm shell	53.4	29.7	47.7	[39]
Pineapple peel	10.4	20.9	31.8	[40]
Sunflower shell	17.0	48.4	34.6	[41]
Walnut shell	52.3	25.6	22.7	[41]
Hardwoods stems	18–25	40–55	24–40	[42]
Softwood stems	25–35	45–50	25–35	[42]
Nut shells	30–40	25–30	25–30	[42]
Corn cobs	15	45	35	[42]
Grasses	10–30	25-40	35-50	[42]
Wheat straw	15	30	50	[42]
Newspaper	18-30	40-55	25-40	[42]

Hemicellulose [$(C_5H_8O_4)n$] is mainly composed of xylan and mannan. It is the second most abundant component of the plant cell wall. Compared to cellulose, hemicellulose has a lower level of polymerization, it is chemically different and has an amorphous structure [36]. Lin et al. [19] studied hemicellulose extracted from pomelo peel to prepare carbon and showed the content of the carbon element is up to 90 % at 800 °C. The hemicellulose-derived porous activated carbon materials offer great potential for a wide range of high-performance supercapacitor applications [19].

DOI: 10.14750/ME.2021.008

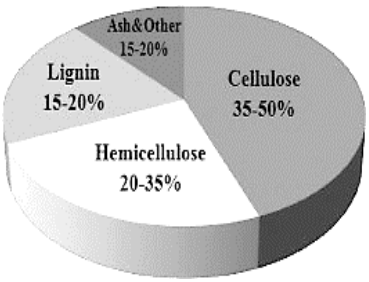

(a)

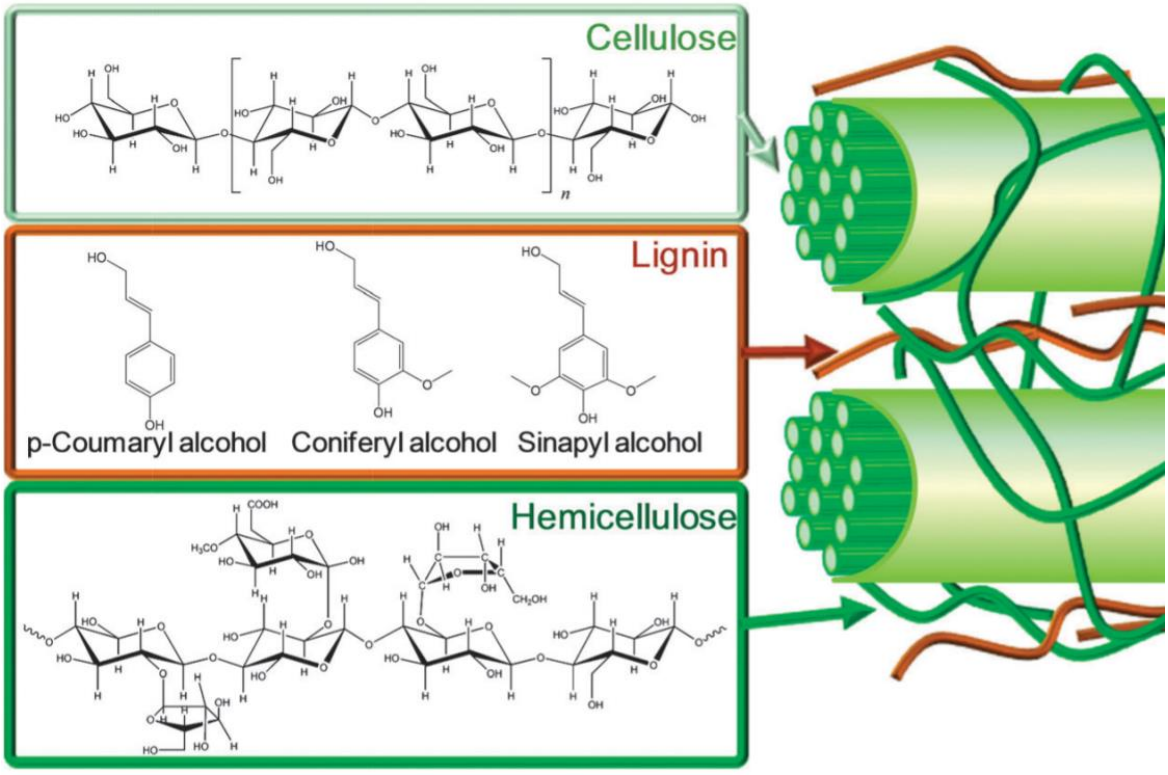

(b)

Figure 2.5 (a) General composition of lignocellulose biomass feedstock (b) structure of lignocellulosic biomass with cellulose, hemicellulose, and lignin [43-44].

Lignin is a complex hydrocarbon polymer with both aliphatic and aromatic constituents, amorphous, and hydrophobic in nature [45]. Xue et al. [37] used pure lignin to produce activated carbon with 33.65 % carbon content and its surface area reached to 558.48 $m^2 g^{-1}$. Lignin contributed to the formation of the layered, microporous structure during the production of activated carbon [37]. Thermal and chemical processes resulted in the lignocellulose structure breaking apart and in smaller particles of the material (Fig 2.6).

DOI: 10.14750/ME.2021.008

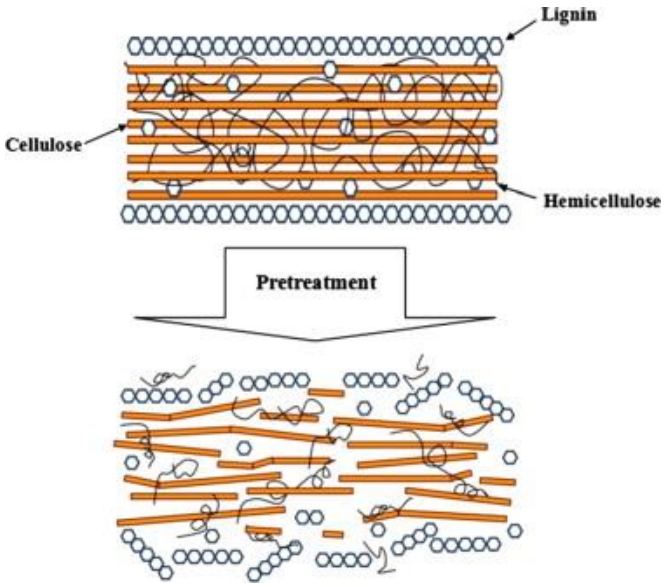

Figure 2.6 Schematic pretreatment of lignocellulose material [43].

2.3 Effect of chemical activation and exfoliation on the surface properties

Chemical activation has been shown as a very efficient method to obtain carbons with high surface area and narrow micropore distribution. Pores come in a variety of sizes to address a very wide range of applications. When considering pore size, a set of standards approved by IUPAC has defined pore size ranges based on different size widths [46]. Pore diameters smaller than 2 nm are referred to as micropores, between 2 nm and 50 nm as mesopores, and macropores as a pore larger than 50 nm (Fig.2.7 and 2.8).

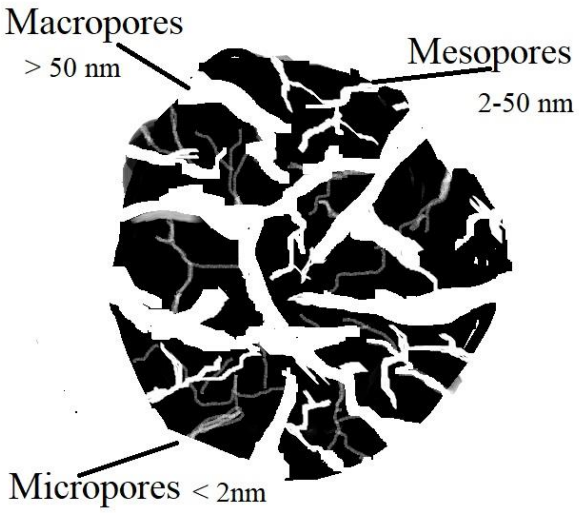

Figure 2.7 Schematic representation pore structure of micropores, mesopores, and macropores.

DOI: 10.14750/ME.2021.008

Within the micropore domain, there is a further subdivision into narrow micropores (ultramicropores, less than 0.7 nm) and wide micropores (supermicropores, from 0.7 nm to 2 nm) [47]. The accessibilities of pore are represented in Fig 2.9. A pore that is completely separated from another pore is called a closed pore. They affect the mechanical properties of materials such as bulk density, mechanical strength and thermal conductivity. Open porosity is porosity with gaps connecting each other within or from the surface of a material. Open pores can also be "blind" (open only at one end) or "through" (open at both ends) [48].

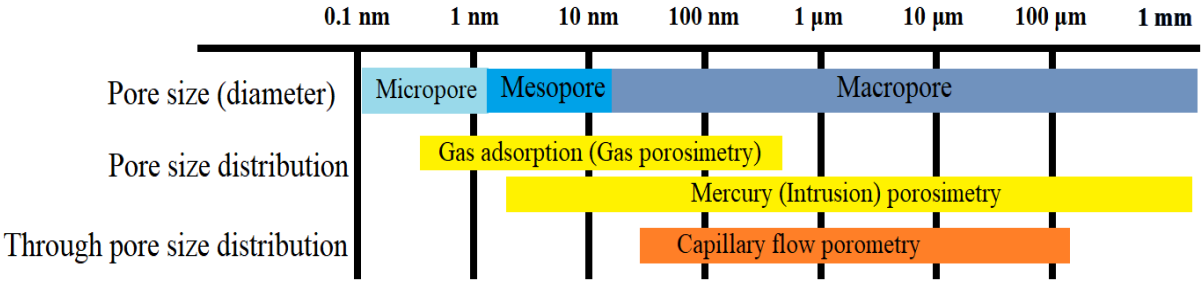

Figure 2.8 The techniques used to measure pore size.

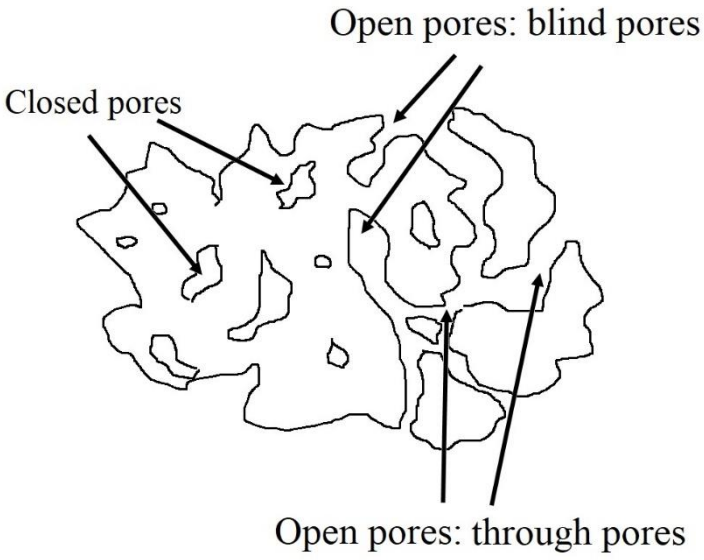

Figure 2.9 Various pore type accessibilities.

Two different methods are employed for the preparation of activated carbons with a wide variety of physicochemical properties. The so-called physical activation usually involves a two-step process: carbonization at 500-700ºC followed by activation via the partial gasification of carbon at 800-1000 ºC in a stream of steam, air, carbon dioxide, etc.

DOI: 10.14750/ME.2021.008

On the other hand, chemical activation involves mixing the precursor with an activating reagent such as KOH, NaOH, $ZnCl_2$ etc. (Table 2.2) and subsequent pyrolysis in the absence of air. Depending on the activating agent, the temperature usually ranges between 500 and 900 ºC. The resulting carbon is washed extensively to remove the chemical reagent [35].

According to the literature, activation with H_3PO_4 is commonly used for lignocellulosic material and carried out at lower temperatures. $ZnCl_2$ generates more surface area than H_3PO_4 but it is harmful to the environment. Activating with KOH in terms of surface area and efficiency shows better results than NaOH for various applications [49]. Therefore, the choice of activating agent depends on the type of raw materials and the purpose of the experiment.

Table 2.2 Comparison of surface properties of activated carbons at different activating agents.

Materials	**Activating agent**	**Specific surface area (m^2 g^{-1})**	**Average pore diameter (nm)**	**Ref.**
Coffee residue	$ZnCl_2$	511.55	2.20	[50]
	H_3PO_4	259.53	2.19	
	H_2SO_4	44.84	2.04	
	KOH	28.34	2.04	
	NaOH	27.15	2.02	
Coffee residue	$ZnCl_2$	890	2.60	[51]
Van apple pulp	$ZnCl_2$	1,067.01	2.46	[52]
Water hyacinth	H_3PO_4	423.6	7.3	[53]
Apricot stone	H_2SO_4	393.2	-	[54]
Jackfruit peel	H_3PO_4	907–1,260	-	[55]
Pumpkin seed shell	H_3PO_4	1,421	-	[56]
Sugar cane bagasse	KOH/ HNO_3	69-806	9-28	[57]
Litchi shells	KOH	3,164	-	[58]
Bambusa vulgaris	NaOH	1,042	2.4	[59]

Among all the chemical activation agents, alkaline hydroxides such as potassium hydroxide (KOH) or sodium hydroxide (NaOH) are reported to be interesting from the performance point of view, allowing activated carbons to be prepared from many kinds of

DOI: 10.14750/ME.2021.008

carbonaceous precursors. Although it is a frequently used process to prepare activated carbons, the general mechanism of chemical activation is not well understood, and the various interpretations found in literature underline the process complexity. In general terms, chemical activation by alkalis consists of solid-solid or solid-liquid reactions which involve the hydroxide reduction and carbon oxidation to generate porosity. During the reactions, CO, CO_2 and H_2 evolution is observed, and additional reactions between active intermediates produced on the surface and the constituents of the gas phase are possible. A recent study [60] suggests that the carbon/MOH (M = Na or K) reaction mechanism is independent of the hydroxide used and consists in the overlapping of redox processes. The hydroxide reduction leads to H_2 and Na or K metals, and carbon is oxidised to carbonates (Na or K) according to the global reaction (2.1):

$$6\ MOH + C \leftrightarrow 2M + 3H_2 + 2M_2CO_3 \qquad (2.1)$$

Alkaline hydroxide activation is a well-known method to generate pore network in carbons and to expand the carbon layer. The process of activation by KOH or NaOH was described in two main mechanisms that contribute to chemical activation [61-64]. The first one consists of the consumption of carbon by oxygen, producing carbon monoxide and carbon dioxide; this process is catalysed by alkali metals. The second one consists of the reduction of the hydroxide to free alkaline metal, the intercalation of free metal into the lattice of the carbon, the expansion of the lattice by the intercalated potassium or sodium, and the rapid removal of the intercalate from the carbon matrix. Below 700˚C, the main products are hydrogen, water, carbon monoxide, carbon dioxide, potassium oxide and carbonate. The dehydration of MOH to M_2O (2.2) results in carbon consumption through the reaction of CO_2, produced in reactions (2.3) and (2.4), with M_2O to form M_2CO_3 (2.5) and (2.6) [61-64]:

$$2MOH \leftrightarrow M_2O + H_2O \qquad (2.2)$$

$$C + H_2O \leftrightarrow CO + H_2 \qquad (2.3)$$

$$CO + H_2O \leftrightarrow CO_2 + H_2 \qquad (2.4)$$

$$CO_2 + M_2O \leftrightarrow M_2CO_3 \qquad (2.5)$$

$$2CO + M_2O \leftrightarrow M_2CO_3 + C \qquad (2.6)$$

DOI: 10.14750/ME.2021.008

Above 700˚C, however, an important activation mechanism occurs alongside with the formation of metallic potassium. This mechanism, described in (2.7-2.9), is directly related to the formation of sub-nanometer pores.

$$M_2O + CO \leftrightarrow 2M + CO_2 \quad (2.7)$$

$$M_2O + H_2 \leftrightarrow 2M + H_2O \quad (2.8)$$

$$M_2O + C \leftrightarrow 2M + CO \quad (2.9)$$

In case of solution activation, the hydrated ionic radius of K^+ ion is lower than that of Na^+ ion which facilitates the immigration of K^+ ion into carbon layers/pores. (Table 2.3).

Table 2.3 Characteristics of the radius ions.

Ion	**Ionic radius (nm)** [65]	**Hydrated radius (nm)** [66]
Na^+	0.095	0.36
K^+	0.133	0.33

In the case of NaOH activation, Raymundo-Pinero et al. [60] reported - as shown in the XRD patterns (Fig. 2.10) - that the redox reaction (Na_2CO_3 formation) starts at a higher temperature (600 ºC) than for KOH (400 ºC). This observation is in agreement with the higher reactivity of KOH when compared with NaOH.

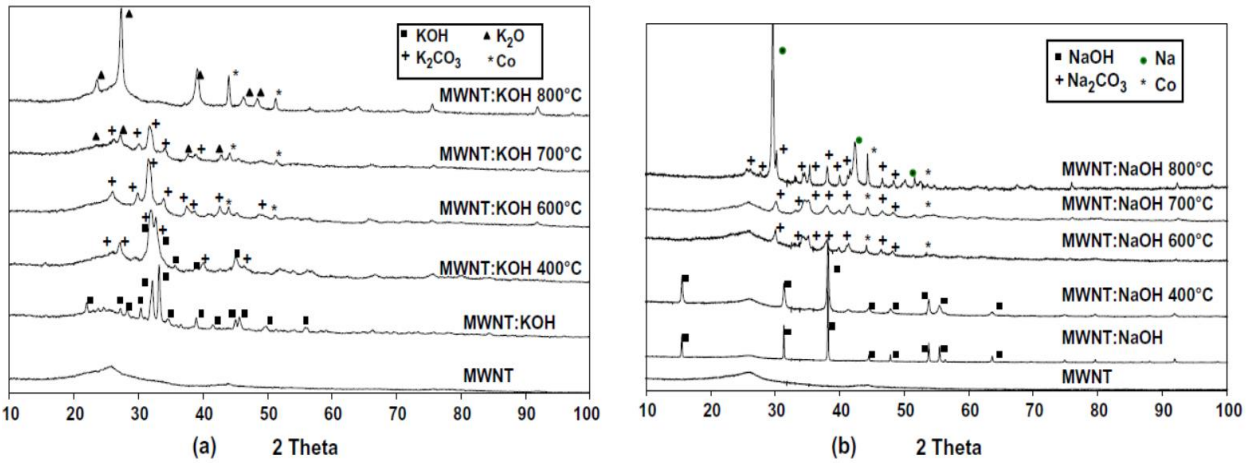

Figure 2.10 XRD patterns of MWNTs during the reaction with (a) KOH at different temperatures and (b) NaOH at different temperatures [60].

DOI: 10.14750/ME.2021.008

Romanos et al. [61] reported that at the activation above 700 ˚C, metallic potassium can penetrate between graphitic layers. The stretching of the lattice and the removal of intercalated potassium result in the expansion of the pore network. This expansion corresponds to an increase in surface area and porosity. This leads to the formation of fragmented carbon sheets as represented in Fig. 2.11 [61].

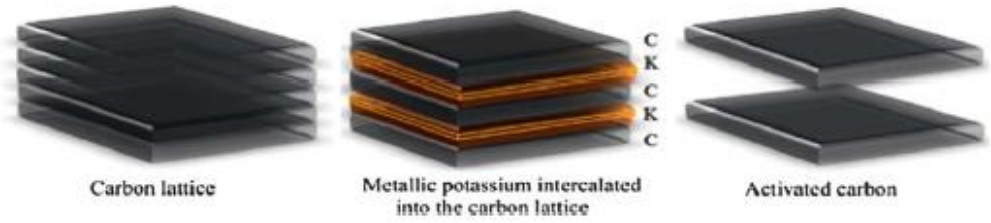

Figure 2.11 Potassium hydroxide activation mechanism above 700˚C [61].

Chemical acids are used as intercalates for obtaining exfoliated graphite by different processes [67-70, 97]. Nicolosi et al. [71] explained liquid exfoliation by the brief outlines of the four main liquid exfoliation techniques for layered materials as shown in Fig. 2.12: (A) Ion intercalation. Ions (yellow spheres) are intercalated between the layers in a liquid environment, swelling the crystal and weakening the interlayer attraction. Then, agitation (such as shear, ultrasonication, or thermal) can completely separate the layers, resulting in an exfoliated dispersion. (B) Ion exchange. Some layered compounds contain ions between the layers so as to balance the surface charge on the layers. These ions (red spheres) can be exchanged in a liquid environment for other, often larger ions (yellow spheres). As above, agitation results in an exfoliated dispersion. (C) Sonication assisted exfoliation. The layered crystal is sonicated in a solvent, resulting in exfoliation and nanosheet formation. This mechanism also describes the dispersion of graphene oxide in polar solvents, such as water [71].

DOI: 10.14750/ME.2021.008

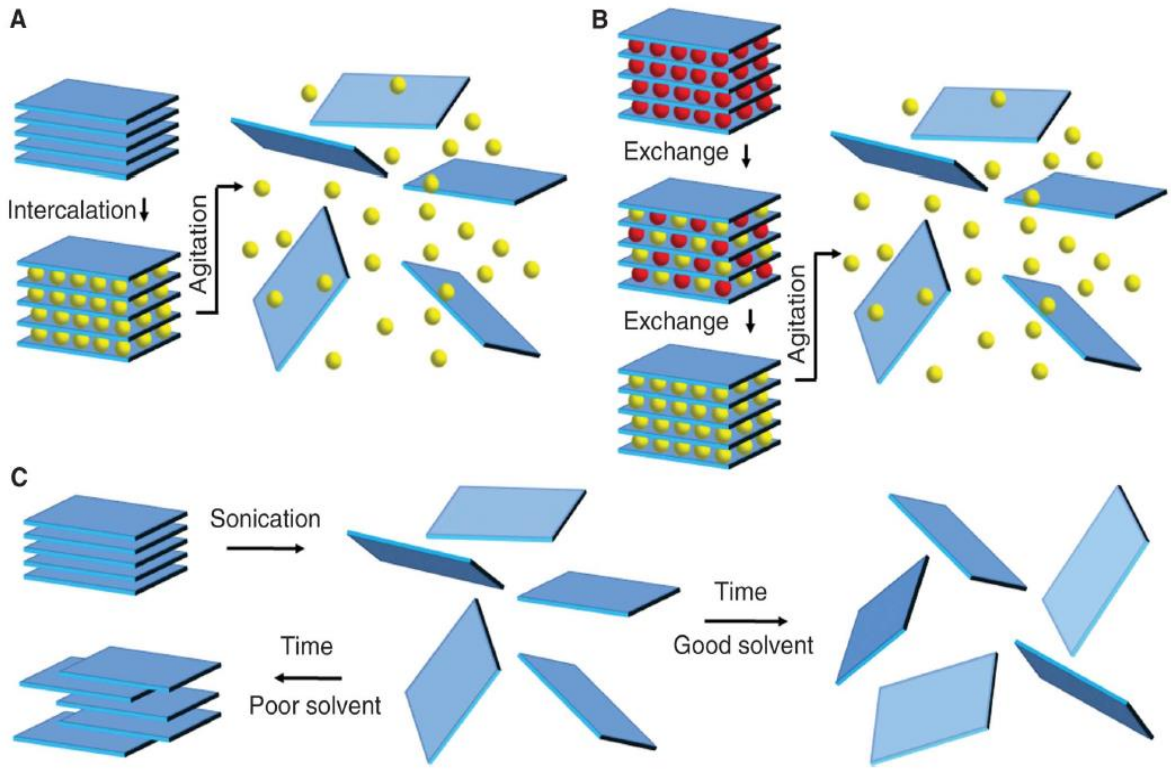

Figure 2.12 Schematic description of the main liquid exfoliation mechanisms (A) Ion intercalation, (B) Ion exchange and (C) Sonication assisted exfoliation [71].

Fan et al. [72] reported that the chemical composition of carbon nanosheets can be adjusted by varying the kinds of precursors, the synthesis temperatures, and post-treatment processes. Chemical exfoliation is effective for achieving thinner carbon nanosheets, leading to an increase in the amount of carbon fillers with larger aspect ratios. The interaction force between the layers is less than that of interplanes of carbon precursors. The application of graphite oxide as a precursor is becoming an approved approach to obtain graphene or carbon nanosheets because the graphite layers swell and are exfoliated after oxidization with strong oxidants. Carbon nanosheets with a thickness of 2–5 nm were prepared by direct chemical exfoliation of expandable graphite (EG), as illustrated in Fig. 2.13. When the resultant carbon nanosheets were used in composites, electromagnetic attenuation was enhanced due to good electrical and dielectric properties of carbon nanosheets [72].

DOI: 10.14750/ME.2021.008

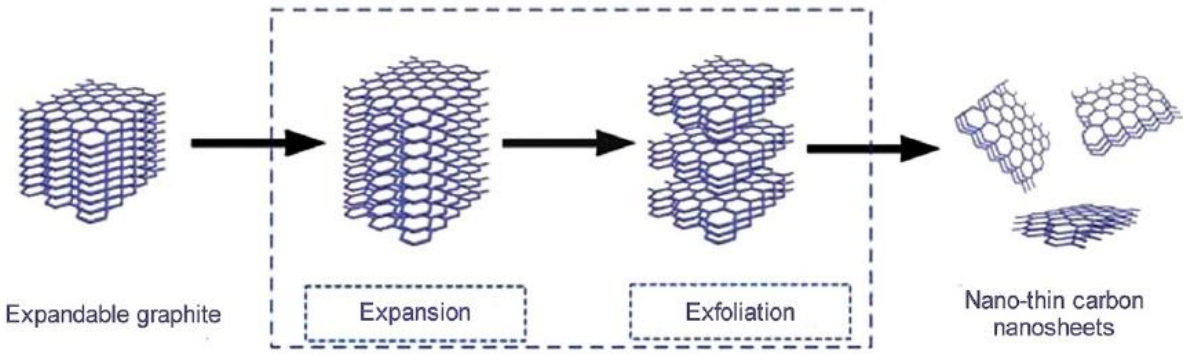

Figure 2.13 Schematic of expansion and exfoliation of expandable graphite [72].

BET analysis is a precise assessment of the specific surface area of material by sorption of multilayer nitrogen as measured as a function of relative pressure. The information from this technique is important to study the effects of surface porosity and particle size in many applications. Gas adsorption is a well-established tool for the characterisation of the texture of porous solids and fine powders. IUPAC (Physisorption of gases) manual was for determination of surface area and porosity of materials.

According to Thommes et al. [47], the IUPAC classification of adsorption isotherms for nitrogen and argon adsorption at 77 K and 87 K are illustrated in Fig. 2.14. The types of isotherm characteristic of adsorbents that are microporous presented by type I, type I isotherms are given by microporous solids having relatively small external. Type I (a) isotherms are given by microporous materials having mainly narrow micropores (of width <∼ 1 nm). Type I (b) isotherms are found in materials having pore size distributions over a broader range including wider micropores and possibly narrow mesopores (<∼ 2.5 nm). Types II are given by the physisorption of most gases on nonporous or macroporous adsorbents. Type III are given by a nonporous or macroporous, types IV are given by mesoporous materials. Type V are observed for water adsorption on hydrophobic microporous and mesoporous adsorbents and Type VI is representative of layer-by-layer adsorption on a highly uniform nonporous surface [47].

DOI: 10.14750/ME.2021.008

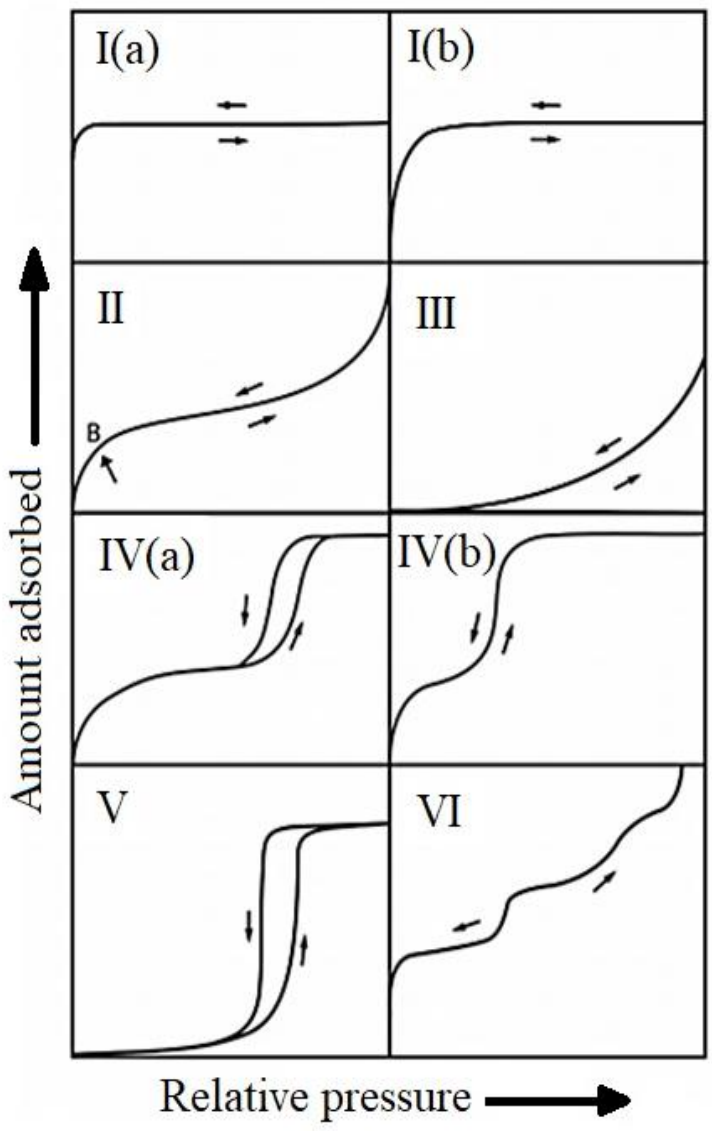

Figure 2.14 IUPAC classification of physisorption isotherms. Type I = microporous, Type I (a) = microporous, Type I (b) micropores and mesopores, Types II = nonporous or macroporous, Type III = nonporous or macroporous, Type IV = mesoporous, Type V = microporous and mesoporous and Type VI = nonporous [47].

DOI: 10.14750/ME.2021.008

Table 2.4 Characterization of the biomass types [73].

	Hemp	**Flax**	**Jute**	**Coir**	**Abaca**
Lignin (%)	3.3	2.5	11.8	41-45	5.1
Cellulose (%)	67.0	56.5	64.4	36-43	63.2
Hemicellulose (%)	16.1	15.4	12.0	0.2-0.3	19.6
Carbon (wt.%)	41.2	43.3	44.1	46.6	43.7
Carbon (wt.%, after activating)	82.4	78.9	87.4	82.7	79.5
BET surface area (m^2 g^{-1})	877	776	840	822	860
Micropore surface area (m^2 g^{-1})	555	436	396	685	587
Mesopore surface area (m^2 g^{-1})	322	340	444	137	273

The properties of carbon depend on the organic composition (lignin, cellulose and hemicellulose) of the precursor (Table 2.4). Deng et al. [74] studied the synthesis of porous carbon by pyrolysis method and established that the self-activation process of cellulose and lignin under higher temperature treatment may result in micropores. However, because lignin contains a robust aromatic structure, its products at low temperature are featured by nonporous structure or give an extremely low specific surface area even at high temperature [74].

2.4 Effect of chemical and thermal treatment to the electrochemical properties

Supercapacitors are very interesting materials that are widely studied today, due to their excellent properties in power density, long cycle life and good efficiency for charging/discharging (Table 2.5). Carbonaceous materials are very attractive to use as an electrode material for supercapacitors [75].

DOI: 10.14750/ME.2021.008

Table 2.5 Comparison of the properties of different electrochemical storage systems [76].

Parameter	Battery	Supercapacitor	Conventional capacitor
Energy density (Wh $kg^{-1)}$	30-40	1-10	<0.1
Power density (W kg^{-1})	1,000	<10,000	<100,000
Life cycle	1,000	> 500,000	> 500,000
Charging time	1-5 h	0.3-30 s	10^{-3}-10^{-6} s
Discharging time	0.3-3 h	0.3-30 s	10^{-3}-10^{-6} s
Charging/discharging efficiency	70-85%	85-98%	95%

According to the mechanism of the storage capacity, supercapacitors can be classified into two types. The first one is defined as an electrolytic double-layer capacitor (EDLC) in which the accumulation of static charge at the electrode interface creates a capacitance. The surface area of the electrode material and the ionic diffusion pathway play an important role in the EDLC capacitance. In another type the charge is stored by a reversible faradic and normally called pseudocapacitor [77] (Fig. 2.15).

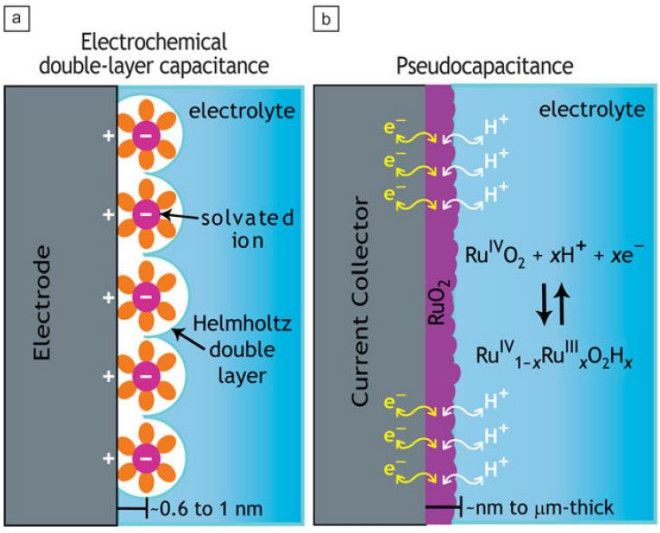

Figure 2.15 Schematic of charge storage of (a) electrochemical double-layer capacitance or (b) pseudocapacitance [77].

DOI: 10.14750/ME.2021.008

The high specific capacitance of EDLC arises from the high area of interface and atomic range separation of positive and negative charge. Carbon-based materials are the most extensively used supercapacitor electrodes due to their attractive physical and chemical properties. Furthermore, the development of supercapacitor needs accurate control over the electrical conductivity, surface area and pore size of the electrode materials. Carbonaceous materials show high electrical conductivity and large specific surface area ensuring low solution resistance and facile diffusion of the electrolyte. The specific surface area and the pore size of the activated carbon can be controlled by the various method of activation [78]

The high surface area value is a crucial factor for energy storage applications. It is normally obtained by controlling the porosity of carbon. Redondo et al. [79] derived activated carbon from olive pits precursor by chemical activation (KOH) process. It was found from the study that several parameters like specific surface area, accessible average pore size and effective dielectric permittivity can affect the specific capacitance of the activated carbon electrode. Formation of different pore size was the reason for variation of specific capacitance of activated carbon electrode [79].

2.5 Electrochemical performance of the carbon nanosheets electrode

Carbon materials have been studied and used as electrodes for supercapacitors (Table 2.6) due to their very attractive chemical and physical performance and low price. The difference in the surface properties of carbon materials can highly affect their electronic properties. The carbon materials can be classified as conductor or semiconductor depending on their orientation of the structure. Moreover, the electronic and electrochemical properties of the carbon nanomaterial can be improved by modifying the surface [78, 80].

DOI: 10.14750/ME.2021.008

Table 2.6 Comparison of different electrode materials for flexible supercapacitors.

Electrode material	Specific capacitance ($F\ g^{-1}$)	Power density ($kW\ kg^{-1}$)	Energy density ($Wh\ kg^{-1}$)
Activated 3D porous graphene [81]	202	109	51
Activated graphene-like carbonnanosheets [81]	~160	77	~40
Activated carbons [82]	400	13.9	35
Activated carbon fibre [82]	430	2.98	8.1
Graphene [82]	341	338	74
Graphene [83]	81.7	1.5	7.13
Carbon nanotubes [83]	22	1.5	13
Carbon aerogel [83]	200	4	20

Performance parameters, such as operating voltage, internal resistance, capacitance, power density, energy density, the time constant and life cycle should be calculated based on currently established and accepted procedures. To calculate these parameters, some fundamental electrochemical measurements should be performed on the supercapacitor cells or electrochemical systems. Electrochemical characteristics distinguish ideal and practical supercapacitors as shown in Fig. 2.16. Cyclic Voltammetry (CV), Galvanostatic Charging/Discharging (GCD), Electrochemical Impedance Spectroscopy (EIS) and other measurements are employed as electrochemical measurement techniques in evaluating the performance of supercapacitors [84].

DOI: 10.14750/ME.2021.008

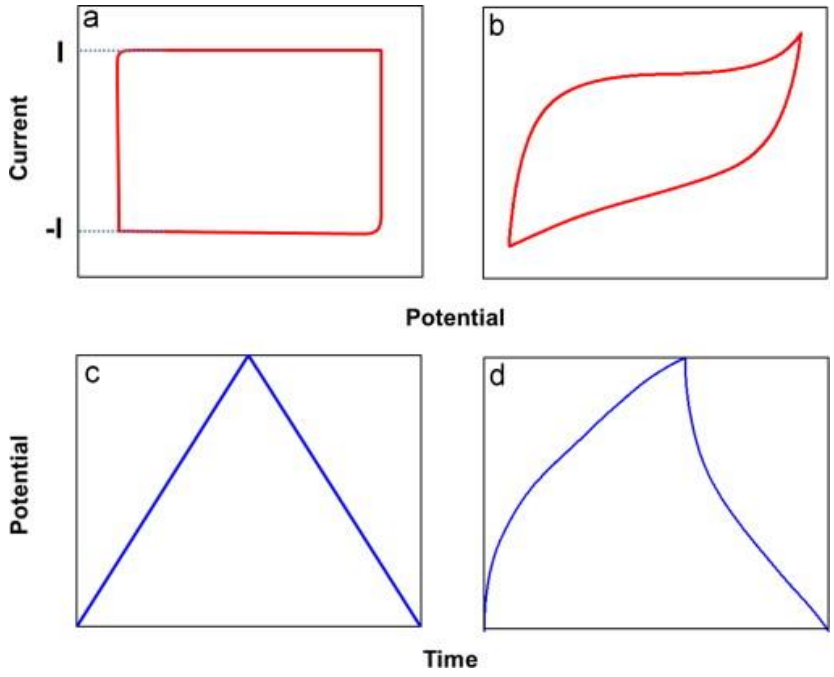

Figure 2.16 Electrochemical characteristics distinguish an ideal and practical supercapacitor. CV curves of an ideal supercapacitor (a) where the current is constant (I) and a practical supercapacitor (b) with variable current. (c) Galvanostatic charge and discharge behaviour for an ideal supercapacitor is linear and symmetric, but (d) it can be distorted for a practical supercapacitor [84].

In the condition of EDLC, carbon materials and their derivatives have been investigated and used in EDLC electrodes. The EDLCs generally store charges through surface absorption, so they reveal high power density, long cycle life but low energy density. In pseudocapacitors, electrochemical energy storage is associated with electron transfer, which is Faradic in origin, involving the passage of charges across the double layer, achieved by surface redox reactions with specifically adsorbed ions from the electrolyte, intercalation of atoms in the layer lattice or electrosorption, underpotential deposition of hydrogen or metal adatoms in surface lattice sites which result in a reversible faradaic charge-transfer. Pseudocapacitors usually possess much higher energy density than EDLCs. The materials primarily for pseudocapacitor mainly are metal oxides/nitrides/sulfides and conducting polymers [84].

DOI: 10.14750/ME.2021.008

- *Calculation of capacitance of single electrode from galvanostatic charge/discharge curves*

The specific capacitance (Cs) could be calculated from the charge-discharge curves by the following equation [85]:

$$C_s = \frac{I\Delta t}{m\Delta V} \tag{2.10}$$

where I is the discharge current (mA or A), Δt is the discharge time difference in seconds, V is the voltage window between the positive and negative electrodes (v), and m is the active material mass of the electrode (g). For the electrodes under the same testing condition, a longer discharge time usually represents larger specific capacitance of the material.

- *Calculation of capacitance of single electrode from cyclic voltammetry curves*

The specific capacitance (Cs) could be calculated from the cyclic voltammetry curves by the following equation:

$$C_s = \frac{Q}{m} \times \Delta V \tag{2.11}$$

Where Cs is the specific capacitance in F g^{-1}, Q is the total charge obtained by integrating the positive and negative sweeps in a curve (in coulomb, C), V and m is the mass of the active materials electrode.

Activated carbon is the form of disordered carbon with high surface area and small pore. According to theory, high specific capacitance is expected from activated carbon due to large surface area [79, 86-94]. Common activated carbon shows low surface area and wide pore size distribution, due to low specific capacitance. The challenging issue for the commercial use of activated carbon electrode consisted of precise control over the pore structure distribution and large surface area. Extensive research was carried out for the improvements in activation processes to achieve quality pore distribution and surface area. However, the relationship between the specific capacitance and specific surface area was not linear. Rather, the capacitance value found to be dependent on several other parameters like decomposition of the electrolyte through active sites of activated carbon, presence of oxygen functional groups, pore conductivity, compatibility of the carbon surface with

DOI: 10.14750/ME.2021.008

a specific electrolyte solution and growth of narrow micropores. The presence of oxygen functional groups on the surface of activated carbon generated additional redox activity (pseudocapacitance). In addition, the internal resistance and leakage current also changes abruptly depending on the amount of oxygen functionalities on activated carbon. Furthermore, the creation of narrow micropores reduces the accessibility of the electrolyte ions due to which a large portion of the activated carbon materials remain unused. The effect of physical and chemical activation of carbon was further studied by electrochemical impedance spectroscopy (EIS) [78, 80].

Knowledge gap:

The application of activated carbon nanosheets prepared from nettle and peanut shell for supercapacitor material is new. However, there is only a small amount of research which systematically studied the effect of different exfoliating acids on the behaviour of carbon materials, while the effect of the state of alkaline hydroxide activation on the carbon nanostructures formation of nettle and peanut shell has not been investigated so far. Most research studies carbon preparation using a single activating agent for chemical activation. Therefore, it is worth to study the chemical treatment of carbon using various chemicals activating and exfoliating agent to enhance its. Since no research have synthesized carbon using two processes: activation (KOH and NaOH) and exfoliation (HNO_3, H_2SO_4 and H_3PO_4), therefore, it is worth to investigate.

DOI: 10.14750/ME.2021.008

3 Materials and methods

3.1 Organic composition of materials

The organic composition of the nettle stem and peanut shell (Fig. 3.1), collected from Miskolc (Hungary), was investigated using chemical analysis at the commercial laboratory Mezőlabor Szolgáltató és Kereskedelmi Kft, Hungary (Appendix 10.1). The acid detergent fibre content (ADF), acid detergent lignin content (ADL), and neutral detergent fibre content (NDF) were determined. The cellulose content was calculated by subtracting ADF from ADL. Similarly, hemicellulose content was calculated by subtracting NDF from ADF and lignin was calculated using ADL (Table 3.1). As nettle leaf has low organic (cellulose, hemicellulose and lignin) and carbon content [95-96], I chose to use the nettle stem to produce carbon in this dissertation.

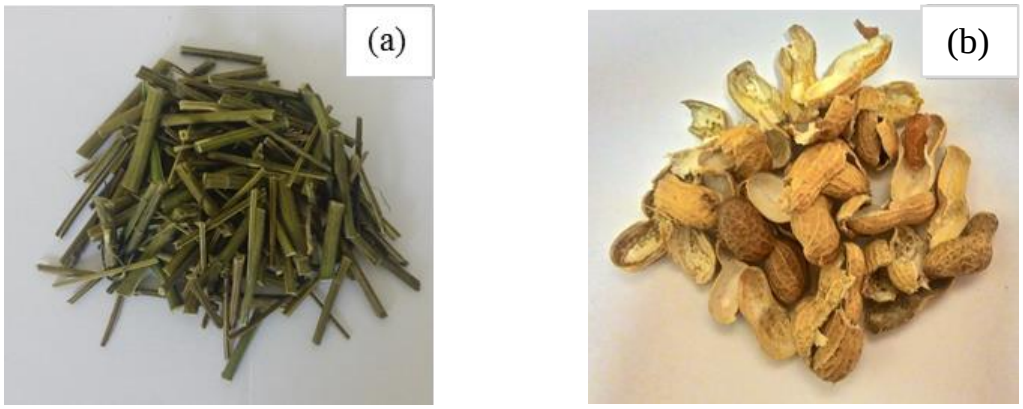

Figure 3.1 Raw materials (a) Nettle stem and (b) Peanut shell.

Table 3.1 Organic composition of natural materials

Materials	**DM[a] (g/kg)**			**Cellulose (wt.%)**	**Hemicellulose (wt.%)**	**Lignin (wt.%)**
	ADF[b]	**NDF[c]**	**ADL[d]**			
Nettle stem	617 ± 31	770 ± 39	119 ± 6	49.8	15.3	11.9
Nettle leaf	183 ± 9	308 ± 15	22 ± 5	16.1	12.5	2.2
Peanut shell	699 ± 35	783 ± 39	272 ± 14	42.4	8.4	27.2

[a]DM, Dry Matter, [b]ADF, Acid Detergent Fibre, [c]NDF, Neutral Detergent Fibre and [d]ADL, Acid Detergent Lignin

DOI: 10.14750/ME.2021.008

3.2 Synthesis of the carbon nanosheets

The synthesis of carbon nanostructured materials from nettle stem or peanut shell was carried out as explained below (Fig. 3.5).:

3.2.1 Sample preparation: The nettle stem (NS), nettle leaf (NL) and peanut shell (PS) were separately washed and dried at 80 ºC for 24 hours, followed by cleaning with HCl [0.5M] for another 24 hours. This facilitates the removal of organic compounds and residual metallic oxides [12]. It was finally washed with distilled water and dried at 80 ºC for 24 hours.

3.2.2 Pre-Carbonization: The samples were pre-carbonized in a stainless-steel tubular furnace at 450 ºC for 2 hours under argon environment (Fig. 3.2). The pre-carbonized samples are identified as char NS, char NL or char PS. As for nettle leaf, the synthesis process was finished with the pre-carbonization step (activation and exfoliation steps were not executed on this material).

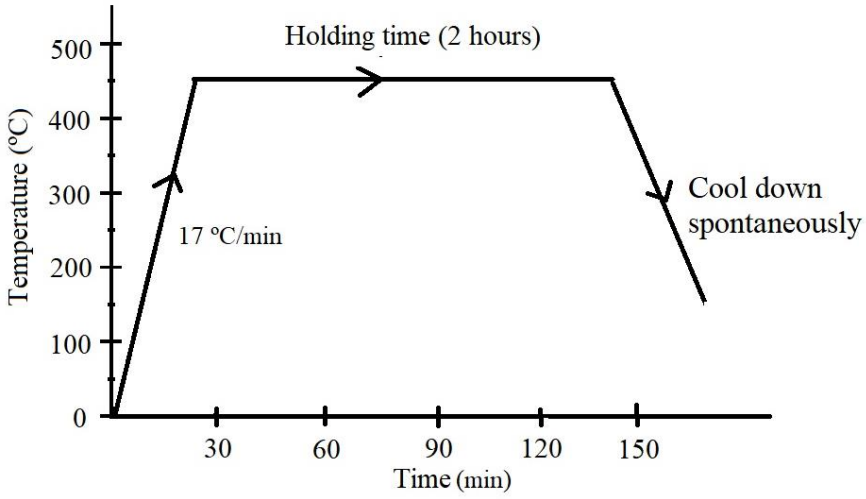

Figure 3.2 Temperature-time curves for pre-carbonization.

Figure 3.3 Char samples (a) Nettle stem (b) Peanut shell.

DOI: 10.14750/ME.2021.008

3.2.3 Activation: The pre-carbonized sample (Fig. 3.3) was milled with a mortar for 1 hour before being adding to aqueous [1 mol L^{-1}] KOH or NaOH with a weight ratio of 1:1 [KOH or NaOH: Char sample (nettle stem or peanut shell)]. The mixture was stirred for an hour and dried at 80 ºC for 24 hours. This method is referred to solute activation. KOH and NaOH were used in solid-state as well. In this case, KOH or NaOH pellet/powder with a weight ratio of 1:1 [KOH or NaOH: Char sample (nettle stem or peanut shell)] was milled with pre-carbonized samples in a mortar for 1 hour. This method is referred to solid activation.

3.2.4 Carbonization: The activated sample was carbonized under Ar atmosphere in a tubular furnace for about 2 hours. The temperature was maintained at 800 ºC for the process (Fig. 3.4). Then these samples were exfoliated by different acids.

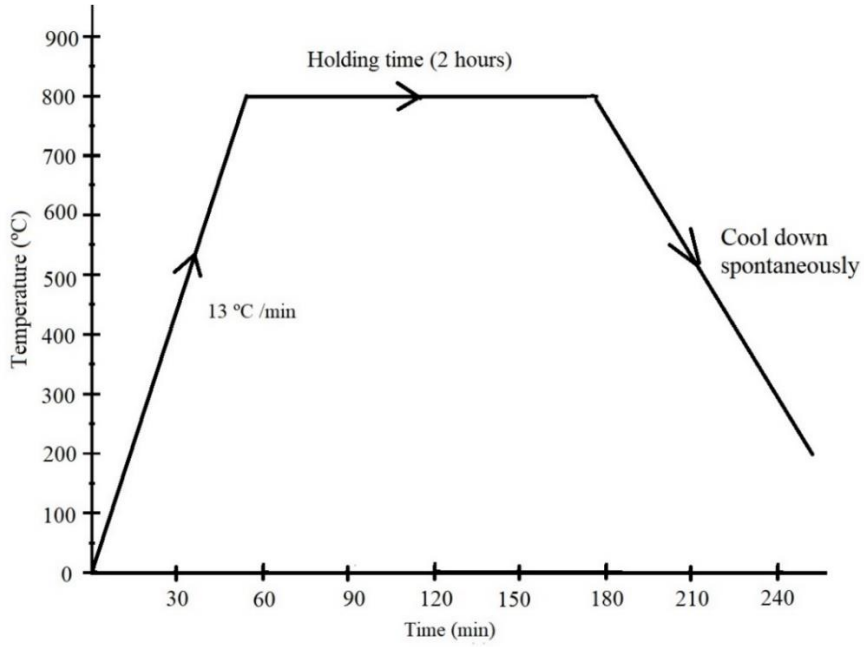

Figure 3.4 Temperature-time curves for carbonization samples.

3.2.5 Exfoliation: The exfoliation process was carried out by three different acids; hence, three different samples were obtained. 2 mol L^{-1} of nitric acid, sulfuric acid, or phosphoric acid was used as exfoliators. The samples were stirred for 1 hour and washed with distilled water several times until a neutral pH was obtained. The samples were then dried at 80 ºC for 24 hours before subjecting them to characterization tests.

For peanut shell, I changed the type of exfoliating acid with other diprotic and triprotic acids (ascorbic acid and boric acid, respectively) to study the relationship between the type of acids and the specific surface of the samples. Lignin is another sample in which

DOI: 10.14750/ME.2021.008

I have done KOH activation and exfoliation by three types of acids (nitric acid, sulfuric acid, or phosphoric acid) to compare their effects with nettle stem and peanut shell.

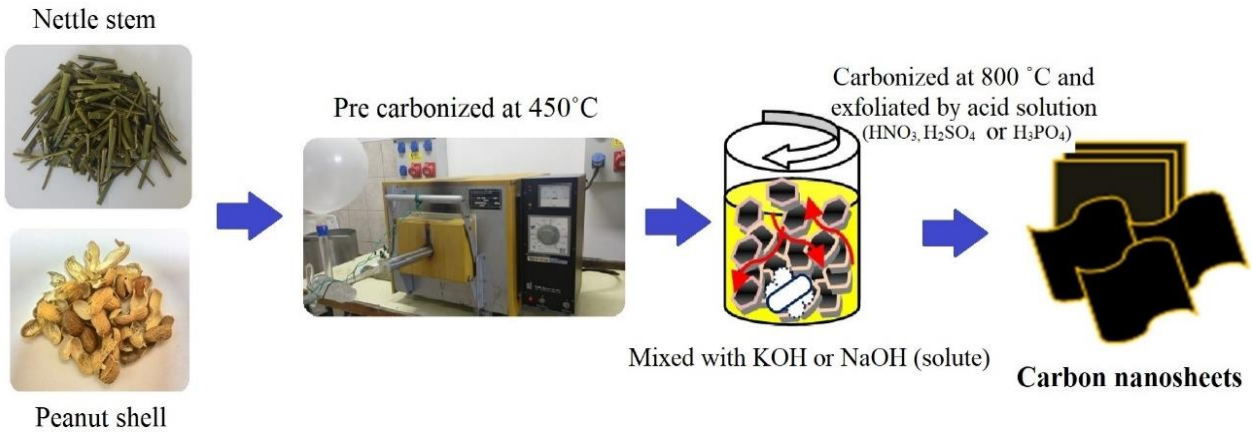

Figure 3.5 Schematic description of the carbon nanosheets preparation.

3.3 Physical and chemical characterization

3.3.1 Scanning electron microscopy: The exfoliated samples were coated with gold and investigated by scanning electron microscopy (SEM, HITACHI S-4800, Zeiss EVO-MA 10 and Helios G4 PFIB CXe DualBeam). The chemical composition was analysed by energy-dispersive X-Ray spectrometry (EDS, BRUKER AXS, EDAX Genesis and EDAX Octane Elect Plus) and CHNS analyser (Carbon, Hydrogen, Nitrogen and Sulfur analyser, Carlo Erba EA1108).

3.3.2 Transmission electron microscopy: The nanosheet structure was investigated by transmission electron microscopy (TEM, FEI TECNAI G2 20 X-TWIN).

3.3.3 Brunauer-Emmett-Teller analyser: The specific surface area of the raw materials and carbon nanosheets (CNs) was examined by the Brunauer-Emmett-Teller method (BET, Micrometrics TriStar 3000).

3.3.4 X-Ray Diffraction: For crystal structure, X-Ray Diffraction was used (XRD, Bruker D8 Advance diffractometer using Cu Kα radiation 40KV, 40mA, in parallel beam geometry obtained with Gobel mirror, equipped with Vantec-1 position sensitive detector (1º window opening)). Patterns were recorded at 0.007º speed 2θ/29 sec and within 2-100º angular range of 2θ.

DOI: 10.14750/ME.2021.008

3.4 Electrochemical characterization

For characterizing electrochemical properties, synthesized CNs sample, carbon black, and PTFE poly-tetrafluoroethylene were weighed in a mass ratio of 90:5:5 and mixed in the mortar. The mixture was pressed to form an electrode pellet (diameter = 10 mm). The electrode material was characterized by a three-electrode system of nettle stem carbon nanosheets (NSCNs) or peanut shell carbon nanosheets (PSCNs), Pt, and Ag/AgCl, where the latter two are used as the counter electrode and reference electrode respectively (Fig. 3.6-3.7). 1 M sodium sulphate (Na_2SO_4) aqueous solution was used as an electrolyte. The electrochemical properties of the electrode material and cell were characterized by cyclic voltammetry (CV), galvanostatic charge-discharge (GCD), and electrochemical impedance spectroscopy (EIS). The specific capacitance of a symmetric supercapacitor (Cs) is calculated by the following equation (3.1) [98].

$$C_s = \frac{I \times \Delta t}{\Delta V \times m} \tag{3.1}$$

where *Cs, I, Δt, ΔV* and *m* are the specific capacitance (F g^{-1}), discharge current (A), discharge time (s), voltage change after a full charge or discharge (V) and mass of active material on the electrode (g), respectively. The energy density (E, Wh kg^{-1}) (3.2) and power density (P, W kg^{-1}) (3.3) of the electrode were calculated based on the following equations:

$$\mathrm{E} = \frac{C_s \times \Delta V^2 \times 1000}{2 \times 3600} \tag{3.2}$$

$$P = \frac{E}{\Delta t} \times 3600 \tag{3.3}$$

DOI: 10.14750/ME.2021.008

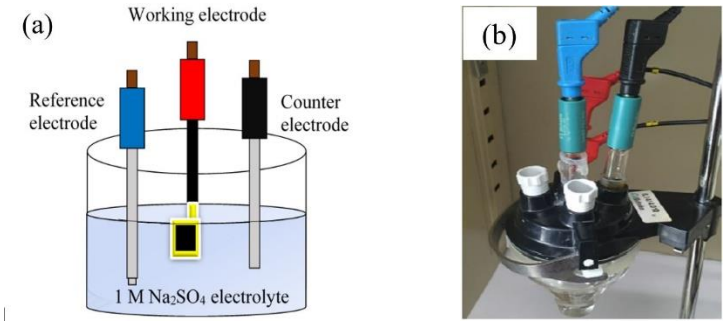

Figure 3.6 (a) Schematic diagram and (b) photograph of 3 electrode setup for electrochemical analysis.

Figure 3.7 A Photograph of Metrohm autolab PGTST 302 [99].

DOI: 10.14750/ME.2021.008

4 Results and discussions

4.1 The structure of carbon nanosheets synthesized from natural materials

4.1.1 Microstructure of raw material

4.1.1.1 Nettle stem

The microstructure of the dried nettle stem was examined by SEM (Fig.4.1). The cell wall in fibre is not a homogeneous layer. The cell walls of a plant cell (the primary and the secondary cell wall) can be considered as a composite consisting of cellulose fibrils embedded within a matrix of lignin and hemicellulosic polysaccharides [100].

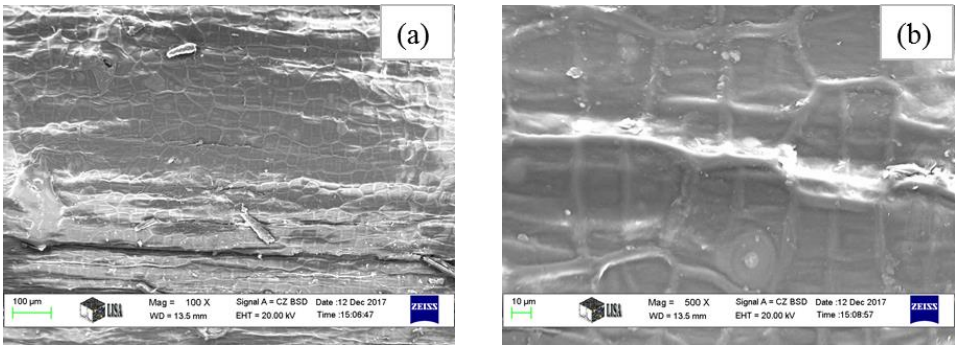

Figure 4.1 SEM micrographs of dried nettle stem at (a) 100X and (b) 500X.

It has a groove and hollow surface, composed of fibrous structure and has many hollow stinging hairs called trichomes on the surface (Fig. 4.1 a-b, see the chemical element in Appendix 10.2).

4.1.1.2 Peanut shell

The SEM micrographs in Fig.4.2 revealed the agglomerate of thin layered surface, interconnect hollow and micro-sized pores on the surface of the peanut shell (Fig. 4.2 a-b).

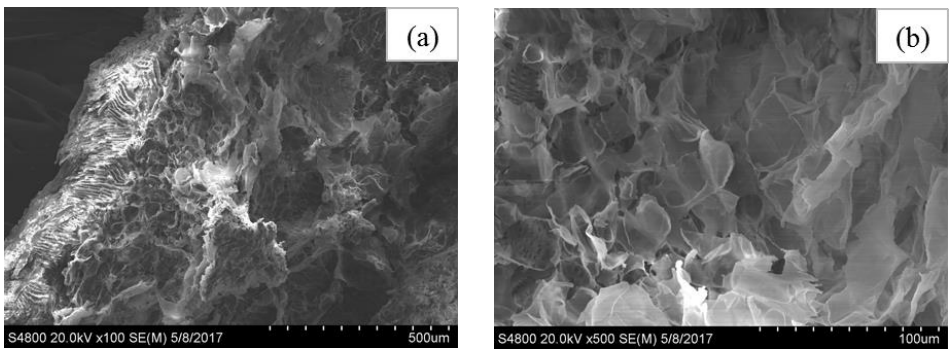

Figure 4.2 SEM micrographs of dried peanut shell at (a) 100X and (b) 500X.

DOI: 10.14750/ME.2021.008

4.1.2 Effect of KOH activation

The samples were activated by KOH (solid and solute) as written in chapter 3.2.3. The microstructures of the samples observed by SEM are shown in Fig.4.3-4.4.

4.1.2.1 KOH (solid) activation

The microstructure of nettle stem activated by KOH (solid) show lots of small angular and flake particles of carbon product in Fig.4.3(a), (c). Porous and thin plate structures were found in peanut shell carbon products (Fig.4.3(b)) after activating with KOH (solid) and carbonizing for 1 hour. The small sheet and network of thin-wall structures were found after activating with KOH (solid) and carbonizing for 2 hours (Fig.4.3 d).

	Carbonized at 800 ˚C for 1 hour	**Carbonized at 800 ˚C for 2 hours**
Nettle stem	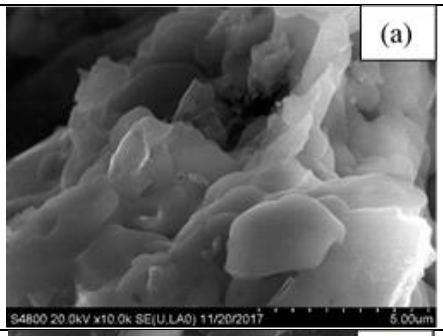	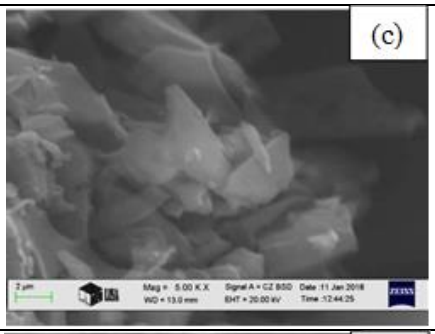
Peanut shell	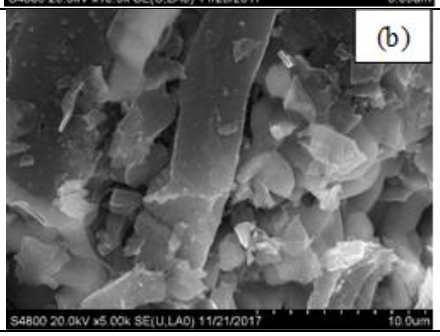	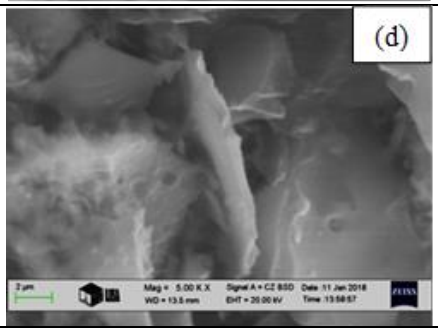

Figure 4.3 SEM micrographs of the samples after KOH (solid) activation and carbonized at 800 ˚C: for 1 hour and 2 hours of (a), (c) nettle stem and (b), (d) peanut shell.

4.1.2.2 KOH (solute) activation

Activation by KOH (solute) forms angulated and nano-sized sheets from nettle stem (Fig.4.4 a, c). Peanut shell has thin-layered (nano-) structure Fig.4.4(b), (d) with micro sized pores and fibrous structure at longer activation time.

The SEM micrographs from Fig.4.3 and Fig. 4.4 show the different microstructure of the samples. After carbonizing for 2 hours, they show the small and clear carbon nanostructure formation compared to the activation time at 1 hour as longer activation time is more efficient. The possible reason is that longer activation time facilitated the burn-off

DOI: 10.14750/ME.2021.008

of carbon and the release of volatile compounds. As a result, the carbon structure was opened to increase surface area [101]. The carbon nanostructures in KOH (solute) activation were separated and distributed better than KOH (solid) activation.

The KOH (solute) activation affected better the carbon nanostructure formation compared to KOH (solid) as nanosheets having smaller thickness were obtained after treating with KOH (solute) and carbonizing for 2 hours. Potassium hydroxide has good penetration and is distributed well in the sample solution.

	Carbonized at 800 ˚C for 1 hour	**Carbonized at 800 ˚C for 2 hours**
Nettle stem	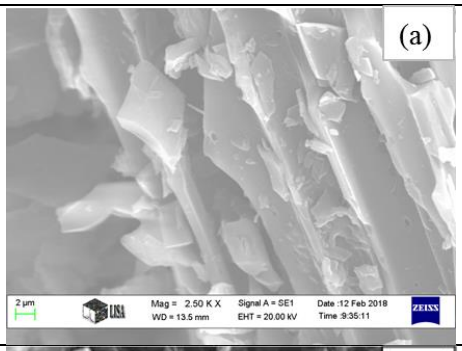	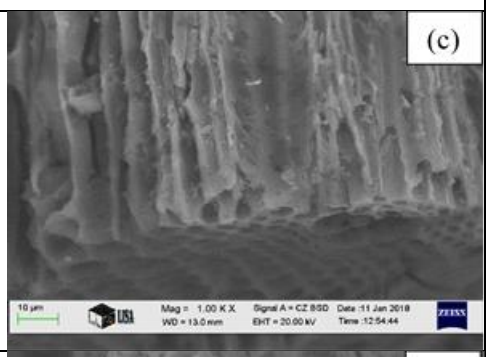
Peanut shell	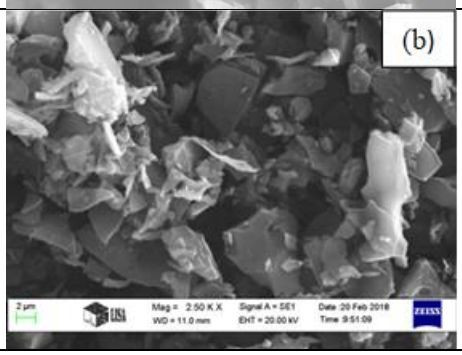	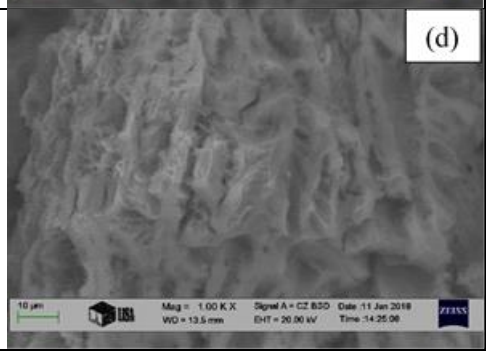

Figure 4.4 SEM micrographs of the samples after KOH (solute) activation and carbonized at 800 ˚C: for 1 hour and 2 hours of (a), (c) nettle stem and (b), (d) peanut shell.

In the case of solids, particles are held together very closely. This makes them very strong and difficult to break. So, it's difficult for KOH to distribute and penetrate with carbon compared to liquid. **In the case of solute**, particles in liquids are quite close to each other. However, they can move past each other very easily. This makes liquids very easy to break apart. The particles in liquids move around quite a bit, bumping gently past each other [102]. In my work, the KOH (solid) is mixed with the samples by milling with mortar, and the KOH (solute) is mixed by stirring. The KOH (solute) is well distributed, coated, and penetrated in the samples. For this reason, after heat treating, the KOH (solute) affected the microstructure more than the solid.

DOI: 10.14750/ME.2021.008

Therefore, from the results of this experiment, I decided to use a hydroxide solution to activate carbon before acid exfoliation to produce carbon nanosheets.

4.1.3 Effect of NaOH activation (carbonized at 800 ˚C for 2 hours)

The activation process is described in chapter 3.2.2. After activation by NaOH (solute), lots of angular and flake particles were found on the surface of the nettle stem (Fig. 4.5 a). The SEM micrograph in Fig. 4.5 (b) revealed the agglomerate of thin layered surface and interconnected hollow on the peanut shell's surface. The activated peanut shell shows multi-layered thin plates. It can be seen that both of the activated nettle stem and peanut shell have micropore structure and carbon fragmented structure dispersed in these samples.

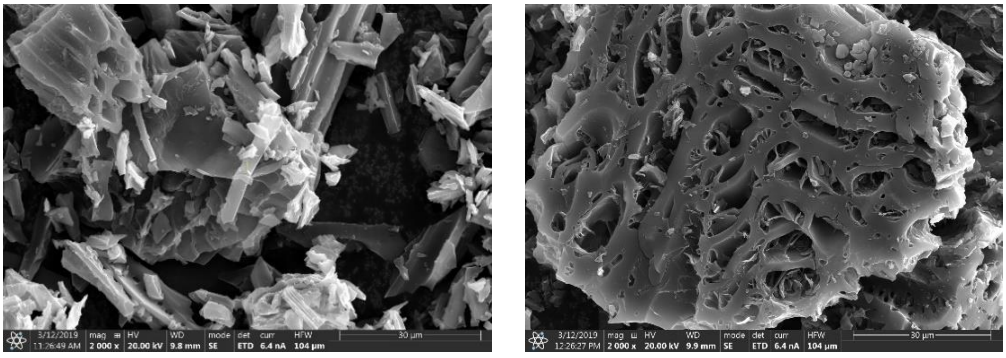

(a) **(b)**

Figure 4.5 SEM micrograph of (a) nettle stem activated by NaOH (solute) and (b) peanut shell activated by NaOH (solute).

From the results, it was found that solute activation gives better results than solid activation and in the case of the carbonization, 2 hours gives better results than 1 hour. So, I decided to use solute activation and carbonization time at 2 hours.

4.1.4 Effect of activation and exfoliation

4.1.4.2 Effect of activation and exfoliation to nettle stem

a) NSCNs activated by KOH and exfoliated by HNO_3, H_2SO_4 or H_3PO_4

The exfoliation process was carried out by using either nitric, sulfuric or phosphoric acid. Angular, thin sheets were found in NSCNs exfoliated by nitric acid (Fig. 4.6) showing thickness varying from 89 to 95 nm and having 70.70 wt.% carbon. The SEM micrograph of NSCNs exfoliated by sulfuric acid shows a smooth surface and clearly reveals the formation of separated carbon nanosheets with thickness from 42 to 71 nm. Chemical

DOI: 10.14750/ME.2021.008

composition results show that carbon nanosheets mainly contain carbon (71.52 wt.%). Ultra-thin structures and overlapping carbon nanosheets were identified in the structure of NSCNs exfoliated by phosphoric acid. The thickness of the carbon nanosheets is ranging from 49 to 60 nm. Exfoliation with phosphoric acid yielded the highest carbon content (71.99 wt.%) among the exfoliated nettle specimens.

Exfoliated by	**KOH activated**	**NaOH activated**
HNO_3	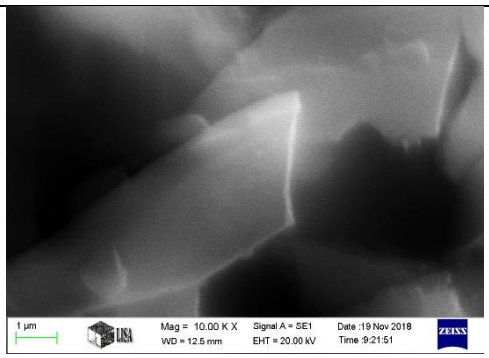	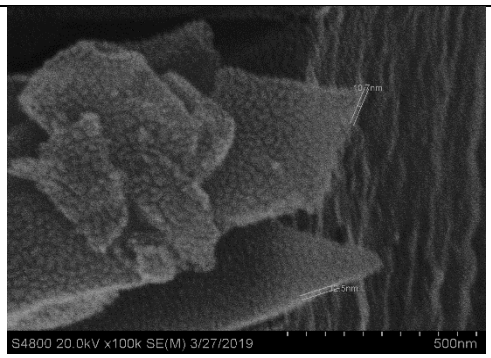
H_2SO_4	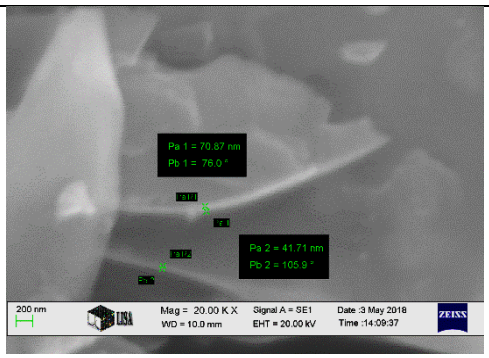	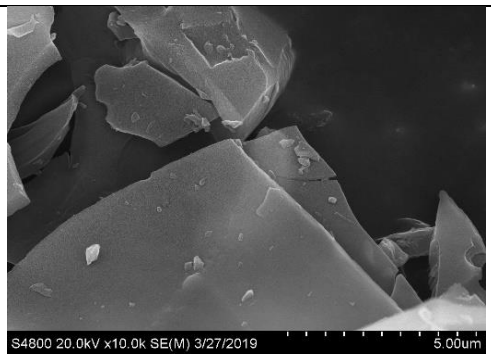
H_3PO_4	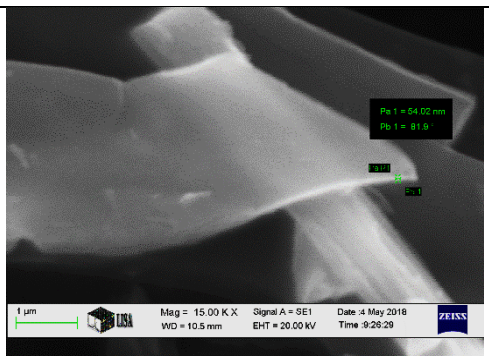	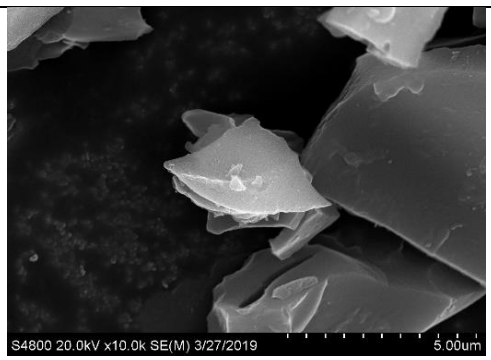

Figure 4.6 SEM micrographs of activated and exfoliated NSCNs obtained by different agents.

b) NSCNs activated by NaOH and exfoliated by HNO_3, H_2SO_4, or H_3PO_4.

The microstructure of NSCNs exfoliated by nitric acid shows the angular plates with thickness from 13 to 20 nm (76.5 wt.% carbon). The small particles and thin sheets with

DOI: 10.14750/ME.2021.008

sharp edges and thickness from 55 to 60 nm (79.2 wt.% carbon) were found after exfoliating by sulfuric acid. Small thin sheets that are overlapped can be found in NSCNs exfoliated by phosphoric acid. The thickness of the carbon nanosheets is ranging from 9 to 15 nm (78.9 wt.% carbon).

The carbon nanosheets' structure after activating with two alkaline hydroxide and exfoliating by three different acids is quite similar (Fig. 4.6). By comparing the microstructures, it was found that carbon nanosheets are separated, and their surface is clean.

4.1.4.3 Effect of activation and exfoliation to peanut shell

a) PSCNs activated by KOH and exfoliated by HNO_3, H_2SO_4, or H_3PO_4.

The SEM micrograph of PSCNs exfoliated by nitric acid shows small thin sheets and multilayer sheets with thickness varying from 31 to 92 nm and having 69.7 wt.% carbon. Thin nanosheets with thickness from 45 to 75 nm were found in PSCNs exfoliated by sulfuric acid. Carbon nanosheets mainly contain carbon (72.2 wt.%). Micropore and thin layer carbon nanosheets were identified in the structure of PSCNs exfoliated by phosphoric acid. The thickness of the carbon nanosheet is ranging from 28 to 54 nm. Exfoliation with phosphoric acid yielded the highest carbon content (74.3 wt.%).

b) PSCNs activated by NaOH and exfoliated by H_2SO_4, H_3PO_4 or HNO_3

The agglomerated thin nanosheets and angular plates with thickness from 10 to 80 nm were found after exfoliating by nitric acid (77.2 wt.% carbon). The microstructure of PSCNs exfoliated by sulfuric acid shows small particles, hollows, and thin sheets with sharp edges with thickness from 10 to 50 nm (79.5 wt.% carbon). Small plates, angular and thin sheets can be found in PSCNs exfoliated by phosphoric acid. The thickness of carbon nanosheets is ranging from 10 to 60 nm (79.8 wt.% carbon).

DOI: 10.14750/ME.2021.008

Exfoliated by	KOH activated	NaOH activated
HNO_3	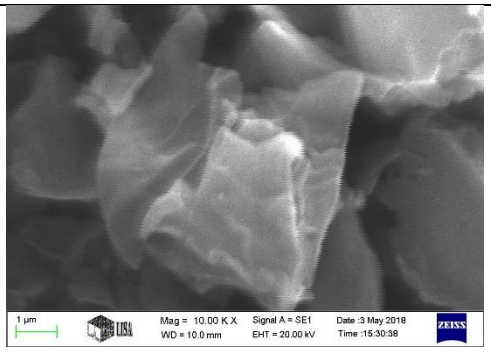	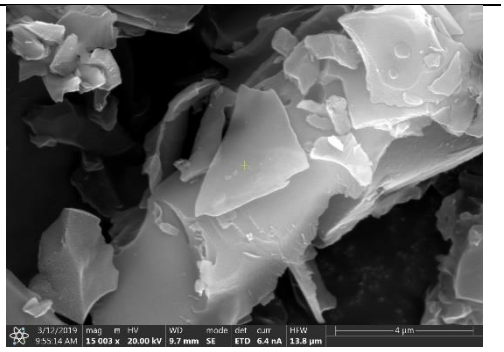
H_2SO_4	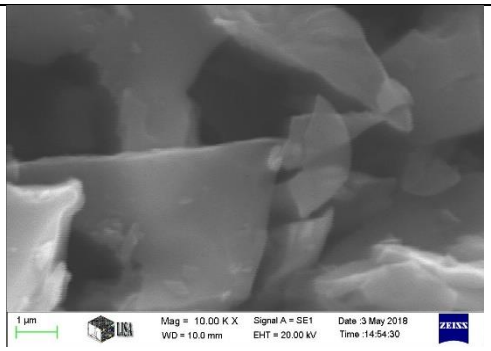	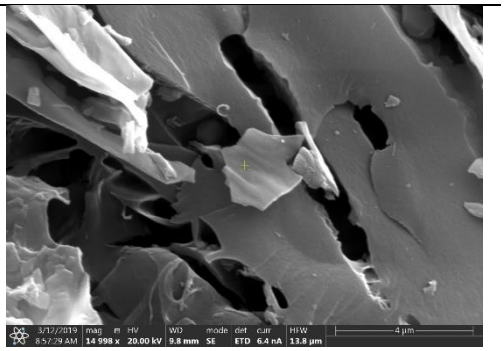
H_3PO_4	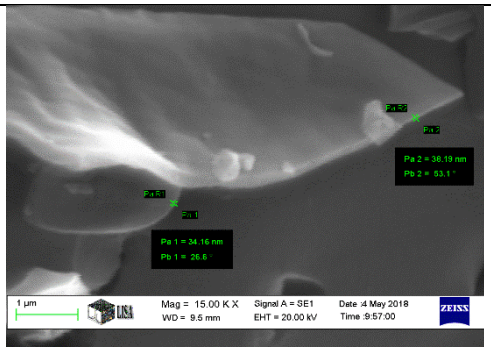	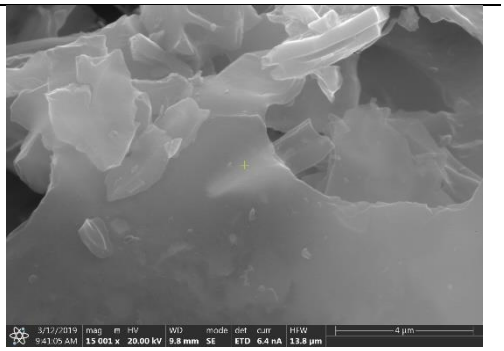

Figure 4.7 SEM micrographs of activated and exfoliated PSCNs obtained by different agents.

The nanosheet structure was confirmed by TEM images (Fig. 4.8 a-c), where the amorphous two-dimensional nanosheet porous structure of NSCNs is clearly seen. In the TEM images, the bright and transparent regions are the ultrathin nanosheet. The less transparent areas reveal the overlapped or folding areas of NSCNs, which further imply the ultrathin structure. The structure of the exfoliated NSCNs was explored further with high-resolution TEM (HRTEM) imaging (Fig. 4.8 d-f). The layered nanosheet structure is highly porous and becomes thinner toward the edges of the material. NSCNs have a monolayer property, further demonstrating their ultrathin nature. The pore distribution can be seen by the white dots in the grey areas from HRTEM images. These figures are representative for the samples. After the exfoliation process, carbon nanosheets with the thickness lower than

DOI: 10.14750/ME.2021.008

100 nm were found and it was confirmed later by the results from the specific surface area measurements as well.

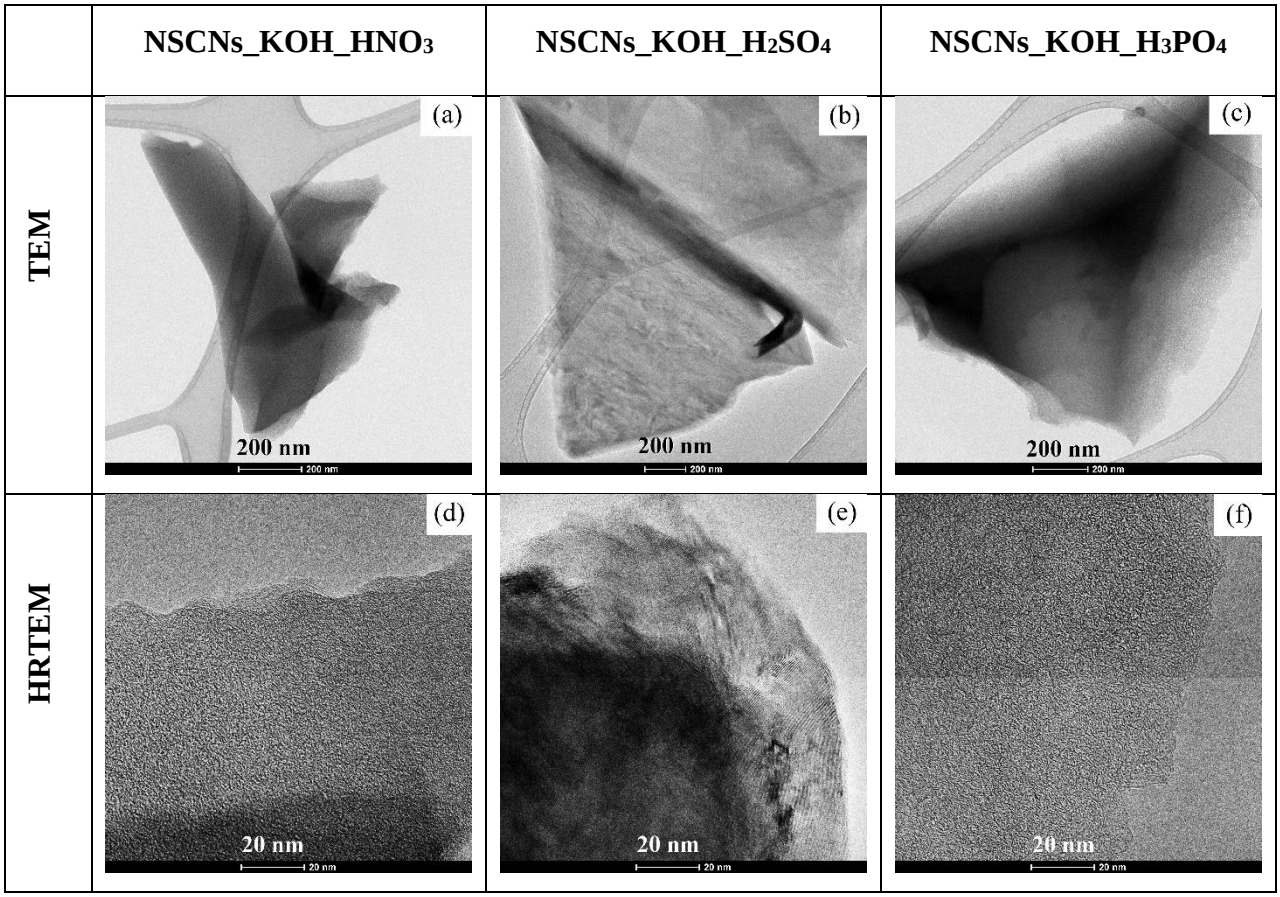

Figure 4.8 TEM (a-c) and HRTEM (d-f) micrographs of the NSCNs activated by KOH and exfoliated by (a, d) HNO_3, (b, e) H_2SO_4, or (c, f) H_3PO_4.

4.1.5 Structure of carbon nanosheets

X-ray diffraction (XRD) was used to determine the structure of NSCNs and PSCNs. The results show (Fig. 4.9-4.11) a glassy carbon structure [103-107] was developed in the exfoliated samples. Both the large peaks at 2θ = ~22° and 44°, and the weak and board diffraction peak occurring in the 2θ range 79° to 81° can be attributed to the typical glassy amorphous carbon structure. The XRD patterns are quite similar. Some sodium carbonate (Na_2CO_3) was found in NaOH activated samples. According to references [60] and [108], this suggests that the exfoliating acids do not have a significant effect on the crystal structure of carbon nanosheet. The alkaline hydroxide and acid solution does not dissolve the carbon material.

DOI: 10.14750/ME.2021.008

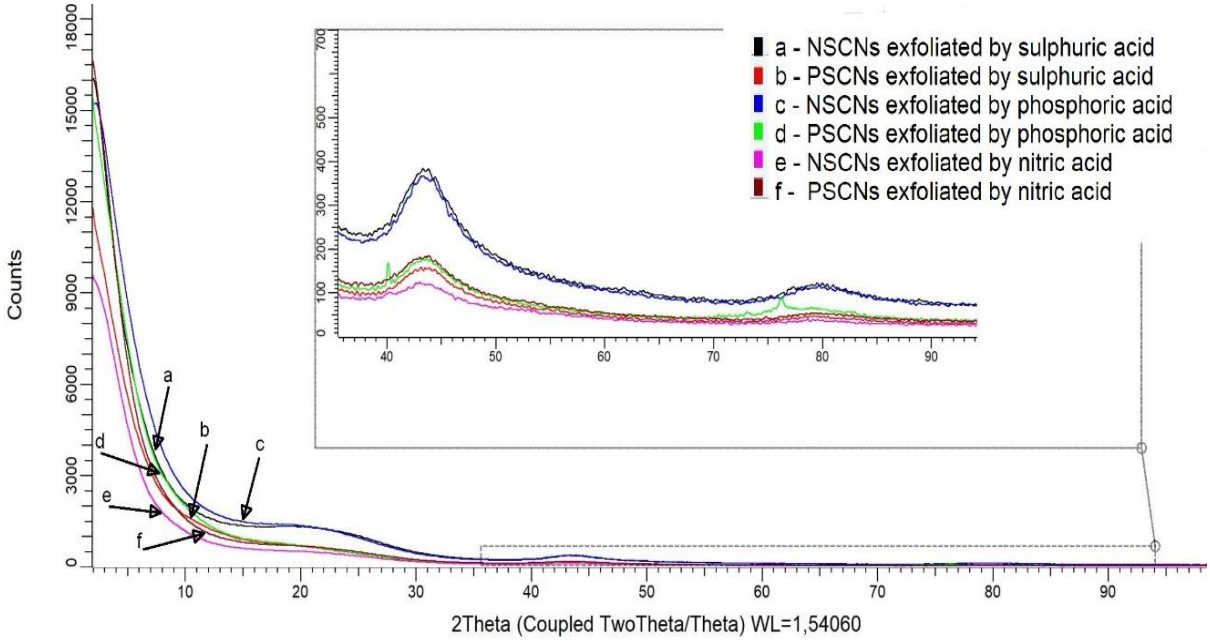

Figure 4.9. XRD patterns of NSCNs and PSCNs activated by KOH.

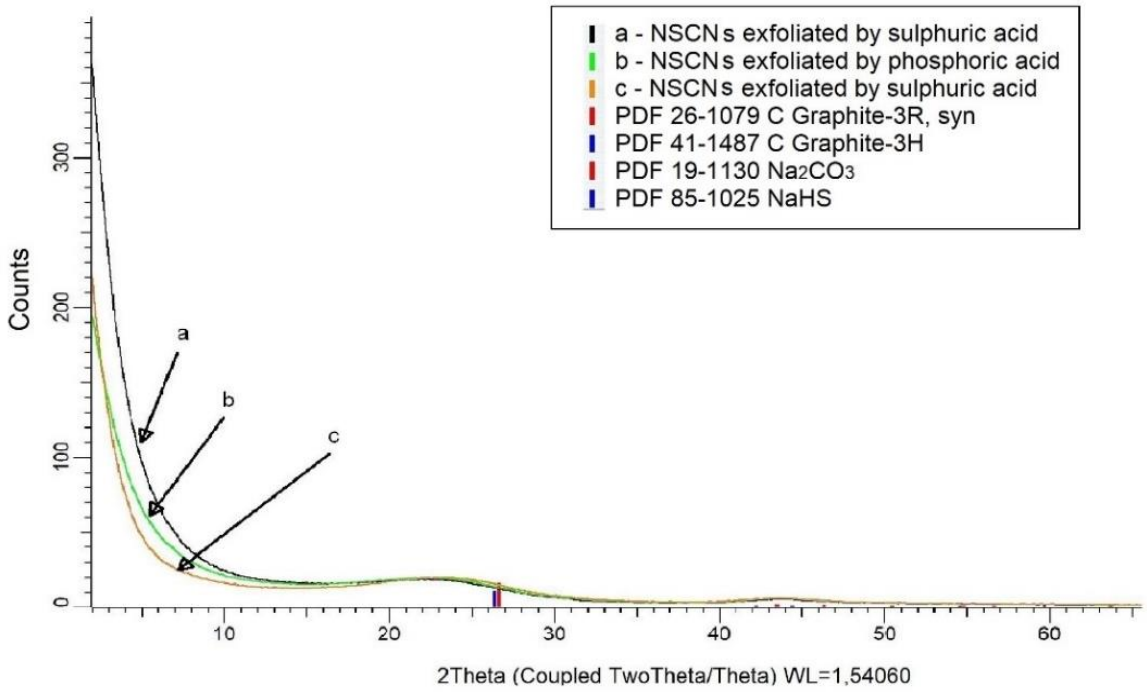

Figure 4.10. XRD patterns of NSCNs activated by NaOH.

DOI: 10.14750/ME.2021.008

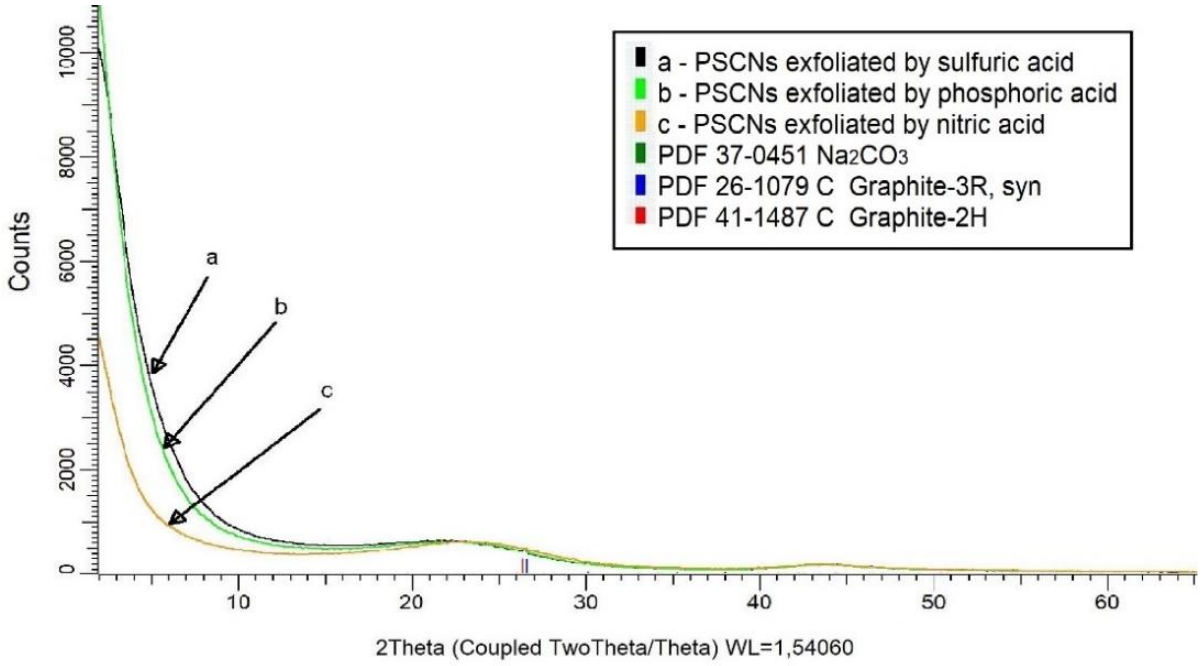

Figure 4.11. XRD patterns of PSCNs activated by NaOH.

During the chemical activation with KOH, K intercalation can be considered as a relevant step which will have an important influence on the total reaction mechanism. The metal intercalation favours the process by separating the layers, that generates micropores or even new high energy sites for the redox reactions. The differences of efficiency found between KOH and NaOH for the activation of carbon of different crystallinity is explained by the fact that K intercalates better than Na [60].

All exfoliating agents (H_2SO_4, H_3PO_4, and HNO_3) were suitable to disrupt the layers in the material. During the exfoliation process, acids penetrated the carbon layers and rupture interlayer bonds. Water was used to clear away contaminants (Fig. 4.12). The exfoliation process has increased the specific surface area (BET results, Table 4.4-4.5) and through these processes, high-purity carbon is obtained (more than 70 wt.%, Table 4.2).

DOI: 10.14750/ME.2021.008

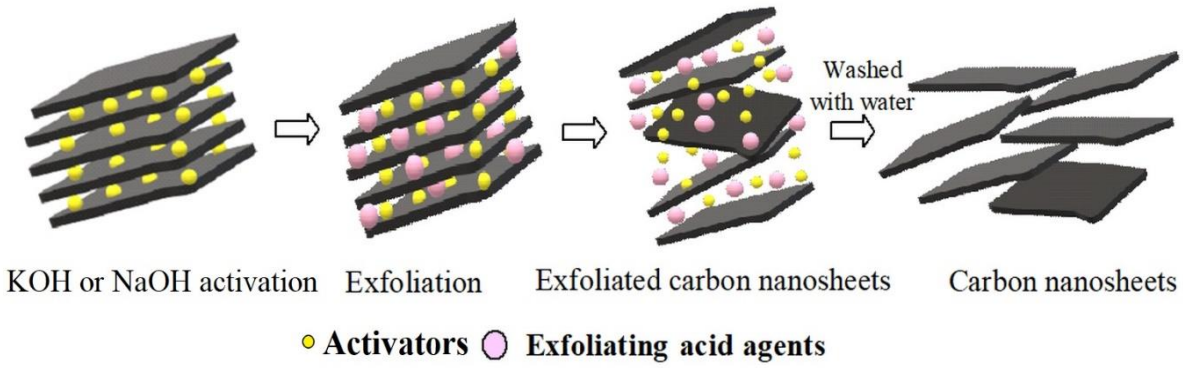

Figure 4.12 Schematic illustration of the mechanism of activation–exfoliation.

Phosphoric acid affected the surface of carbon nanosheets more than sulfuric acid or nitric acid because it is a strong, polyprotic acid that is capable of donating more than one proton. Phosphoric acid is a triprotic acid having three dissociable protons that undergo stepwise dissociation as follows [109]:

$$H_3PO_4 \rightleftharpoons H^+ + H_2PO_4^- \quad (4.1)$$

$$H_2PO_4^- \rightleftharpoons H^+ + HPO_4^{2-} \quad (4.2)$$

$$HPO_4^{2-} \rightleftharpoons H^+ + PO_4^{3-} \quad (4.3)$$

All three protons can be successively lost to yield $H_2PO_4^-$ (4.1) followed by HPO_4^{2-} (4.2), and finally PO_4^{3-} (4.3). A triprotic acid reacts more intensely with the materials than diprotic sulfuric acid or monoprotic nitric acid. The reactions result in higher micropore volume (more porous carbon surface), higher specific surface area and higher specific volume.

The specific surface area of the samples after exfoliating by H_3PO_4 acid are higher than H_2SO_4 acid and HNO3 acid because the bond length of H_3PO_4 is longer than those of H_2SO_4 and HNO_3 (Fig. 4.13). This leads to the breaking of van der Waals bonds more effectively and allowing more PO_4^{3-} anions move to be inserted into bilayer of carbon. Due to the much larger radius of ions, the interlayer distance of graphite is significantly larger and the surface area is higher [110]. Moreover, the microstructure of peanut shell contains

DOI: 10.14750/ME.2021.008

higher amount of micropore than nettle stem. Consequently, the BET surface area of peanut shell is higher than that of nettle stem.

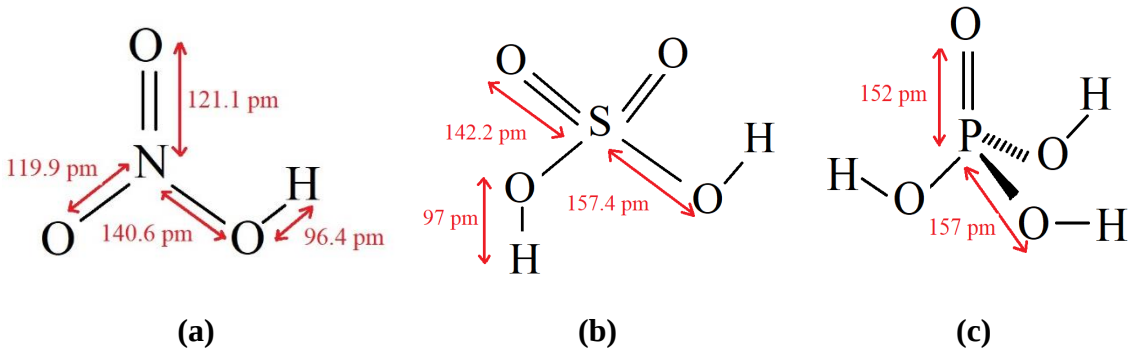

(a) **(b)** **(c)**

Figure 4.13 Molecular chemical structure of (a) Nitric acid, (b) Sulfuric acid, and (c) Phosphoric acid.

4.2 Effect of organic components on carbon properties

The nettle and peanut shell are mainly composed of cellulose, lignin and hemicellulose (nettle stem: 49.8, 11.9 and 15.3 wt.% /peanut shell: 42.4, 27.2 and 8.4 wt.%, respectively). The cell wall in the fibre is inhomogeneous, layered and mainly composed of cellulose, lignin and hemicellulose.

Table 4.1 Chemical composition of raw materials (CHNS analyser).

Dried materials	**Elemental analysis by CHNS analyser (wt.%)**				
	C	**H**	**N**	**S**	**Others**
Nettle stem	44.86	5.98	0.91	<0.01	48.25
Peanut shell	47.34	5.95	1.62	<0.01	45.09

The chemical composition (Table 4.1) analysis shows the presence of carbon lower than 50 wt.% for dried materials (others can see in EDS results, Appendix 10.2). Due to its higher cellulose and carbon content, nettle stem and peanut shell were used to prepare carbon nanostructure. Its higher carbon content can further be increased by activation and exfoliation processes (Table 4.2).

DOI: 10.14750/ME.2021.008

Table 4.2 Chemical composition of carbon nanosheets prepared from nettle stem and peanut shell (CHNS analyser).

	Samples		**Elemental analysis by CHNS analyser (wt.%)**				
	Activation	**Exfoliation**	**C**	**H**	**N**	**S**	**Others**
Nettle stem	KOH	HNO_3	70.70	1.09	0.89	<0.01	27.32
	NaOH	HNO_3	76.48	0.88	1.15	<0.01	21.49
	KOH	H_2SO_4	71.52	0.89	0.61	0.18	26.80
	NaOH	H_2SO_4	79.21	0.64	0.61	0.13	19.41
	KOH	H_3PO_4	71.99	0.70	0.72	<0.01	26.59
	NaOH	H_3PO_4	78.90	0.91	1.00	0.03	19.16
Peanut shell	KOH	HNO_3	69.74	0.67	0.91	<0.01	28.68
	NaOH	HNO_3	77.16	0.78	1.13	<0.01	20.93
	KOH	H_2SO_4	72.19	0.81	0.74	0.21	26.05
	NaOH	H_2SO_4	79.45	0.81	0.75	0.08	18.91
	KOH	H_3PO_4	74.31	0.49	0.76	<0.01	24.44
	NaOH	H_3PO_4	79.75	0.94	0.99	<0.01	18.32

The chemical composition of nettle stem carbon nanosheets (NSCNs) after exfoliating with different acids is slightly different. Besides the high amount of carbon (more than 70 wt.% from CHNS analyser), only some elements remained in a small amount. The chemical composition of peanut shell carbon nanosheets (PSCNs) after exfoliating with different acids is similar to NSCNs samples.

Dried nettle stem and peanut shell have 11.9 and 27.2 wt.% lignin, 44.9 and 47.3 wt.% carbon content, respectively. After exfoliation, the carbon was found in the range of 70-80 wt.% (CHNS analyser). In the case of KOH activation, NSCNs and PSCNs have a higher carbon yield than dried samples up to 57-60 % and 47-57 %, respectively. In the case of NaOH activation, NSCNs and PSCNs have a higher carbon yield than dried samples up to 70-77 % and 63-68 %, respectively.

DOI: 10.14750/ME.2021.008

Dried nettle stem has higher wt.% of cellulose and hemicellulose than peanut shell (by 17.5 and 82.1 %, respectively) and has higher wt.% of carbon content after exfoliation. The carbon content of NSCNs and PSCNs is up to > 70% and reach in the range of 80% for NaOH activation.

The difference in cellulose, lignin, and hemicellulose content affects carbon yields after activation and exfoliation processes. The activation and exfoliation of carbon have a greater impact on carbon yields than the organic composition.

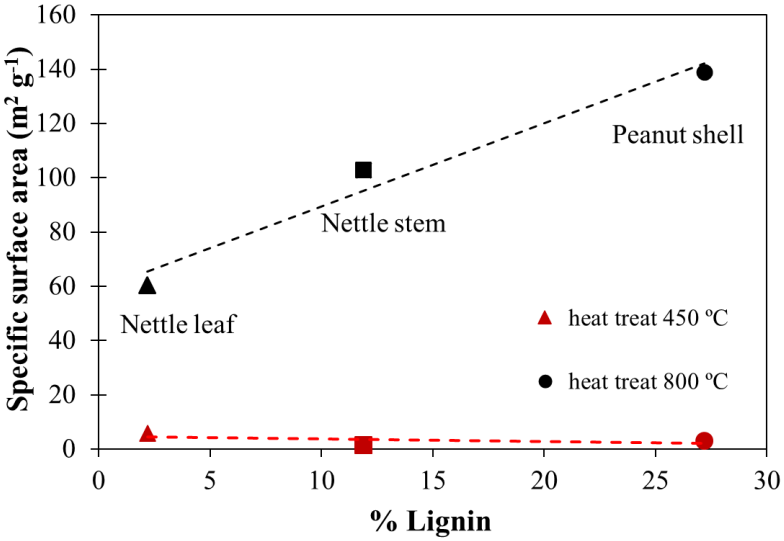

Figure 4.14 Relationship between specific surface area after heat treating (without chemical treatment) as a function of weight percent lignin from different materials.

Plotting the specific surface area after heat treating against the weight percentage of lignin from different materials show a linear correlation (see Fig. 4.14). The specific surface area of carbon after heat treating at high temperature (800 ºC) is higher than at low temperature (450 ºC). It was found that the highest weight percentage of lignin (from peanut shell) resulted the surface area increasing from 3 to 139 m^2 g^{-1} compared to the thermal treatment at 450 ºC. Material containing the mixture of cellulose, hemicellulose, and lignin can be a precursor to produce a three-dimensional porous structure (micropores, mesopores, and mesopores) when lignin has less than 50% [74].

At different raw materials, lignin to cellulose ratio has a linear relationship with the surface area of carbon after potassium hydroxide activating and phosphoric acid exfoliating (Fig. 4.15). The experimental results indicated that the appropriate ratio of lignin and cellulose (lignin/(cellulose+lignin) ratios: nettle leaf, nettle stem and peanut shell is 0.1, 0.2

DOI: 10.14750/ME.2021.008

and 0.4, respectively) induced the activated carbon to develop a microporous and mesoporous structure. After thermal and chemical treatment processes, the specific surface area of carbon is higher than 500 m^2 g^{-1}.

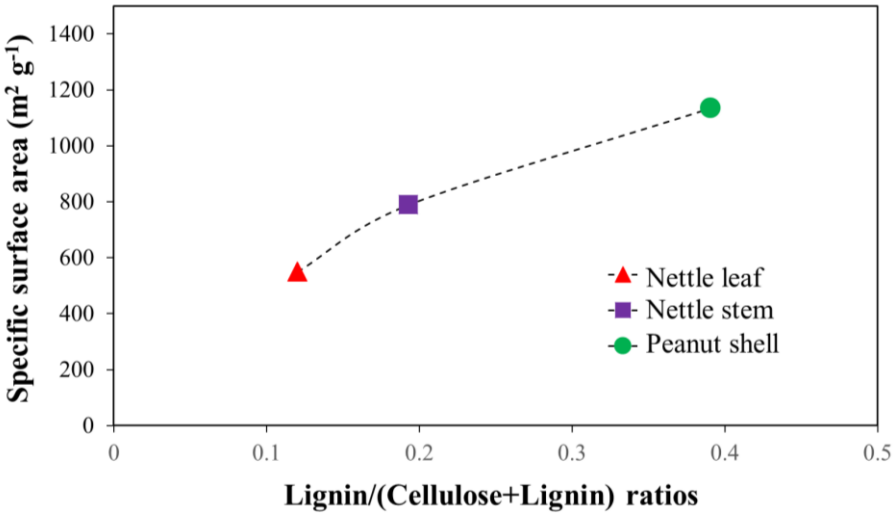

Figure 4.15 Specific surface area as function of lignin/cellulose ratios of KOH activated/H_3PO_4 exfoliated samples.

4.3 Effect of chemical activation and exfoliation to the surface properties

During activation, KOH or NaOH can penetrate the pores of the carbonized material. Interlayered KOH or NaOH residue can react with the exfoliation acids (HNO_3, H_2SO_4, and H_3PO_4); thus, some chemical compounds, such as KNO_3, K_2SO_4, K_3PO_4, $NaNO_3$, Na_2SO_4, and Na_3PO_4 are possible to form (Table 4.3). Based on their thermochemical properties, the formation of K_3PO_4 is the most likely as it has the most negative $\Delta_f G$.

Table 4.3 Thermochemical properties and molar volume of compounds at 25 °C.

Compounds	**$\Delta_f G$ (kJ mol^{-1})** [111]	**$\Delta_f H$ (kJ mol^{-1})** [111]	**$\Delta_f S$ (J $mol^{-1}\cdot K^{-1}$)** [111]	**Molar Volume (cm^3 mol^{-1})**
KNO_3	-394.70	-494.63	-335.16	47.94
K_2SO_4	-1,319.67	-1,437.79	-396.17	65.51
K_3PO_4	-1,876.38	-2,005.70	-433.72	82.79
$NaNO_3$	-366.80	-467.70	-338.43	37.61
Na_2SO_4	-1,270.02	-1,387.90	-395.39	53.40
Na_3PO_4	-1,788.25	-1,916.90	-431.50	101.20

DOI: 10.14750/ME.2021.008

The molar volume of KNO_3, K_2SO_4, and K_3PO_4 is 47.9, 65.5, and 82.8 cm^3mol^{-1}. The molar volume of $NaNO_3$, Na_2SO_4, and Na_3PO_4 is 37.6, 53.4, and 101.2 cm^3mol^{-1}, respectively. These compounds cause tension in the pores of the activated carbon. K_3PO_4 has a 26.4-72.7% higher molar volume than K_2SO_4 or KNO_3, resulting in the carbon nanosheets with the highest specific surface area. But in the case of NaOH, it is different. The specific surface area of carbon nanosheet after NaOH activating and exfoliating is lower.

The changes in surface properties (including the specific surface area, micropores volume, adsorption and desorption, the average pore diameter) were investigated using the BET nitrogen adsorption result. Based on the adsorption isotherms, porous materials are also defined in terms of their adsorption properties. According to the alkaline hydroxide and exfoliating agent, the identification of the activated carbon nanosheets is given in Table 4.4-4.5.

Table 4.4 BET surface properties of nettle stem carbon nanosheets (NSCNs).

Samples		Specific surface area (m^2 g^{-1})	Micropore volume (cm^3 g^{-1})	Adsorption average pore diameter (nm)	Desorption average pore diameter (nm)
Activation	**Exfoliation**				
Dried nettle stem		0.17	0.0001	15.11	27.78
KOH	HNO_3	106	0.04	2.63	2.89
NaOH	HNO_3	72	0.02	2.31	2.44
KOH	H_2SO_4	705	0.29	1.92	1.93
NaOH	H_2SO_4	220	0.07	2.08	2.13
KOH	H_3PO_4	789	0.33	2.68	1.81
NaOH	H_3PO_4	3	0.001	6.80	9.10

For activators, molar mass and solubility in water are 56.1 g mol^{-1}, 121 g 100 ml^{-1} (25 ºC) for KOH, and 39.9 g mol^{-1}, 100 g 100 ml^{-1} (25 ºC) for NaOH, respectively. The wettability angle (θ) of KOH and NaOH on the graphite surface is 81.85º and 67.40º, respectively. During the activation process, KOH (having higher molar mass and solubility) is dissolved easily in water. It can react and penetrate to carbon and increase the specific

DOI: 10.14750/ME.2021.008

surface area of carbon better than NaOH. Similarly, the atomic and ionic radius of potassium (0.231 nm and 0.133 nm, respectively) are larger than that of sodium (0.186 nm and 0.095 nm, respectively). They can penetrate between the layers of carbon and increase the porosity or surface area of materials. The significant increase in potassium penetration compared to sodium is due to the inserting ion's size, which in turn caused effective porosity in material [112].

Table 4.5 BET surface properties of peanut shell carbon nanosheets (PSCNs).

Samples		Specific surface area (m^2 g^{-1})	Micropore volume (cm^3 g^{-1})	Adsorption average pore diameter (nm)	Desorption average pore diameter (nm)
Activation	**Exfoliation**				
Dried peanut shell		0.29	0.0001	7.70	21.39
KOH	HNO_3	468	0.15	1.93	1.95
NaOH	HNO_3	266	0.07	2.17	2.01
KOH	H_2SO_4	1,104	0.37	2.27	2.29
NaOH	H_2SO_4	395	0.11	2.11	2.13
KOH	H_3PO_4	1,135	0.39	2.46	2.52
NaOH	H_3PO_4	420	0.12	2.11	2.19

4.3.1 Surface properties of nettle stem

Nettle stem activated by KOH shows a higher specific surface area than carbonized or NaOH activated nettle stem. The adsorption isotherm shape can provide qualitative information on the adsorption process and the extent of the surface area available to the adsorbate. The adsorption isotherms of NSCNs after chemical activation and exfoliation process in Fig. 4.16 show that all isotherms of all NSCNs belong to type I according to the IUPAC classification.

As for KOH activation (Fig. 4.16 a), the carbon products contained mostly micropores (type I (a) isotherm). However, in the case of NaOH activation, the carbon products revealed wider micropores with a contribution of narrow mesopores (type I (b), Fig. 4.16 b). The dried nettle stem shows nonporous and macroporous structure (type III). The isotherms of NSCNs activated by NaOH and exfoliated by H_3PO_4 revealed types II,

DOI: 10.14750/ME.2021.008

which can be described with a nonporous or macroporous structure related to lower micropore volume and higher average adsorption and desorption pore diameter.

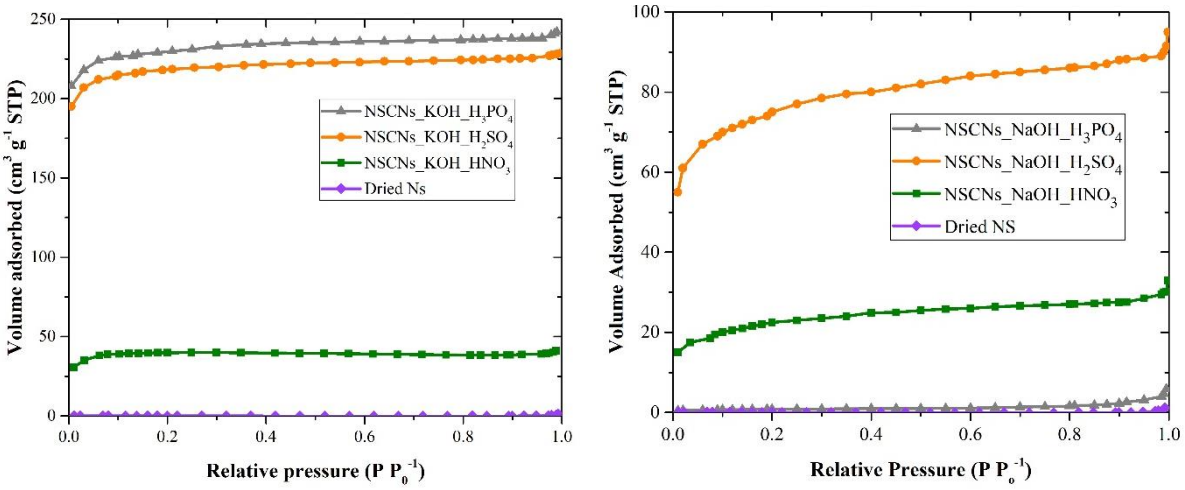

(a) **(b)**

Figure 4.16 Nitrogen adsorption isotherms of nettle stem (a) KOH activation and (b) NaOH activation.

The specific surface area of NSCNs activated by NaOH after exfoliating by H_2SO_4 is smaller than that of NSCNs activated by KOH (Table 4.4). The micropore volume is lower in the NaOH activated samples than in the KOH activated samples, but the average adsorption and desorption pore diameter is higher in the case of NaOH activated samples compared with other samples.

4.3.2 Surface properties of peanut shell

For peanut shell samples, the adsorption isotherm of dried peanut shell, according to the IUPAC classification, shows nonporous and macroporous material presented by type III isotherm (Fig. 4.17). The adsorption isotherms of peanut shell after activation with KOH or NaOH are quite similar to type I isotherm, which means that the carbon nanosheets contained micropores. For KOH activation (Fig. 4.17 a), the carbon products had micropores (type I (a) isotherm) and narrow mesopores (type I (b)). Carbon products of NaOH activation (Fig. 4.17 b) revealed wider micropores with only a small contribution of narrow mesopores (type I (b) isotherm). However, when considering the isotherm information, it can be seen that it is quite similar, but the volume adsorbed of KOH activated samples are higher than

DOI: 10.14750/ME.2021.008

NaOH activated samples (Table 4.5) because KOH affected the activated structure of materials more than NaOH similar to Raymundo-Pinero et al. [60].

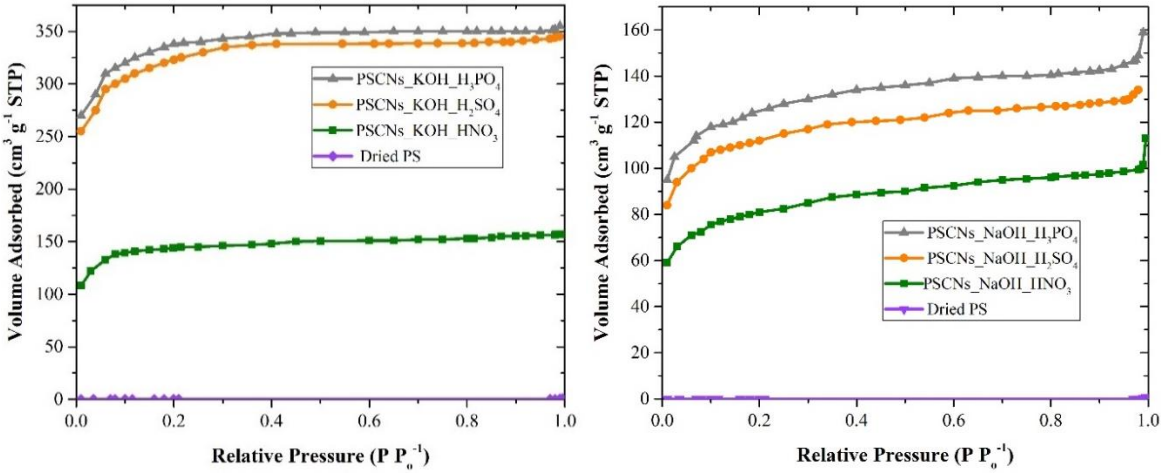

(a) **(b)**

Figure 4.17 Nitrogen adsorption isotherms of peanut shell KOH activation and (b) NaOH activation.

The isotherms from nitrogen adsorption presented porous structure (micropore/ IUPAC, Type I isotherm) in the carbon materials, which can be changed by chemical activation and exfoliation. Without chemical activation or exfoliation, the dried samples (nettle stem and peanut shell) show the mesoporous structure with a low specific surface area. The quantitative property of carbon nanosheets was confirmed by BET. The investigations assure the formation of carbon nanosheets with a higher specific surface area (which can describe the separation ability of carbon layer from this process) and small pore diameter and higher micropore volume. The specific surface area of carbon nanosheets related with micropore volume (Fig. 4.18), the highest specific surface area and micropore volume of NSCNs and PSCNs were found after activating with KOH and exfoliating by phosphoric acid.

DOI: 10.14750/ME.2021.008

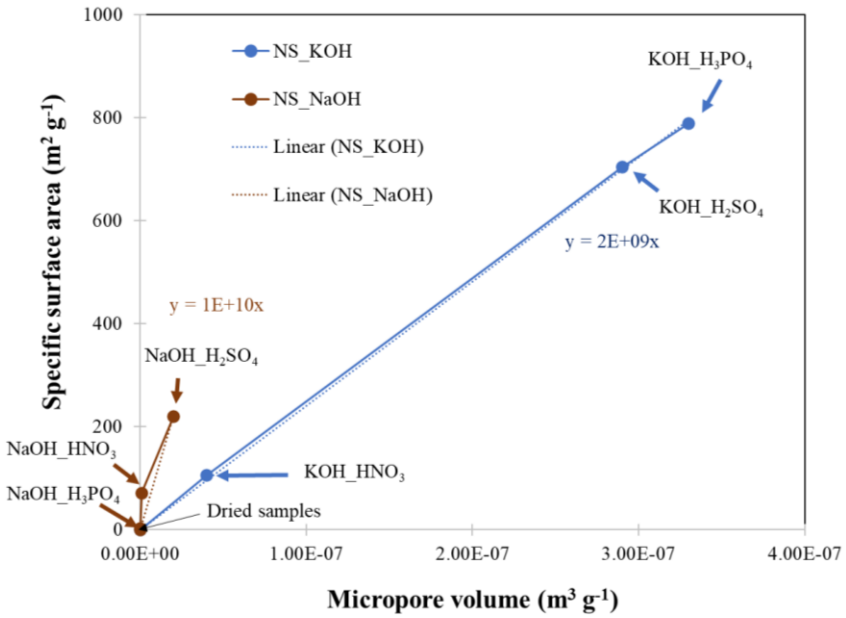

(a)

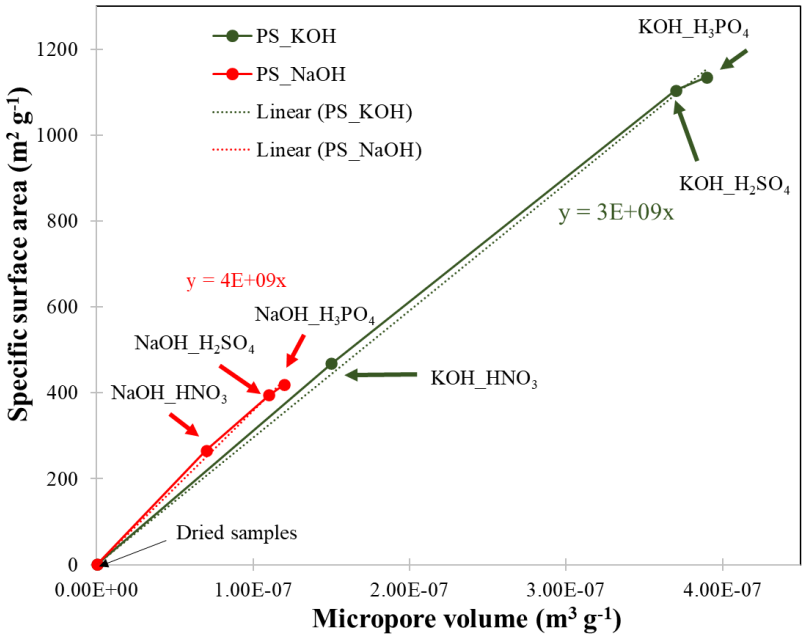

(b)

Figure 4.18 Specific surface area of samples as function of micropore volume of (a) nettle stem and (b) peanut shell.

When lignin was prepared under the same conditions as the nettle stem and peanut shell, it was found that the specific surface area of carbon obtained after exfoliation with phosphoric acid was the highest at 668 m^2 g^{-1}, followed by sulfuric acid at 497 m^2 g^{-1} and nitric acid at 367 m^2 g^{-1}, respectively (Fig. 4.19). The result is the same as for the nettle and peanut shell. After that, I changed the type of exfoliating acid to other diprotic and triprotic

DOI: 10.14750/ME.2021.008

acids (ascorbic acid and boric acid, respectively). The results in Fig. 4.20 show that the specific surface area of carbon (peanut shell) after exfoliating by boric acid is 825 m^2 g^{-1} and 14% higher than as for ascorbic acid. It means that triprotic acid (boric acid) resulted in a higher carbon specific surface area than that of diprotic acid (ascorbic acid).

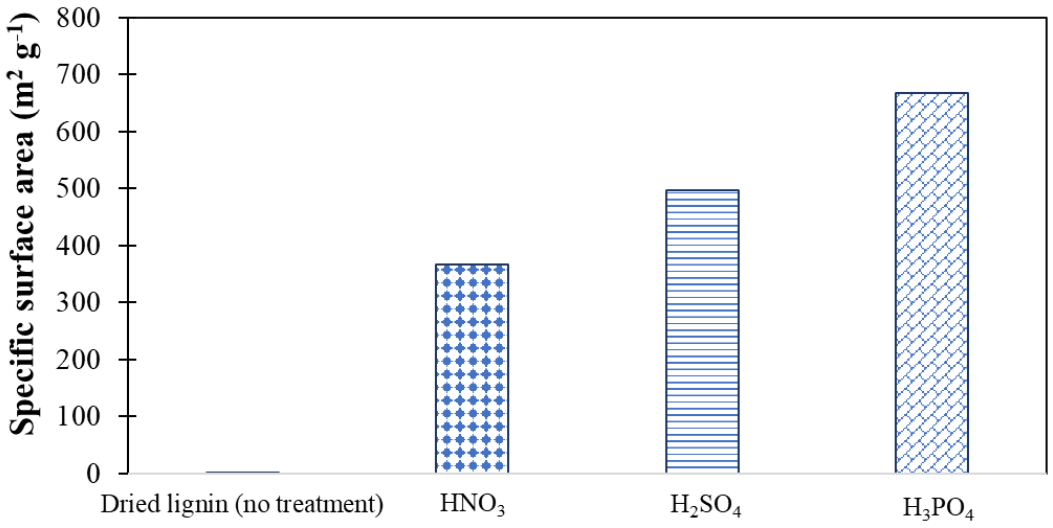

Figure 4.19 Specific surface area of lignin derived carbons as function of different acid exfoliators (using KOH activation).

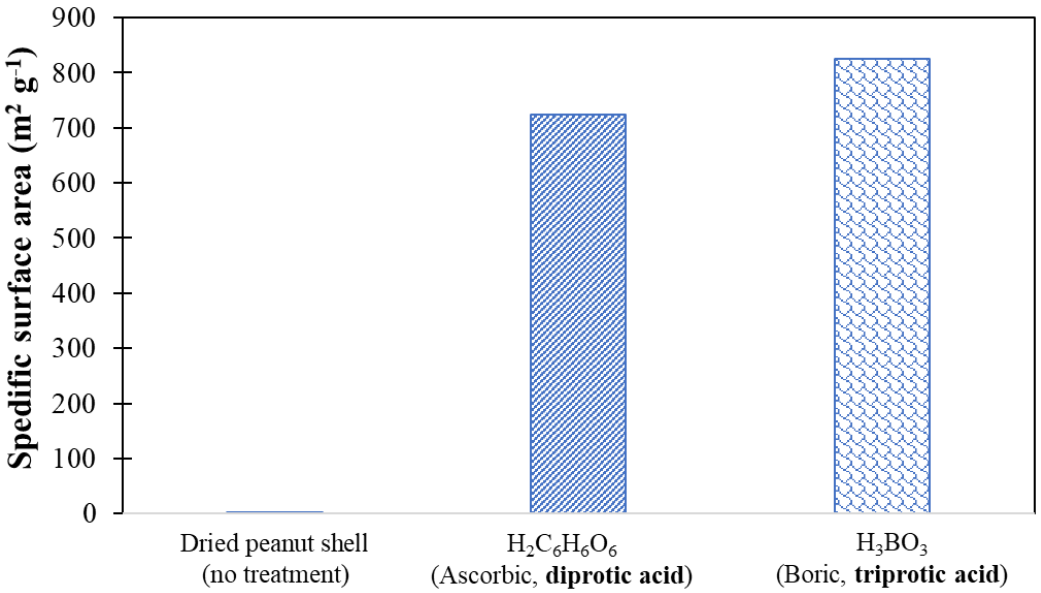

Figure 4.20 Specific surface area of peanut shell derived carbonas function of different acid exfoliators (using KOH activation).

DOI: 10.14750/ME.2021.008

During activation, KOH or NaOH can penetrate into the pores of the carbonized material. Interlayered KOH or NaOH residue can react with the exfoliation acids (HNO_3, H_2SO_4, and H_3PO_4), thus some chemical compounds, such as KNO_3, K_2SO_4, K_3PO_4, $NaNO_3$, Na_2SO_4, and Na_3PO_4 may form. Due to the potassium ions (K^+) are larger than sodium ions (Na^+) by 40%, the specific surface area and micropore volume of carbon nanosheets activated by KOH are higher than those activated by NaOH.

Based on their thermochemical properties (Gibbs free energy of formation, Δ_fG, and molar volume) from the database in HSC Chemistry [111] (Table 4.3), all of these compounds can be formed due to negative Δ_fG. These compounds cause tension in the pores of the activated carbon. As K_3PO_4 has 26.4 or 72.7% higher molar volume than K_2SO_4 or KNO_3, respectively, it resulted in the highest specific surface area, and micropore volume in KOH activated carbon nanosheets both for nettle stem and peanut shell. As for the NaOH activation, Na_3PO_4 has 89.5 or 169.1% higher molar volume than Na_2SO_4 or $NaNO_3$. Thus, it resulted in the highest specific surface area and micropore volume in carbon nanosheets prepared from peanut shell (Fig. 4.21). But in the case of nettle stem, the specific surface area of NSCNs after NaOH activation is the lowest for the Na_3PO_4.

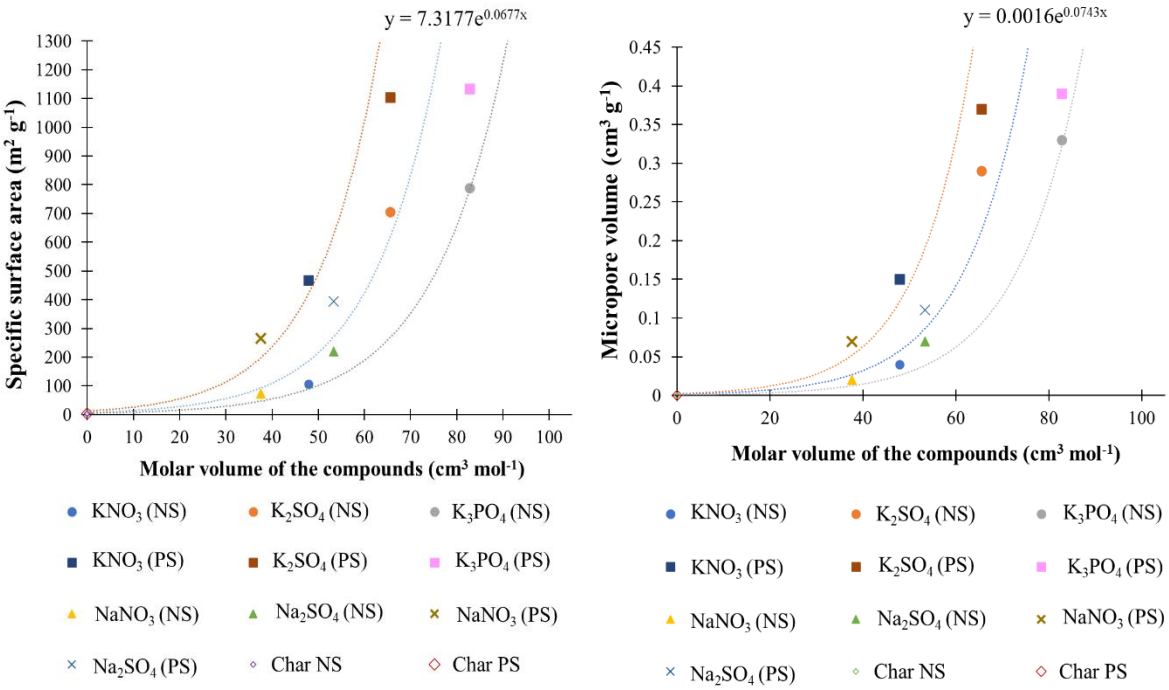

(a) **(b)**

Figure 4.21 Relationship between molar volume of the compounds (formation) and (a) specific surface area, (b) micropore volume of nettle stem derived carbon and peanut shell derived carbon.

DOI: 10.14750/ME.2021.008

4.4 Effect of chemical activation and exfoliation to the electrochemical properties

The electrochemical properties, including specific capacitance, energy density, and power density value of the electrodes are presented in Table 4.6. The specific capacitance of NSCNs and PSCNs is higher than char samples. PSCNs samples have higher specific capacitance than NSCNs due to their higher specific surface area and micropore volume (Table 4.4-4.5). IUPAC classification of carbon nanosheet from nettle stem and peanut shell (Fig. 4.16-4.17) shows mostly micropore structure. Micropores contain bottlenecks that can drastically decrease ion mobility, thus reducing the electrode's power capability [113]. Surface area and porosity are important factors for higher capacitance. As for materials having low porosity, electrolyte and electrode are in minimal contact due to which less charge is stored on the electrode surface; hence low capacitance was observed [114].

The correlation in specific surface area and specific capacitance for some of the samples is too low. The reason could be the stacking of carbon black on the CNs surface (electrode material), which decreases the specific surface area and capacitance characteristics [115], or the agglomeration or re-stacking of CNs resulting reduced specific capacitance or specific surface area [113].

It can be seen that the specific surface area and specific capacitance of NSCNs activated by KOH, exfoliated by HNO_3, H_2SO_4, or H_3PO_4 increases with micropore volume. However, the existence of a too narrow pore size distribution makes the electrolyte's entry into the pores difficult. The non-accessible pores do not contribute to the total double-layer capacitance of the material [116]. High specific capacitance with the high specific surface area was found in samples activated by NaOH and exfoliated by H_2SO_4, both for nettle stem and peanut shell. The highest specific capacitance was found in PSCNs activated by NaOH and exfoliated by H_2SO_4 (122.26 F g^{-1}).

DOI: 10.14750/ME.2021.008

Table 4.6 Electrochemical properties obtained by cyclic voltammetry at scan rate 5 mV s^{-1}.

Samples			Specific surface area (m^2 g^{-1})	Specific capacitance (F g^{-1})	Surface-capacitance (F m^{-2})	Energy density (Wh kg^{-1})	Surface-energy density (Wh m^{-2})	Power density (kW kg^{-1})	Surface-power density (kW m^{-2})
	Activation	Exfoliation							
Nettle stem	Char NS*		1.6	0.15	0.094	0.01	6.3E-06	30.6	0.01913
	KOH	HNO_3	106	1.71	0.016	0.06	5.7E-07	26.7	0.00025
		H_2SO_4	705	9.34	0.013	0.32	4.5E-07	20.9	0.00003
		H_3PO_4	789	27.3	0.035	0.95	1.2E-06	24.8	0.00003
	NaOH	HNO_3	72	0.61	0.008	0.02	2.8E-07	26.4	0.00037
		H_2SO_4	220	7.86	0.036	0.27	1.2E-06	24.7	0.00011
		H_3PO_4	3	0.21	0.070	0.01	3.3E-06	37.9	0.01263
Peanut shell	Char PS*		3	0.14	0.047	0.01	3.3E-06	80.6	0.02687
	KOH	HNO_3	468	115.57	0.247	4.01	8.6E-06	84.2	0.00018
		H_2SO_4	1,104	44.27	0.040	1.54	1.4E-06	18.3	0.00002
		H_3PO_4	1,135	1.73	0.002	0.06	5.3E-08	31.9	0.00003
	NaOH	HNO_3	266	23.62	0.089	0.95	3.6E-06	24.4	0.00009
		H_2SO_4	395	122.26	0.310	4.25	1.1E-05	27.1	0.00007
		H_3PO_4	420	15.57	0.037	0.81	1.9E-06	24.9	0.00006

* Samples were heat treated at 450 ºC (without activation and exfoliation)

Based on the literature and my experimental results, I found a correlation between the composition (lignin/(cellulose+lignin) ratio) of the raw material and the surface capacitance of the carbon nanosheets prepared from the raw materials (Fig. 4.22). The correlation can be described with the following equation:

$$CA=0.33\varphi \quad (4.4)$$

where CA is the surface capacitance (F m^{-2}), φ is the lignin/(cellulose+lignin) ratio.

DOI: 10.14750/ME.2021.008

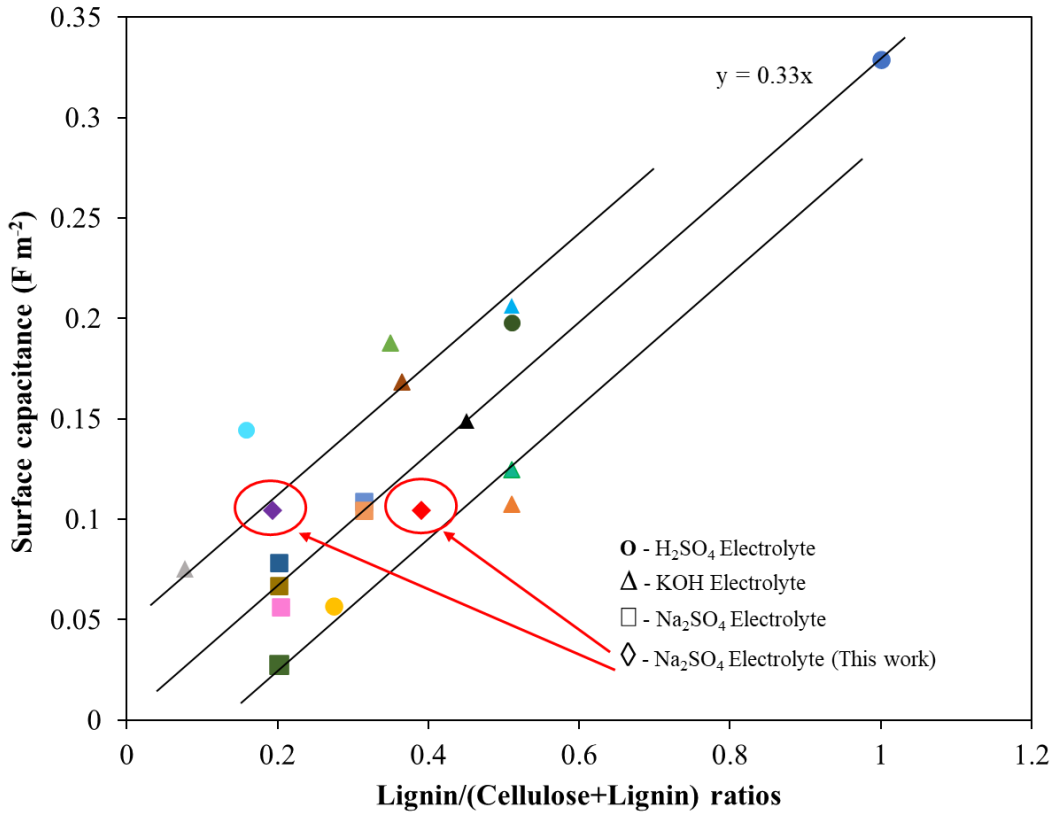

Figure 4.22 Surface-capacitance as function of lignin/(cellulose+lignin) ratios of carbon from difference natural samples (with difference electrolytes).

●	Lignin [117]	▲	Cherry stone (4) [120]
●	Coconut kernel [76, 118]	■	Banana fiber (1) [125-126]
●	Pistachio shell [76, 119]	■	Banana fiber (2) [125-126]
●	Cherry stone (1) [120-121]	■	Banana fiber (3) [125-126]
▲	Coffee shell [76, 122]	■	Bamboo Shoot (1) [127-128]
▲	Corn grains [76, 123]	■	Bamboo Shoot (2) [127-128]
▲	Rice husk [76, 124]	■	Durian husk [129-130]
▲	Coconut shell [76, 119]	◆	**Nettle stem (This work)**
▲	Cherry stone (2) [120]	◆	**Peanut shell (Thiswork)**
▲	Cherry stone (3) [120]		

DOI: 10.14750/ME.2021.008

4.5 Electrochemical performance of the carbon nanosheets electrode

Cyclic voltammetry (CV) measurements at 5, 20, and 100 mV s^{-1} in the potential range -0.2 to 0.8 V were used to calculate carbons' specific capacitance. CV curves show a quasi-rectangular shape at increased scan rates (Fig. 4.23 and Fig. 4.24), indicating that the CNs can be used in energy storage applications [86]. The CV shape for exfoliated CNs is more rectangular, revealing a better charge propagation than char samples. The quasi-rectangle shapes are maintained even at a high scan rate of 100 mV s^{-1}, which is suitable for a typical, stable double-layer capacitor quick and efficient in charge transfer. They also have excellent capacitive behaviour [131].

The galvanostatic charge and discharge (GCD) curves (Fig. 4.25) of the samples at a current density of 0.05 A g^{-1} in the voltage range of -0.2 to 0.8 V show typical triangular shapes. The GCD curves are imperfectly symmetrical; they are slightly distorted due to the pseudocapacitive behaviour [132], which is consistent with the CV graphs.

The GCD curves show that PSCNs activated by NaOH and exfoliated by H_3PO_4 have the longest charge and discharge cycles (1,033 s), which implies the samples' best electrochemical performance. The longest charge and discharge cycles of NSCNs activated by KOH were found for H_3PO_4 exfoliator (27.3 s).

DOI: 10.14750/ME.2021.008

Activator / Exfoliator	KOH	NaOH
	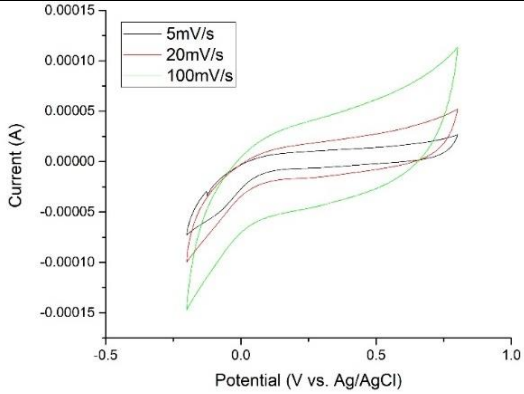 NS char (no activation and exfoliation)	
HNO_3	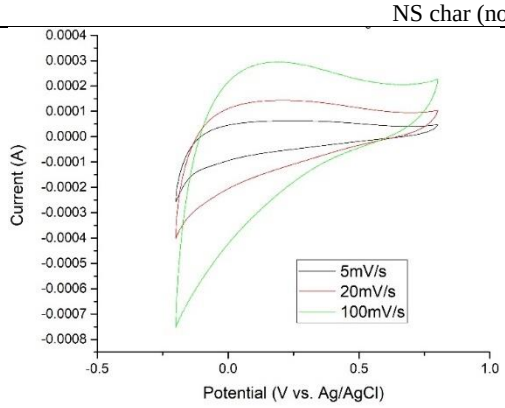	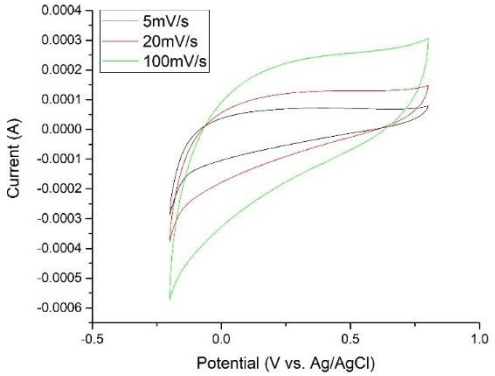
H_2SO_4	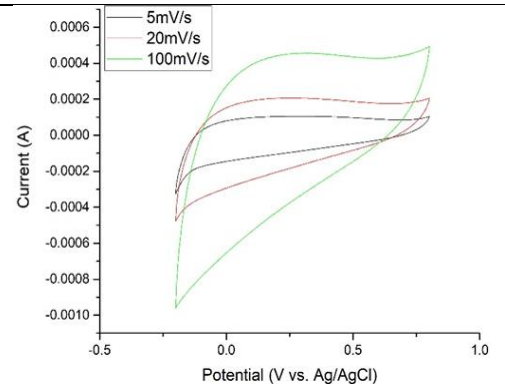	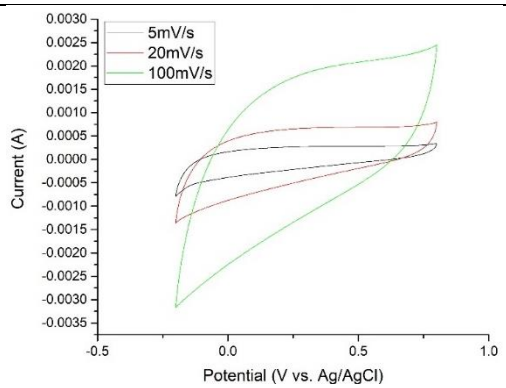
H_3PO_4	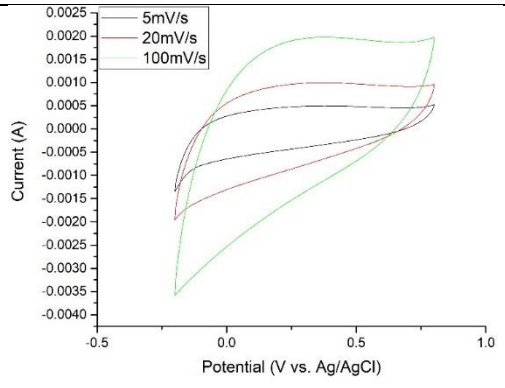	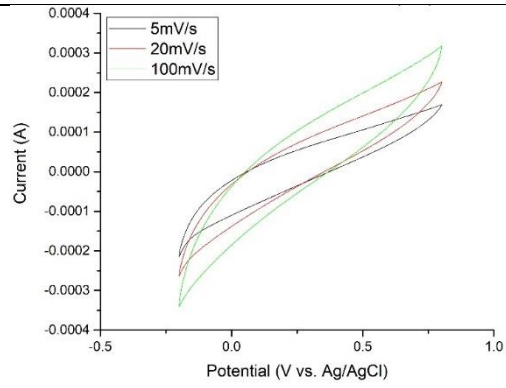

Figure 4.23 Cyclic voltammetry (CV) of nettle stem carbon nanosheets, (a) char NS, (b) exfoliated by HNO_3, (c) exfoliated by H_2SO_4 and (d) exfoliated by H_3PO_4.

DOI: 10.14750/ME.2021.008

Activator / Exfoliator	KOH	NaOH
	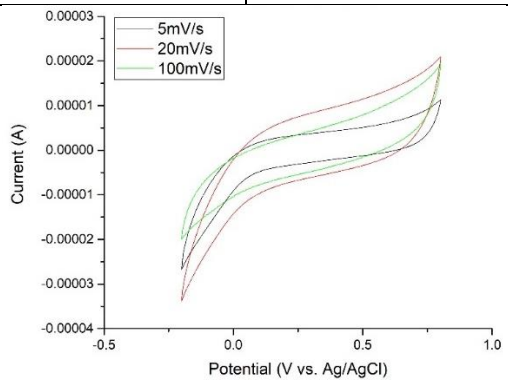 PS char (no activation and exfoliation)	
HNO_3	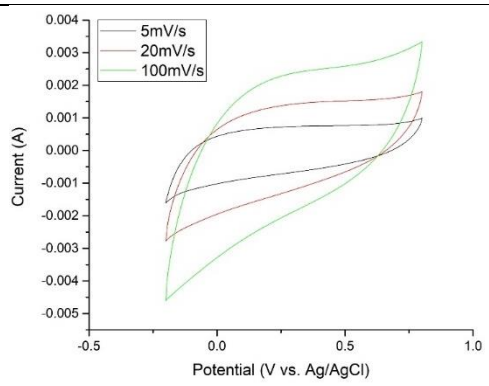	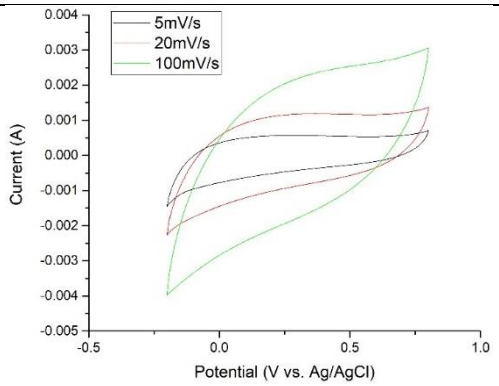
H_2SO_4	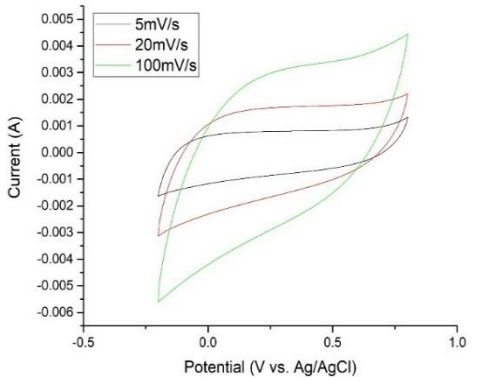	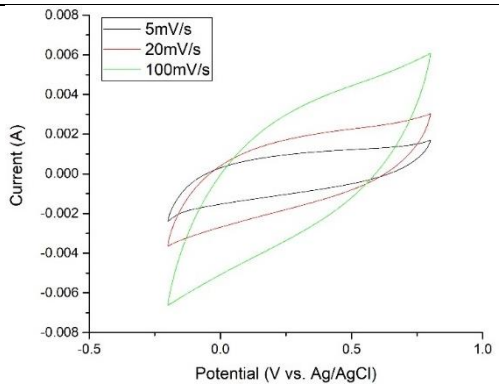
H_3PO_4	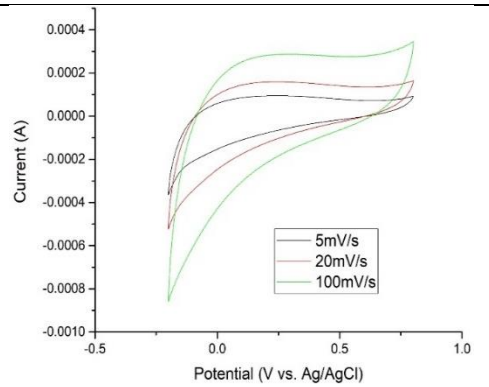	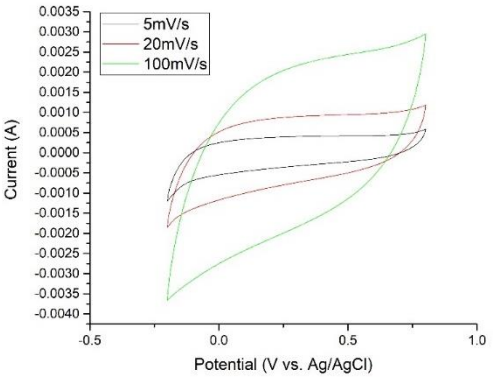

Figure 4.24 Cyclic voltammetry (CV) of peanut shell carbon nanosheets, (a) char PS, (b) exfoliated by HNO_3, (c) exfoliated by H_2SO_4 and (d) exfoliated by H_3PO_4.

DOI: 10.14750/ME.2021.008

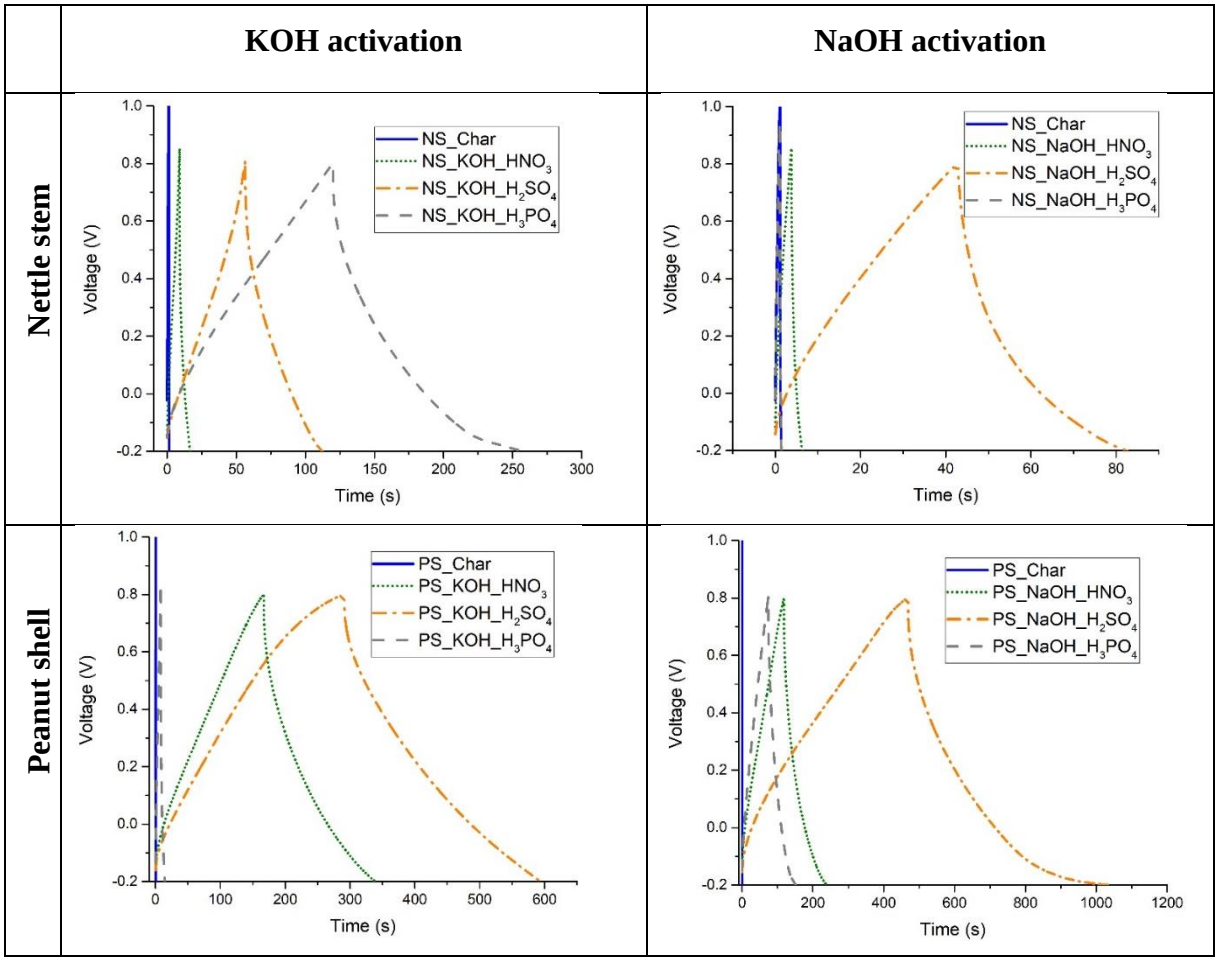

Figure 4.25 Galvanostatic charge and discharge of samples at a current density of 0.05 A g^{-1}.

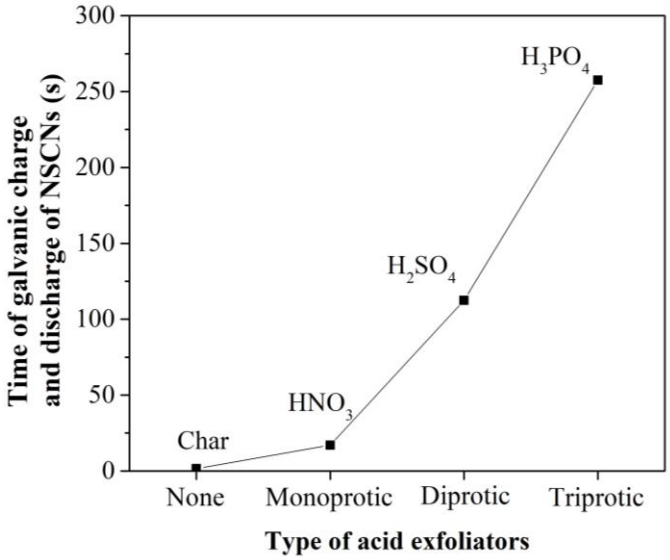

Figure 4.26 The time of galvanic charge and discharge of nettle stem derived carbons as a function of different types of acid exfoliators (at a current density of 0.05 A g^{-1}).

DOI: 10.14750/ME.2021.008

For nettle stem activated by KOH, the increase of dissociable protons (polyprotic acid) affects the longer charge and discharge cycle time, resulting in the same effect as the specific surface area. The type of acid exfoliator affects the charge and discharge cycles. Cycle time for triprotic (H_3PO_4), diprotic (H_2SO_4), and monoprotic (HNO_3) exfoliators were 260, 112, and 17 s, respectively (Fig. 4.26) [133].

The electrochemical impedance spectroscopy (EIS) of CNs samples is presented in Fig. 4.27 [133] with the Nyquist plots of each CNs electrode material in the frequency range between 0.1 Hz to 100 kHz. The straight-line slope is close to 45º in the middle-high frequency and is assumed to diffuse the electrolyte ions in the electrode pores. The steep linear curve in the low-frequency region of CNs is sharp, representing the diffusion-limited charge transfer characteristic close to ideal capacitance performance [134-137]. The equivalent series resistance (ESR) of CNs can be determined from the offsets on the x-axis in the high-frequency region. The ESRs of NSCNs exfoliated by H_3PO_4, H_2SO_4, HNO_3, and char NS were approximately 14.6, 17.8, and 21.3 Ω, respectively, lower than that of char NS (107.0 Ω). The results confirmed NSCNs exfoliated by H_3PO_4 had the best electrochemical performance. This observation agrees with the linear correlation between the peak current and square root of the scan rate in Fig. 4.28. The ESRs of PSCNs exfoliated by H_3PO_4, H_2SO_4, HNO_3, and char PS were approximately 1.3, 0.8, and 1.4 Ω, respectively, lower than that of char PS (2.6 Ω). The small ESRs value proves that the current can easily diffuse through the electrode-electrolyte interface [138].

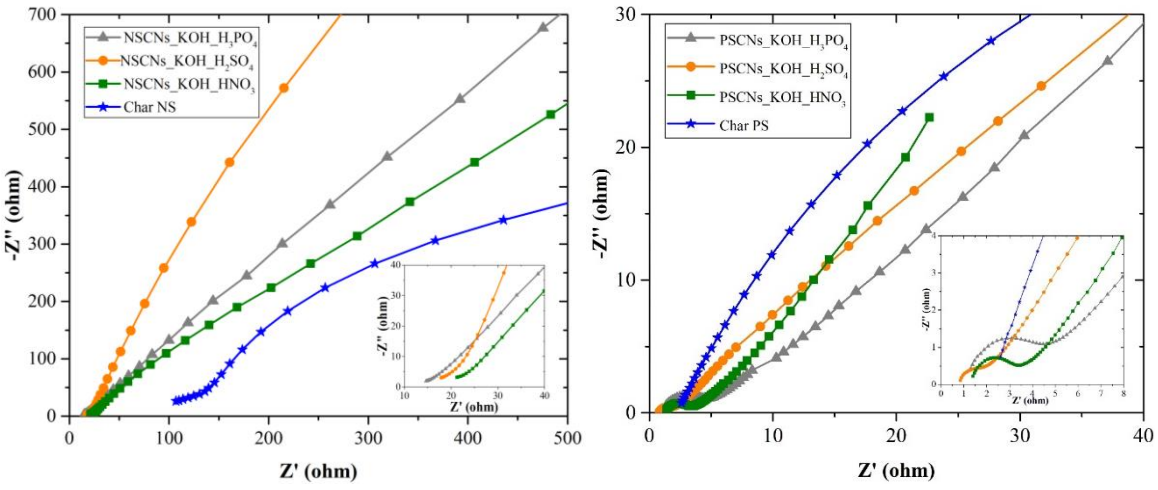

(a) **(b)**

Figure 4.27 Nyquist plots of (a) nettle stem and (b) peanut shell derived carbons at an alternating current amplitude of 5 mV.

DOI: 10.14750/ME.2021.008

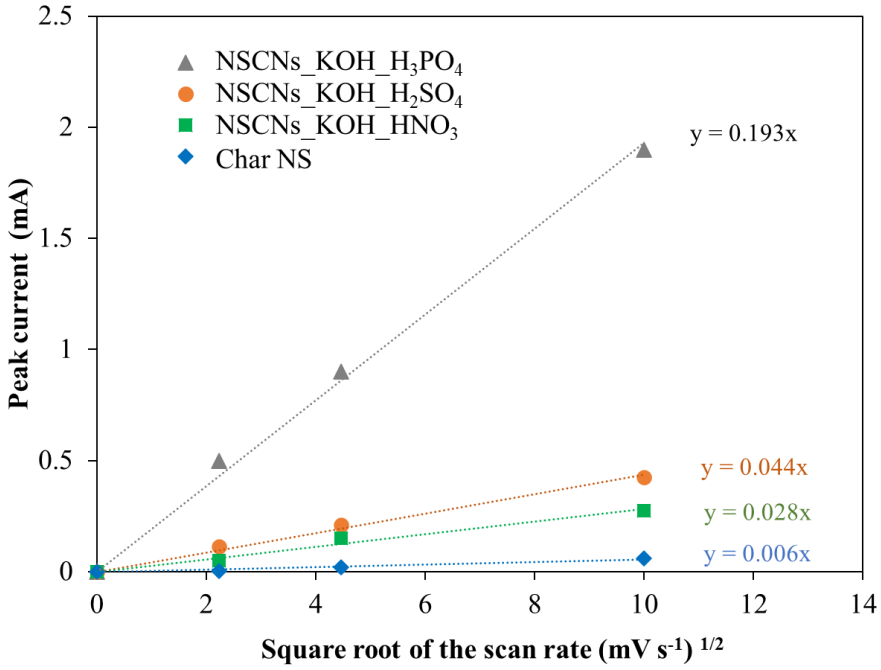

Figure 4.28 Relationship between peak current and the square root of the scan rate of cyclic voltammetry measurement of nettle stem derived carbons (potential range -0.2 to 0.8 V).

The diffusion coefficient in the case of the nettle stem carbon nanosheets (NSCNs), based on the relationship between peak current and the square root of the scan rate of cyclic voltammetry measurement, was identified. The diffusion coefficients were calculated based on the Randles-Sevcik equation (4.5):

$$Ip = (2.69 \times 10^5)\, n^{3/2} A D^{1/2} C \nu^{1/2} \quad (4.5)$$

Where Ip is peak current (A), n is number of electrons involved in the reaction, A is electrode area (cm^2), D is diffusion coefficient ($cm^2\ s^{-1}$), C is the concentration of the electroactive species (mol cm^{-3}) and ν is scan rate (V s^{-1}), respectively. The diffusion coefficient depends on the slope of $Ip \propto \nu^{1/2}$ (Fig. 4.28). The higher diffusion coefficient indicates a better electrode reaction activity due to the faster ionic transportation. The diffusion coefficients obtained by the Randles-Sevcik equation are listed in Table 4.7.

DOI: 10.14750/ME.2021.008

Table 4.7 The diffusion coefficients of samples (at scan rate 100 mV s^{-1}).

Samples/Electrode	Ip (10^{-5} A)	n	A (cm^2)	C (mol cm^{-3})	Ip/$\nu^{1/2}$ (As V^{-1})	D (10^{-8} cm^2 s^{-1})
Char NS	6.1	1	0.79	0.001	0.006	1.37
NSCNs_KOH_HNO_3	27.5	1	0.79	0.001	0.028	6.17
NSCNs_KOH_H_2SO_4	42.5	1	0.79	0.001	0.044	9.53
NSCNs_KOH_H_3PO_4	190	1	0.79	0.001	0.193	42.6

Table 4.8 The capacitive performance of carbon prepared in this work and other typical biomass derived activated carbon reported in literature.

Materials	SSA (m^2 g^{-1})	Specific capacitance (F g^{-1})	Electrolyte	Ref.
Corn straws	3,237	188	$EMIMBF_4$	[139]
Cow dungs	1,984	125	AN	[140]
Coconut shells	154	0.54	H_2SO_4	[141]
Banana fibers	1,097	74	Na_2SO_4	[76]
Nut shells	228	47	Na_2SO_4	[2]
Coconut kernel pulp (Milk free)	1,200	173	Na_2SO_4	[142]
Nettle stem	789	27.3	Na_2SO_4	This work
Peanut shell	395	122.26	Na_2SO_4	This work

A comparison of several supercapacitor electrodes with different precursors are presented in Table 4.8. The specific capacitance depends on the materials and condition of the electrolyte. The abundant availability of nettle stem and peanut shell are the advantages of these samples, so it certainly can be produced at a relatively low cost. This study has successfully demonstrated that nettle stem or peanut shell based carbon can be presented as raw material for a flexible carbon electrode in supercapacitor as an energy storage device.

DOI: 10.14750/ME.2021.008

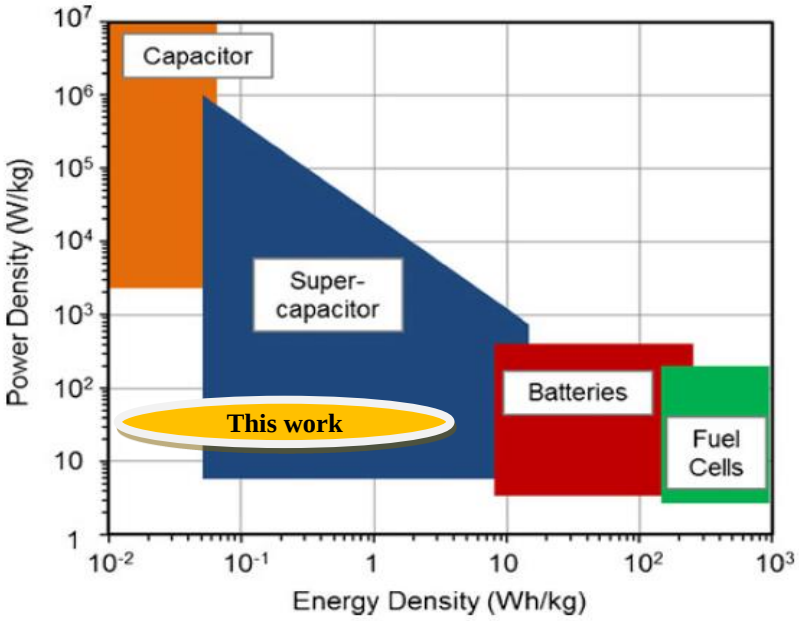

Figure 4.29 Energy density as a function of power density (Ragone plot) for different energy storage and conversion devices [143].

Specific capacitance, which is the intrinsic capacitance of electrode material, is a widely used property to characterize a material. A higher specific capacitance does not necessarily mean that the material will be a high performing supercapacitor electrode. Other factors substantially impact capacitance, such as electrical conductivity (both that of materials and electrode particles), which governs electron and ion transfer into the layer [115]. From the data compiled in Fig. 4.29, it can be seen that carbon from nettle stem and peanut shell in this work can be applied for an energy storage device. The carbons' energy density and power density in this work are in the range of supercapacitor materials at 0.01-4.25 Wh kg^{-1} and 18.3-84.2 W kg^{-1}, respectively.

DOI: 10.14750/ME.2021.008

5 Conclusions

The goal of this research is to systematically study and investigate the effect of different alkaline hydroxides activators and acid exfoliators on the properties of carbon nanosheets, prepared from natural materials. In this work, the carbon nanosheets were studied for capacitor application by using as electrode material for an energy storage device.

- The carbon nanosheets synthesized from nettle stem or peanut shell using KOH or NaOH activation and exfoliation by H_2SO_4 or H_3PO_4 have high specific surface areas, especially peanut shell (activated by KOH and exfoliated by H_3PO_4) having 1,135 $m^2\ g^{-1}$.
- The chemical activation and exfoliation affect the surface property of carbon nanosheets which can be described in terms of quantity of porous carbon. The micropore volume of carbon nanosheets activated by KOH is higher than that of activated by NaOH.
- Pore diameters in the exfoliated NSCNs and exfoliated PSCNs were found to be less than 2.5 nm which belongs to the micropore range (IUPAC, Type I isotherm).
- The process developed is simple and yields a high percentage (up to 70 %) of carbon particles in a nanostructured form.
- The CNs with an electrolyte 1M Na_2SO_4 is a material work as active part of the electrode for an energy storage device. Using this material as an electrode, the measured specific capacitances of NSCNs and PSCNs are higher than char samples (nettle stems and peanut shells without activation and exfoliation). Specific capacitance reached 27.3 F g^{-1} at scan rate of 5 mV s^{-1} for NSCNs activated by KOH and exfoliated by H_3PO_4. PSCNs activated by NaOH and exfoliated by H_2SO_4. had specific capacitance 122.26 F g^{-1} at scan rate of 5 mV s^{-1}.
- Energy density (0.01-4.25 Wh kg^{-1}) and power density (18.3-84.2 W kg^{-1}) of carbons in this work is in the range of supercapacitor materials.

DOI: 10.14750/ME.2021.008

6 Claims/New scientific results

Carbon nanosheets were successfully synthesized from nettle stem or peanut shell with a 5-step method, which consists of the following process: sample preparation (cleaning), pre-carbonization, activation (KOH or NaOH aqueous solution), carbonization, and exfoliation (HNO_3, H_2SO_4, or H_3PO_4). The chemical and thermal activation affects the carbon formation, and the separation of carbon layers. The carbon nanosheets were studied for capacitor application by using as electrode material for supercapacitors.

Claim 1. The structure of carbon nanosheets synthesized from natural materials

Carbon nanosheets were successfully synthesized from nettle stem (NSCNs) and peanut shell (PSCNs) (SEM, Fig. A-B and TEM Fig. C). I established that the layered nanosheet structure is highly porous and becomes thinner toward the edges of the material. In the TEM images, the bright and transparent regions are the ultrathin nanosheet. The less transparent areas reveal the overlapped or folding parts of carbon nanosheets, which further imply the ultrathin structure. These figures are representative for the samples. After the exfoliation process, the carbon nanosheets with the thickness lower than 100 nm were found and the successful exfoliation is confirmed by the increasing the specific surface area.

DOI: 10.14750/ME.2021.008

Exfoliated by	KOH activated	NaOH activated
No exfoliation	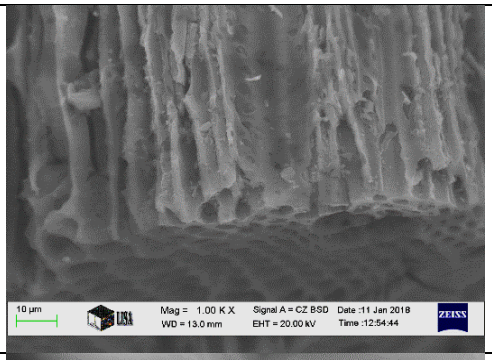	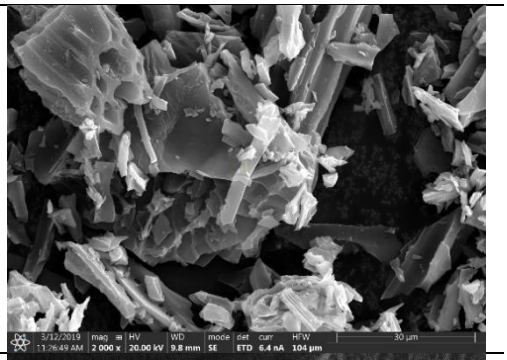
HNO_3	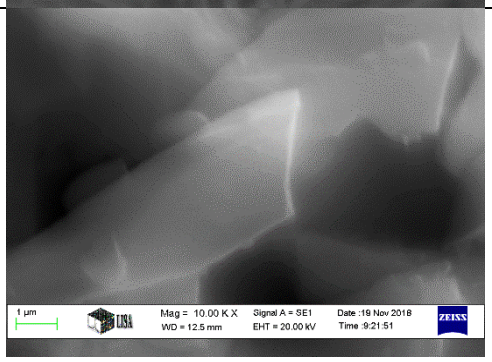	
H_2SO_4	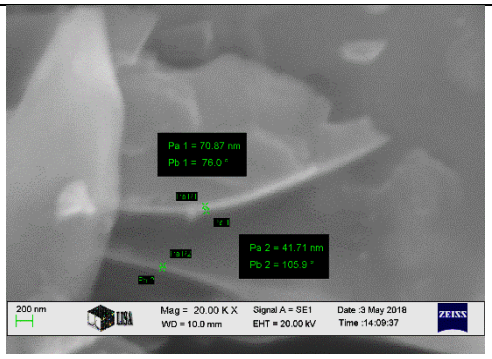	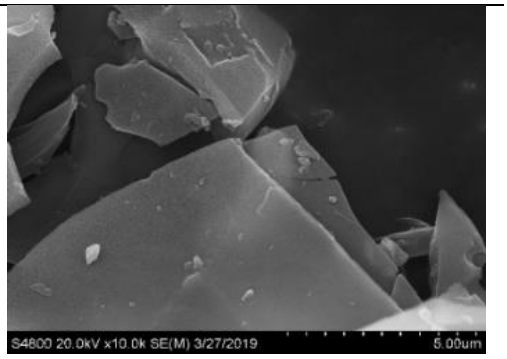
H_3PO_4	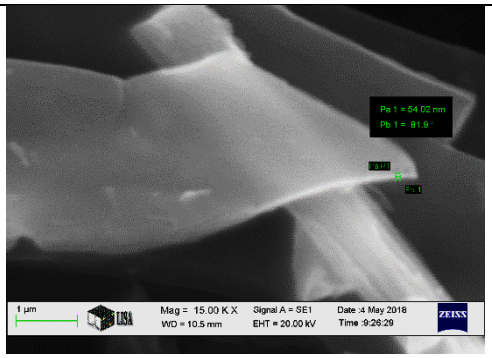	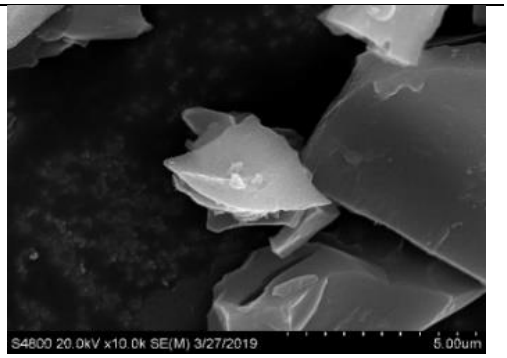

Figure A. SEM micrographs of activated and exfoliated nettle stem carbon nanosheets obtained by different agents.

DOI: 10.14750/ME.2021.008

Exfoliated by	KOH activated	NaOH activated
No exfoliation	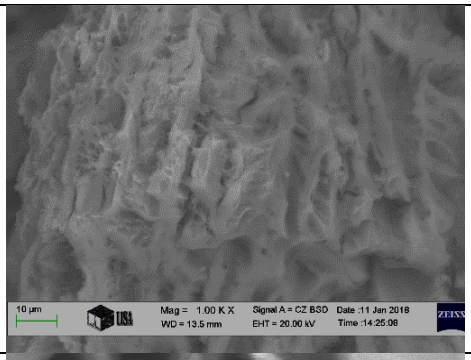	
HNO_3	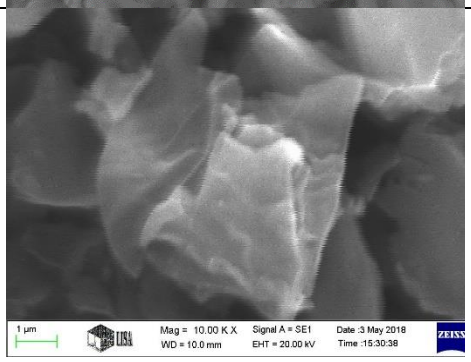	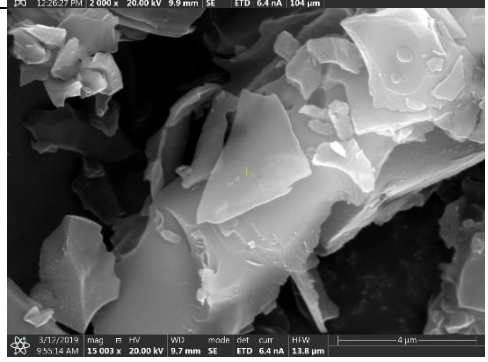
H_2SO_4	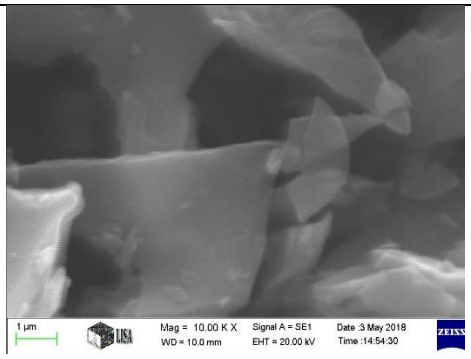	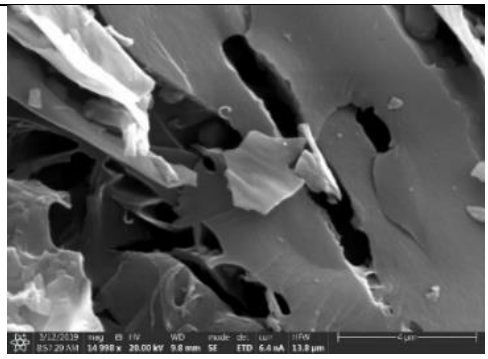
H_3PO_4	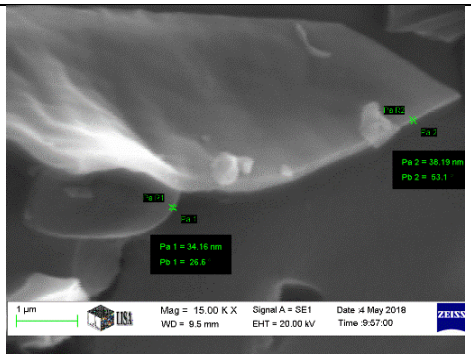	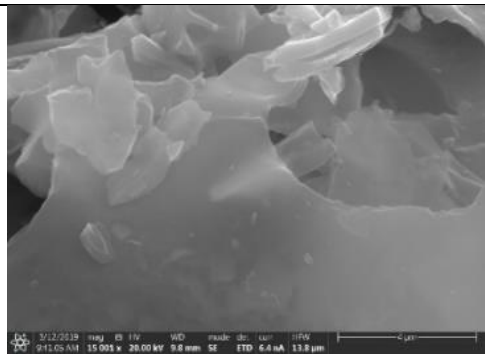

Figure B. SEM micrographs of activated and exfoliated peanut shell carbon nanosheets obtained by different agents.

DOI: 10.14750/ME.2021.008

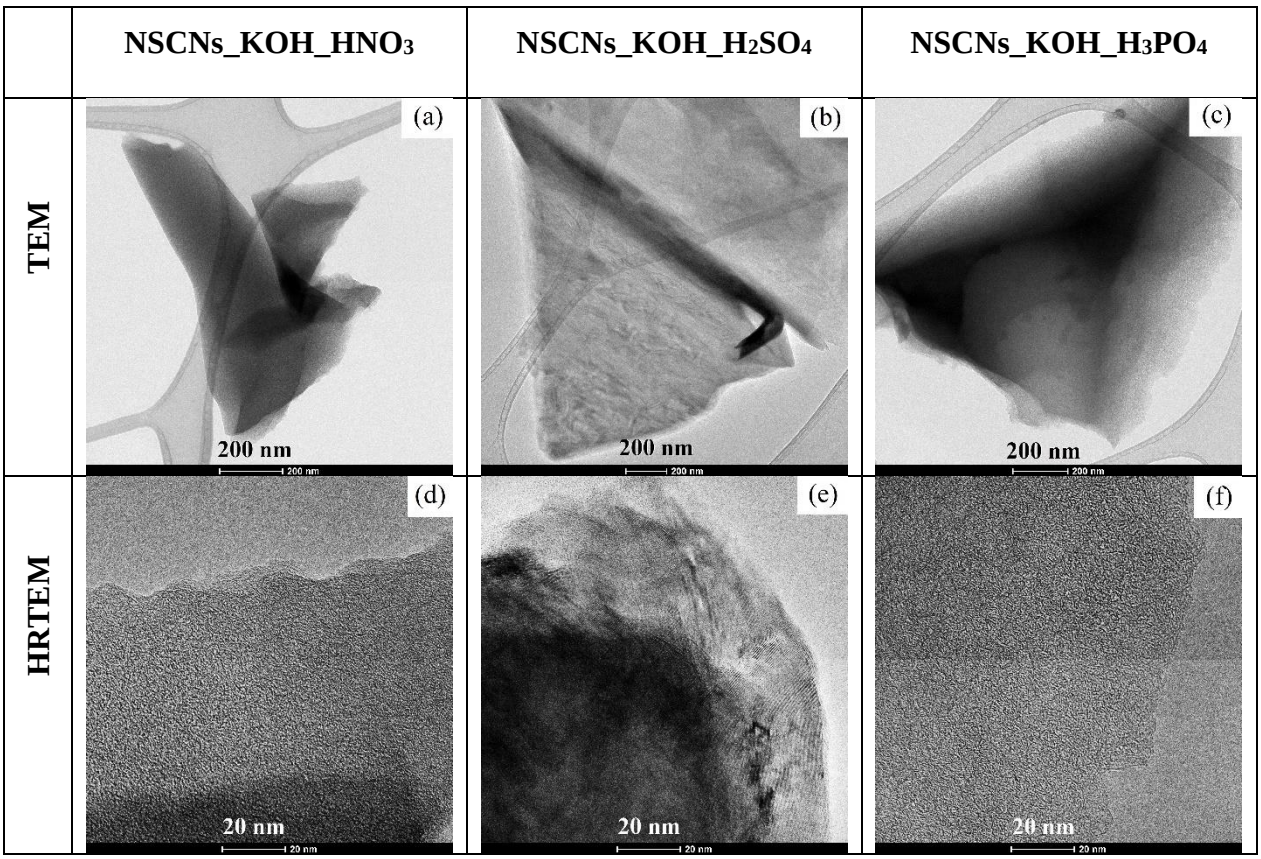

Figure C. TEM (a-c) and HRTEM (d-f) micrographs of the nettle stem carbon nanosheets activated by KOH and exfoliated by (a, d) HNO_3, (b, e) H_2SO_4, or (c, f) H_3PO_4.

Claim 2. Effect of organic components on carbon properties

I established that the natural structure of the material affected the increase of carbon content and the specific surface area of carbon materials after thermal and chemical treatment processes.

2.1 Carbon content: I established that microstructure and carbon content depends on the natural structure of materials. Dried nettle stem and peanut shell have 11.9 and 27.2 wt.% lignin, and 44.86 and 47.34 wt.% carbon content, respectively (as a high wt.% of lignin has a high carbon content). After exfoliation, the carbon was found in the range of 70-80 wt.% (CHNS analyser). In the case of KOH activation, nettle stem carbon nanosheets and peanut shell carbon nanosheets have up to 57-60 % and 47-57 % higher carbon yield than dried samples. For NaOH activation, nettle stem carbon nanosheets and peanut shell carbon nanosheets have up to 70-77 % and 63-68 % higher carbon yield than dried samples.

Dried nettle stem has higher cellulose and hemicellulose content than peanut shell (by 17.5 % and 82.1 %, respectively) and has higher carbon content after exfoliation. The carbon content of nettle stem carbon nanosheets and peanut shell carbon nanosheets is up to > 70

DOI: 10.14750/ME.2021.008

wt.% and reaches the range of 80 wt.% for NaOH activation. The difference in cellulose, lignin, and hemicellulose content affects carbon yields after activation and exfoliation processes. The activation and exfoliation of carbon have a greater impact on carbon yields than the organic composition.

2.2 Specific surface area: I established that at different raw materials, lignin to cellulose ratio has a linear relationship with the surface area of carbon after potassium hydroxide activation and phosphoric acid exfoliation. The BET surface area gradually increased with the cellulose content. The experimental results indicated that the appropriate ratio of lignin and cellulose (lignin/(cellulose+lignin) ratios: nettle leaf, nettle stem and peanut shell is 0.1, 0.2 and 0.4, respectively) induced the activated carbon to develop a microporous and mesoporous structure. After thermal and chemical treatment processes, the specific surface area of carbon is higher than 500 m^2 g^{-1}.

Claim 3. Effect of chemical activation and exfoliation to the surface properties

I established that the chemical activation and exfoliation affect the surface property of carbon nanosheets, which can be described in terms of the quantity of porous carbon. Due to the fact that potassium ions (K^+) are 40% larger than sodium ions (Na^+), the specific surface area and micropore volume of carbon nanosheets activated by KOH are higher than those of activated by NaOH.

3.1 During activation, KOH or NaOH can penetrate the pores of the carbonized material. Interlayered KOH or NaOH residue can react with the exfoliation acids (HNO_3, H_2SO_4, and H_3PO_4). Thus some chemical compounds, such as KNO_3, K_2SO_4, K_3PO_4, $NaNO_3$, Na_2SO_4, and Na_3PO_4 may form. The relationship between the molar volume of these compounds and BET results of the samples is shown in Fig. D (this valid for the investigated system, till the molar volume is 83 cm^3 mol^{-1}). These compounds cause tension in the pores of the activated carbon. As K_3PO_4 has 26.4 and 72.7% higher molar volume than K_2SO_4 and KNO_3, respectively, it resulted in the highest specific surface area, and micropore volume in KOH activated carbon nanosheets both for nettle stem and peanut shell.

DOI: 10.14750/ME.2021.008

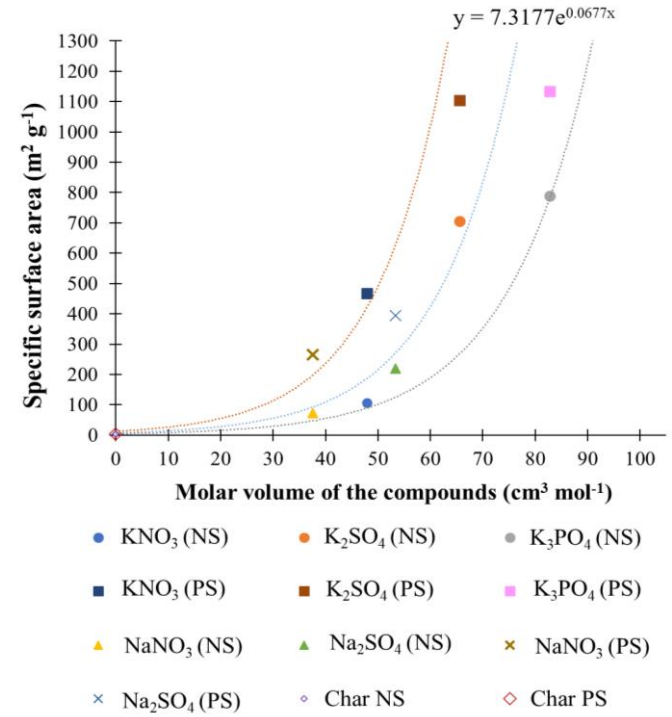

(a)

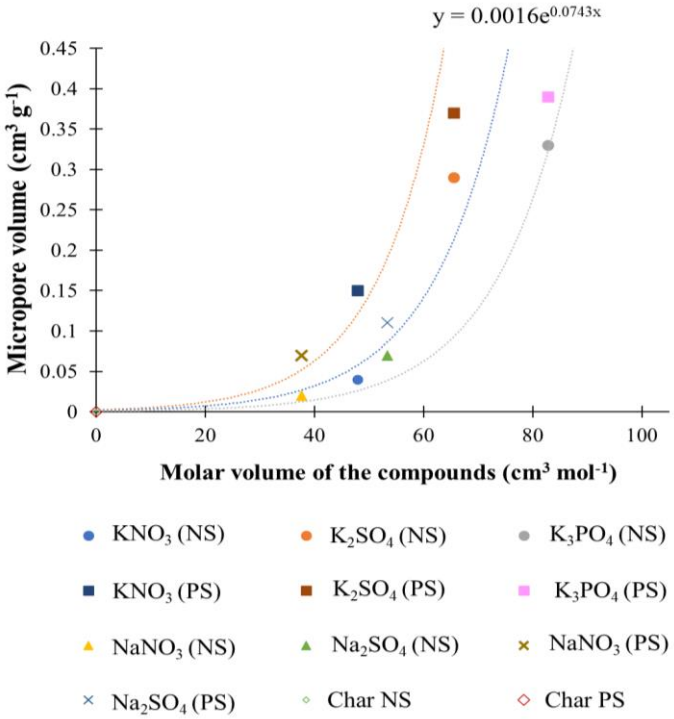

(b)

Figure D Relationship between molar volume of the compounds (formation) and (a) specific surface area, (b) micropore volume of nettle stem derived carbon and peanut shell derived carbon.

DOI: 10.14750/ME.2021.008

3.2 I observed that the triprotic acid (H_3PO_4) reacts more intensely with the materials than diprotic (H_2SO_4) or monoprotic (HNO_3). The reactions result in higher micropore volume with 0.33 and 0.39 $m^3\ g^{-1}$ for nettle stem and peanut shell, respectively (more porous carbon surface) and a higher specific surface with 789, 1,135 and 668 $m^2\ g^{-1}$ for nettle stem, peanut shell, and lignin, respectively (Fig. E-F).

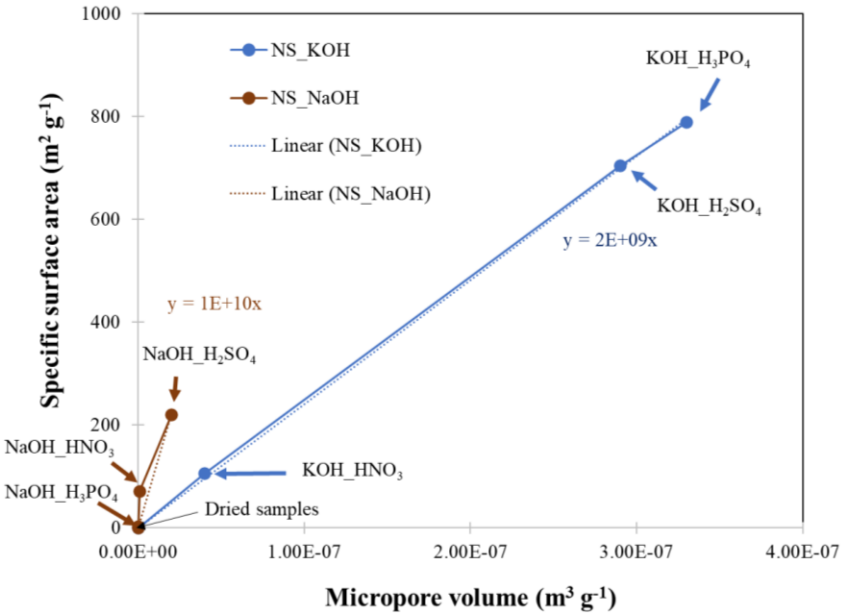

(a)

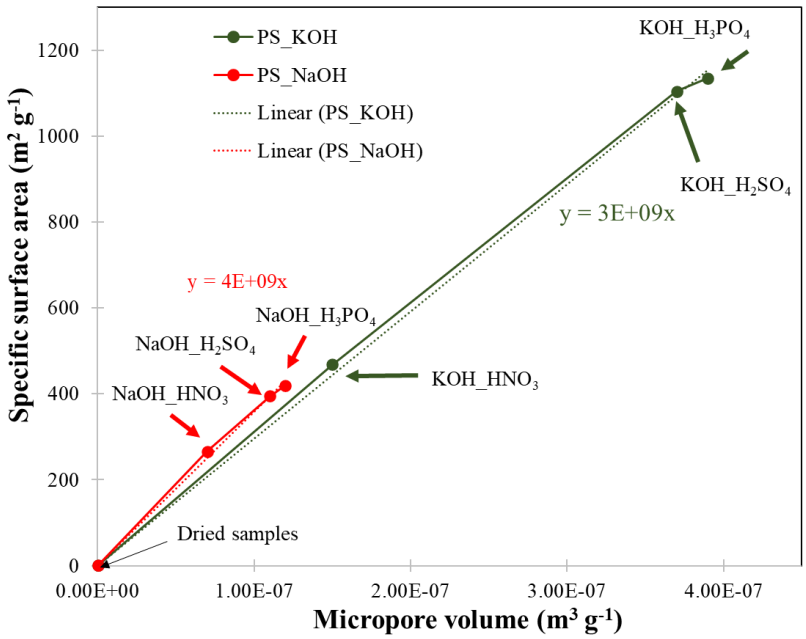

(b)

Figure E Specific surface area of samples as function of micropore volume of (a) nettle stem and (b) peanut shell.

DOI: 10.14750/ME.2021.008

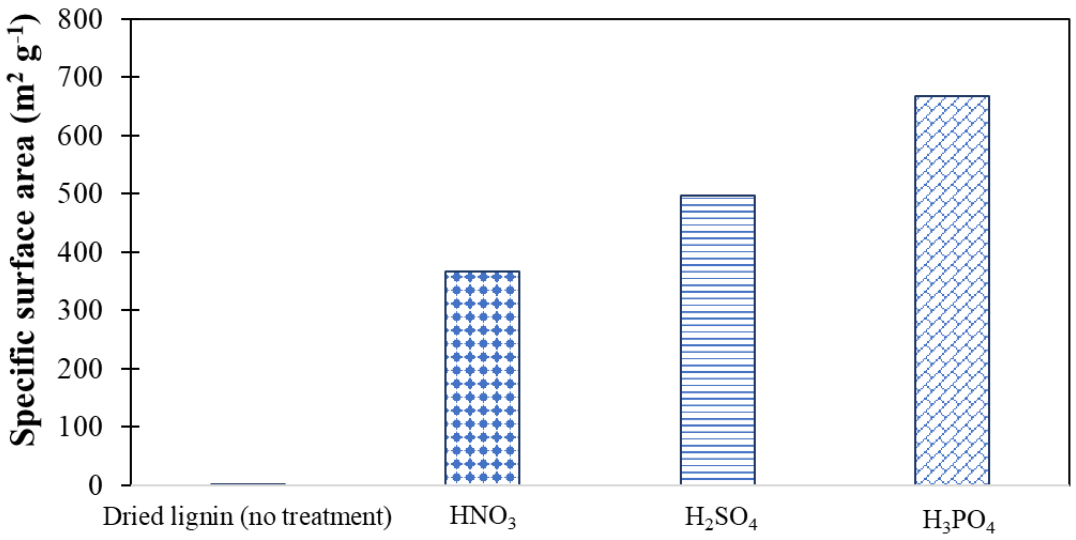

Figure F Specific surface area of lignin derived carbons as function of different acid exfoliators (using KOH activation).

Claim 4. Effect of chemical activation and exfoliation to the electrochemical properties

I established that the energy density (0.01-4.25 Wh kg^{-1}) and power density (18.3-84.2 W kg^{-1}) of carbons in this work is in the range of supercapacitor materials.

The specific capacitance of activated and exfoliated nettle stem carbon nanosheets (KOH activation and H_3PO_4 exfoliation) and peanut shell carbon nanosheets (NaOH activation and H_2SO_4 exfoliation) is 27.3 F $g^{-1}$and 122 F g^{-1}, respectively, and which are higher than the specific capacitance of pre-carbonized nettle stem (0.15 F g^{-1}) and peanut shell (0.14 F g^{-1}) samples. It means peanut shell carbon nanosheets samples have higher specific capacitance (122 F g^{-1}) than nettle stem carbon nanosheets due to their higher specific surface area (1,135 m^2 g^{-1}) and micropore volume (0.39 cm^3 g^{-1}).

Claim 5. Relationship between organic components and electrochemical properties

Based on the literature and my experimental results, I found a correlation between the composition (lignin/(cellulose+lignin) ratio) of the raw material and the surface capacitance of the carbon nanosheets prepared from the raw materials (Fig. G). The correlation can be described with the following equation:

$$C_A=0.33\varphi \quad (6.1)$$

where C_A is the surface capacitance (F m^{-2}), φ is the lignin/(cellulose+lignin) ratio.

DOI: 10.14750/ME.2021.008

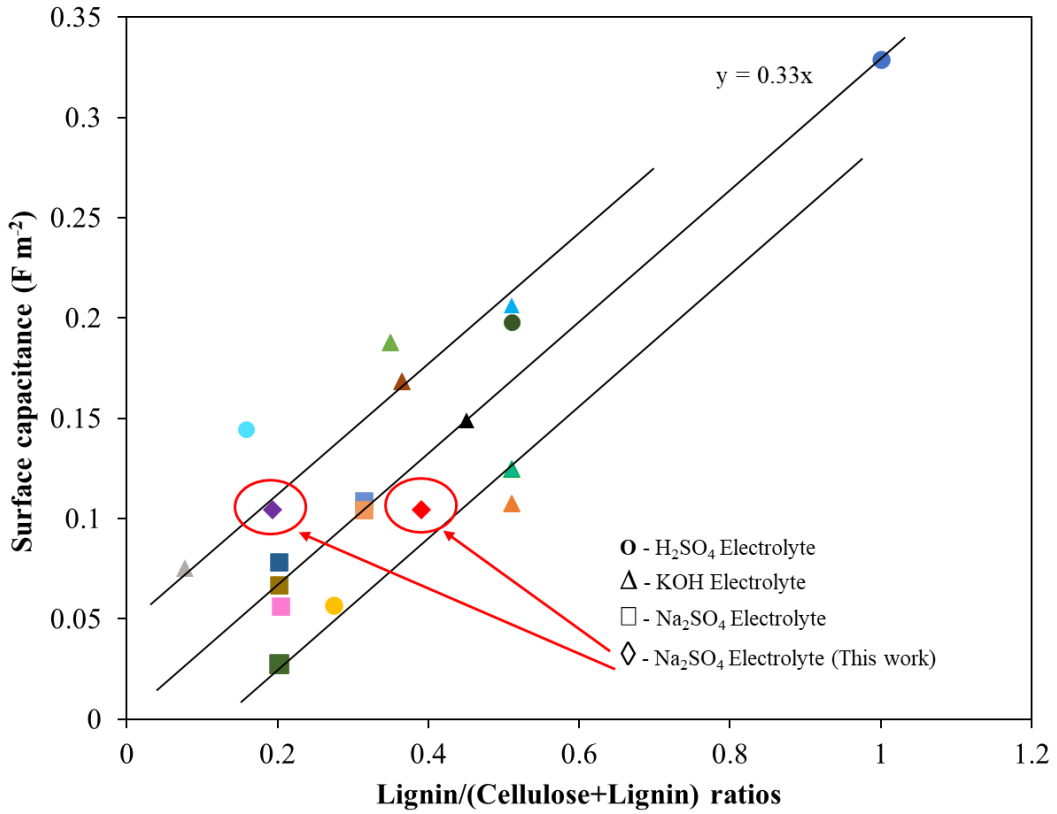

Figure G Surface-capacitance as function of lignin/(cellulose+lignin) ratios of carbon from difference natural samples (with difference electrolytes).

●	Lignin [117]	▲	Cherry stone (4) [120]
●	Coconut kernel [76, 118]	■	Banana fiber (1) [125-126]
●	Pistachio shell [76, 119]	■	Banana fiber (2) [125-126]
●	Cherry stone (1) [120-121]	■	Banana fiber (3) [125-126]
▲	Coffee shell [76, 122]	■	Bamboo Shoot (1) [127-128]
▲	Corn grains [76, 123]	■	Bamboo Shoot (2) [127-128]
▲	Rice husk [76, 124]	■	Durian husk [129-130]
▲	Coconut shell [76, 119]	◆	**Nettle stem (This work)**
▲	Cherry stone (2) [120]	◆	**Peanut shell (Thiswork)**
▲	Cherry stone (3) [120]		

DOI: 10.14750/ME.2021.008

Claim 6. Electrochemical performance of the carbon nanosheets electrode

Carbon materials have been studied and used as electrodes for supercapacitors due to their very attractive chemical and physical performance and low price. The difference in the surface properties of carbon materials affect their electronic properties. Moreover, the electronic and electrochemical properties of the carbon nanomaterial can be improved by modifying the surface.

6.1 I established that for nettle stem activated by KOH, the increase of dissociable protons (polyprotic acid) results in longer charge and discharge cycle time, resulting in the same effect as the specific surface area. The type of acid exfoliator affects the charge and discharge cycles. Cycle time for triprotic (H_3PO_4), diprotic (H_2SO_4), and monoprotic (HNO_3) exfoliators were 260, 112, and 17 s, respectively (Fig. H).

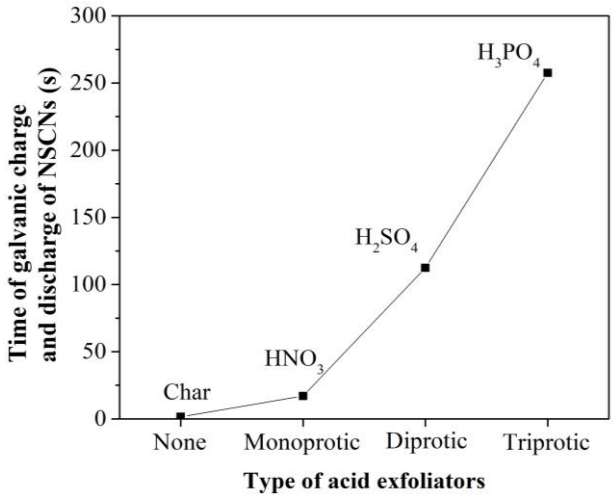

Figure H The time of galvanic charge and discharge of nettle stem derived carbons as a function of different types of acid exfoliators (at a current density of 0.05 A g^{-1}).

6.2 The galvanic charge and discharge curves (Fig. I) show that nettle stem carbon nanosheets activated by KOH and exfoliated by H_3PO_4 have the longest charge and discharge cycles (260 s), which implies the samples' best electrochemical performance. The longest charge and discharge cycles were found from peanut shell carbon nanosheets activated by NaOH and exfoliated H_2SO_4 exfoliator (1,033 s).

DOI: 10.14750/ME.2021.008

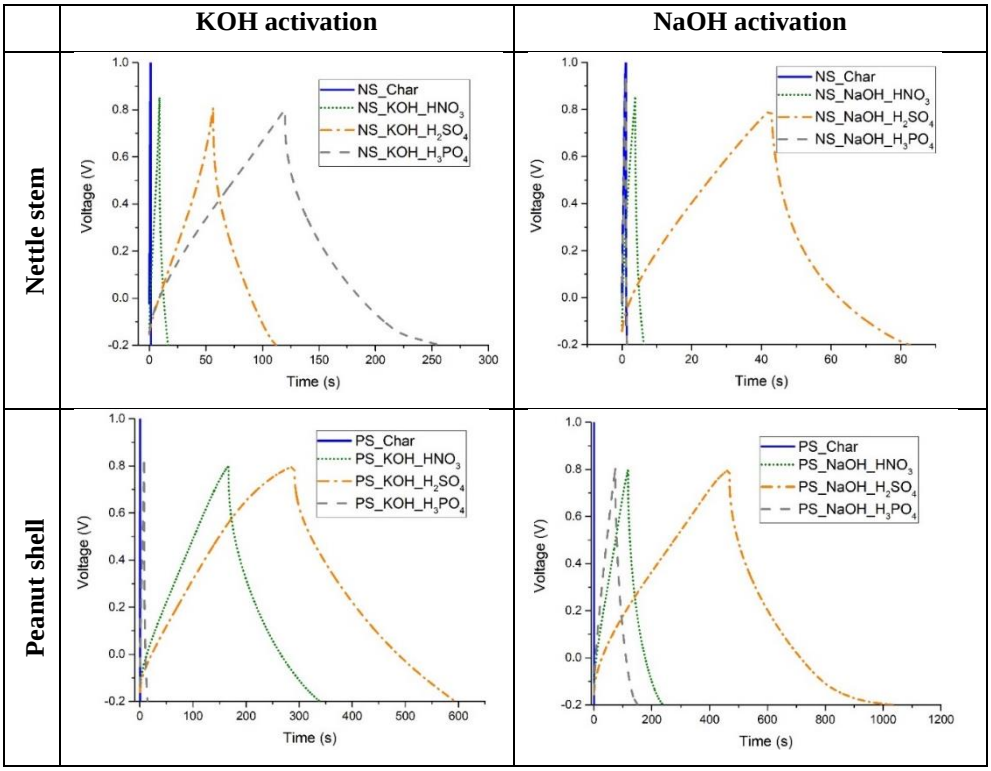

Figure I Galvanostatic charge and discharge of samples at a current density of 0.05 A g^{-1}.

6.3 I identified the electrochemical impedance spectroscopy (EIS, Fig. J) of the carbon nanosheets samples presented with the steep linear curve in the low-frequency region of carbon nanosheets is sharp, representing diffusion-limited charge transfer characteristic close to ideal capacitance performance.

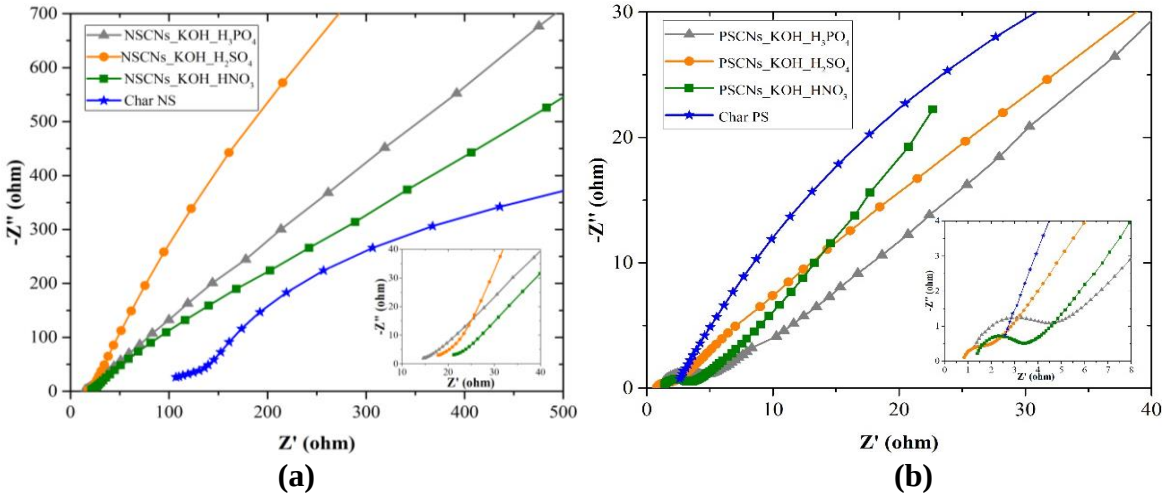

Figure J Nyquist plots of (a) nettle stem and (b) peanut shell derived carbons at an alternating current amplitude of 5 mV.

DOI: 10.14750/ME.2021.008

6.4 I identified the correlation between the peak current and square root of the scan rate of cyclic voltammetry measurement of nettle stem carbon nanosheets. This observation agrees with the linear correlation between the peak current and square root of the scan rate in Fig. K.

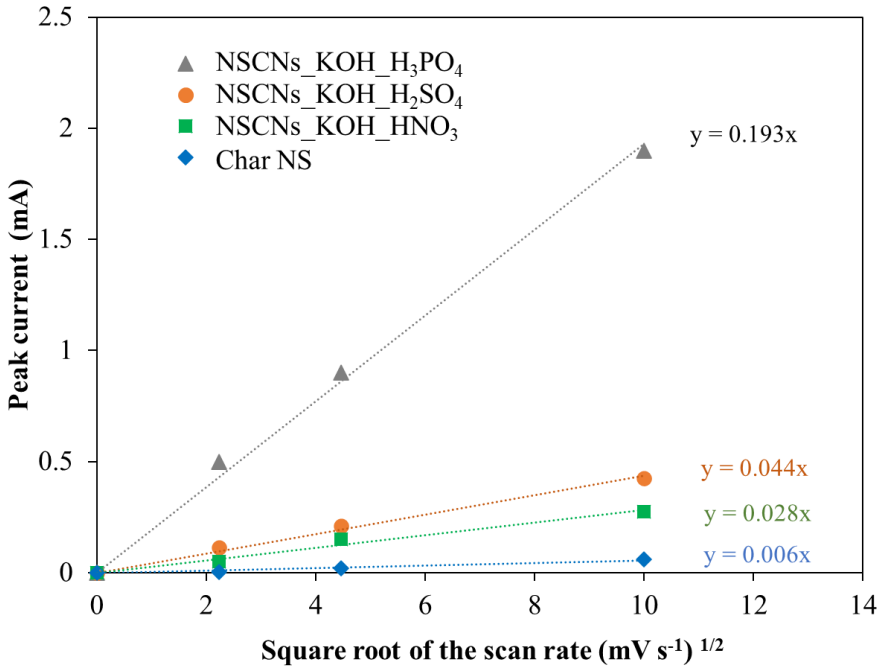

Figure K Relationship between peak current and the square root of the scan rate of cyclic voltammetry measurement of nettle stem derived carbons (potential range -0.2 to 0.8 V).

6.5 I identified the diffusion coefficient in the case of nettle stem carbon nanosheets, based on the relationship between peak current and the square root of the scan rate of cyclic voltammetry measurement. The diffusion coefficients were calculated based on the Randles-Sevcik equation (6.2):

$$Ip = (2.69 \times 10^5)\, n^{3/2} A D^{1/2} C \nu^{1/2} \qquad (6.2)$$

Where Ip is peak current (A), n is number of electrons involved in the reaction, A is electrode area (cm^2), D is diffusion coefficient ($cm^2\ s^{-1}$), C is the concentration of the electroactive species (mol cm^{-3}) and ν is scan rate (V s^{-1}), respectively. The diffusion coefficient depends on the slope of $Ip \propto \nu^{1/2}$ (Fig. K). The higher diffusion coefficient indicates a better electrode reaction activity due to the faster ionic transportation.

DOI: 10.14750/ME.2021.008

The diffusion coefficients obtained by the Randles-Sevcik equation are listed in table A.

Table A The diffusion coefficients of samples (at scan rate 100 mV s^{-1}).

Samples/Electrode	**Ip** **(10^{-5} A)**	**n**	**A** **(cm^2)**	**C** **(mol cm^{-3})**	**$Ip/\nu^{1/2}$** **(As V^{-1})**	**D** **(10^{-8} cm^2 s^{-1})**
Char NS	6.1	1	0.79	0.001	0.006	1.37
NSCNs_KOH_HNO_3	27.5	1	0.79	0.001	0.028	6.17
NSCNs_KOH_H_2SO_4	42.5	1	0.79	0.001	0.044	9.53
NSCNs_KOH_H_3PO_4	190	1	0.79	0.001	0.193	42.6

DOI: 10.14750/ME.2021.008

7 Acknowledgement

I would like to express my sincere gratitude and appreciation to my research supervisors, Assoc. Prof. Dr. Peter Baumli and Assoc. Prof. Dr. Andrea Simon, for their guidance, support and very patience towards the completion of this work. I would like to express my deepest appreciation to my reviewers and committee.

I want to thank Dr. Maria Sveda, Dr. Anna Sycheva and Dr. Daniel Koncz-Horvath for SEM investigation, Mr. Gabor Karacs for TEM investigation, Mr. Tibor Ferenczi for BET investigation, Dr. Ferenc Kristaly for XRD investigation, shell based carbon for CHNS element analysis, Dr. Robert Geber for porosity investigation, Dr. Veres Zsolt for helping with the furnace and Dr. Jaroslav Sychev for the consultation on evaluation of the electrochemical results.

I am always thankful to Ms. Agnes Solczi for always being kind and helpful. I would like to thank Ms. Ildiko Tasnadi, Mrs. Aniko Zoltanne Markus, Mrs. Napsugar Bodnarne Nyari and Mr.Gal Karoly for helping with chemical and equipments.

I have to thank Dr. Winadda Wongwiriyapan, Miss Vichuda Sattayarut and Miss Pundita Ukkakimapan from College of Nanotechnology, King Mongkut's Institute of Technology Ladkrabang in Thailand very much for investigate electrochemical properties of my samples.

I also wish to thank the Institute of Ceramics and Polymer Engineering, Institute of Metallurgy, Metal Forming and Nanotechnology and Antal Kerpely Doctoral School of Materials Science & Technology (Faculty of Materials Science & Engineering) at the University of Miskolc.

I acknowledge the scholarship from the Rajamangala University of Technology Isan (RMUTI, Thailand) for support me to study at the University of Miskolc and I also thank you to my colleagues at RMUTI for helping to coordinate various matters during my studies in Hungary.

Finally, I would like to acknowledge my parents, my older sister for their warmly love, encouragements and understanding throughout my PhD studies.

.

DOI: 10.14750/ME.2021.008

8 References

[1] Saleem, J., Shahid, U. B., Hijab, M., Mackey, H., & McKay, G. (2019). Production and applications of activated carbons as adsorbents from olive stones. *Biomass Conversion and Biorefinery*, 1-28.

[2] Natalia, M., Sudhakar, Y. N., & Selvakumar, M. (2013). Activated carbon derived from natural sources and electrochemical capacitance of double layer capacitor. *Indian Journal of Chemical Technology, 20*(6), 392-399.

[3] Ravula, S., Baker, S. N., Kamath, G., & Baker, G. A. (2015). Ionic liquid-assisted exfoliation and dispersion: Stripping graphene and its two-dimensional layered inorganic counterparts of their inhibitions. *Nanoscale, 7*(10), 4338-4353.

[4] Esparza, Y., Ullah, A., & Wu, J. (2017). Preparation and characterization of graphite oxide nano-reinforced biocomposites from chicken feather keratin. *Journal of Chemical Technology & Biotechnology*, *92*(8), 2023-2031.

[5] Kumar, R., Singh, R. K., & Singh, D. P. (2016). Natural and waste hydrocarbon precursors for the synthesis of carbon based nanomaterials: graphene and CNTs. *Renewable and Sustainable Energy Reviews, 58*, 976-1006.

[6] Baysal, M., Bilge, K., Yılmaz, B., Papila, M., & Yürüm, Y. (2018). Preparation of high surface area activated carbon from waste-biomass of sunflower piths: kinetics and equilibrium studies on the dye removal. *Journal of environmental chemical engineering, 6*(2), 1702-1713.

[7] Wang, B., Gao, B., & Fang, J. (2017). Recent advances in engineered biochar productions and applications. *Critical reviews in environmental science and technology, 47*(22), 2158-2207.

[8] Cheah, W. K., Ooi, C. H., & Yeoh, F. Y. (2016). Rice husk and rice husk ash reutilization into nanoporous materials for adsorptive biomedical applications: A review. *Open Material Sciences, 1*(open-issue).

[9] Yallappa, S., Deepthi, D. R., Yashaswini, S., Hamsanandini, R., Chandraprasad, M., Kumar, S. A., & Hegde, G. (2017). Natural biowaste of Groundnut shell derived nano carbons: Synthesis, characterization and its in vitro antibacterial activity. *Nano-Structures & Nano-Objects, 12*, 84-90.

[10] Afsaneh, D. M., Emad, O., Pradeep, L. M., & Pradeep, K. R. (2015). Mechanical and tribological properties of self-lubricating metal nanocomposites reinforced by carbon nanotubes (CNTs) and grapheme—A review. *Compos. Part B*, 77, 402-420.

[11] Muley, A. V., Aravindan, S., & Singh, I. P. (2015). Nano and hybrid aluminum based metal matrix composites: an overview. *Manufacturing Review*, *2*, 15.

[12] Wu, K., Gao, B., Su, J., Peng, X., Zhang, X., Fu, J., ... & Chu, P. K. (2016). Large and porous carbon sheets derived from water hyacinth for high-performance supercapacitors. *RSC advances*, *6*(36), 29996-30003.

[13] Yun, Y. S., Park, M. H., Hong, S. J., Lee, M. E., Park, Y. W., & Jin, H. J. (2015). Hierarchically porous carbon nanosheets from waste coffee grounds for supercapacitors. *ACS applied materials & interfaces*, *7*(6), 3684-3690.

[14] Liu, H., Wu, X., Geng, H., & Teng, X. (2017). Effects of several nano-carbon materials on the microstructure and properties of copper. *Materials Research Express*, *4*(2), 025801.

[15] Liu, J., Khan, U., Coleman, J., Fernandez, B., Rodriguez, P., Naher, S., & Brabazon, D. (2016). Graphene oxide and graphene nanosheet reinforced aluminium matrix composites: powder synthesis and prepared composite characteristics. *Materials & design*, *94*, 87-94.

[16] Menendez-Diaz, J. A., & Martín-Gullón, I. (2006). Types of carbon adsorbents and their production. In *Interface science and technology* (Vol. 7, pp. 1-47). Elsevier.

[17] Hawari, A. I., Al-Qasir, I. I., & Ougouag, A. M. (2007). Investigation of the impact of simple carbon interstitial formations on thermal neutron scattering in graphite. *Nuclear science and engineering*, *155*(3), 449-462.

[18] Sfiligoj Smole, M., Hribernik, S., Stana Kleinschek, K., & Kreže, T. (2013). Plant fibres for textile and technical applications. *Advances in agrophysical research*, 369-398.

[19] Lin, H., Liu, Y., Chang, Z., Yan, S., Liu, S., & Han, S. (2020). A new method of synthesizing hemicellulose-derived porous activated carbon for high-performance supercapacitors. *Microporous and Mesoporous Materials*, 292, 109707.

[20] Meng, L. Y., Ma, M. G., & Ji, X. X. (2019). Preparation of lignin-based carbon materials and its application as a sorbent. *Materials*, *12*(7), 1111.

[21] Suryawan, I. A., Suardana, N. P. G., Winaya, I. S., Suyasa, I. B., & Nindhia, T. T. (2017, May). Study of stinging nettle (urtica dioica l.) Fibers reinforced green composite materials: a review. In *IOP Conference Series: Materials Science and Engineering* (Vol. 201, No. 1, p. 012001). IOP Publishing.

[22] Di Virgilio, N., Papazoglou, E. G., Jankauskiene, Z., Di Lonardo, S., Praczyk, M., & Wielgusz, K. (2015). The potential of stinging nettle (Urtica dioica L.) as a crop with multiple uses. *Industrial Crops and Products*, *68*, 42-49.

DOI: 10.14750/ME.2021.008

[23] Gülçin, I., Küfrevioğlu, Ö. İ., Oktay, M., & Büyükokuroğlu, M. E. (2004). Antioxidant, antimicrobial, antiulcer and analgesic activities of nettle (Urtica dioica L.). *Journal of ethnopharmacology*, *90*(2-3), 205-215.

[24] Loetscher, Y., Kreuzer, M., & Messikommer, R. E. (2013). Utility of nettle (Urtica dioica) in layer diets as a natural yellow colorant for egg yolk. *Animal feed science and technology*, *186*(3-4), 158-168.

[25] Pua, F. L., Tan, C. Y., Dang, W. H., & Palanisamy, K. (2015). Peanut shells derived solid acid catalyst for biodiesel production. *ARPN Journal of Engineering and Applied Sciences*, *10*(17), 7704-7706.

[26] Dridi-Dhaouadi, S., Douissa-Lazreg, N. B., & M'Henni, M. F. (2011). Removal of lead and Yellow 44 acid dye in single and binary component systems by raw Posidonia oceanica and the cellulose extracted from the raw biomass. *Environmental technology*, *32*(3), 325-340.

[27] Kocherbitov, V., Ulvenlund, S., Kober, M., Jarring, K., & Arnebrant, T. (2008). Hydration of microcrystalline cellulose and milled cellulose studied by sorption calorimetry. *The Journal of Physical Chemistry B*, *112*(12), 3728-3734.

[28] Lapina, V. A., & Akhremkova, G. S. (2006). Correlations between the adsorption and structural properties of SV-1 phytoadsorbent and its main components. *Russian journal of physical chemistry*, *80*(7), 1164-1166.

[29] Bacci, L., Baronti, S., Predieri, S., & di Virgilio, N. (2009). Fiber yield and quality of fiber nettle (Urtica dioica L.) cultivated in Italy. *Industrial crops and products*, *29*(2-3), 480-484.

[30] Sugumaran, P., Susan, V. P., Ravichandran, P., & Seshadri, S. (2012). Production and characterization of activated carbon from banana empty fruit bunch and Delonix regia fruit pod. *Journal of Sustainable Energy & Environment*, *3*(3), 125-132.

[31] Yahya, M. A., Al-Qodah, Z., & Ngah, C. Z. (2015). Agricultural bio-waste materials as potential sustainable precursors used for activated carbon production: A review. *Renewable and Sustainable Energy Reviews*, *46*, 218-235.

[32] Gupta, V. K., Carrott, P. J. M., Singh, R., Chaudhary, M., & Kushwaha, S. (2016). Cellulose: a review as natural, modified and activated carbon adsorbent. *Bioresource technology*, *216*, 1066-1076.

[33] Lu, H., & Zhao, X. S. (2017). Biomass-derived carbon electrode materials for supercapacitors. *Sustainable Energy & Fuels*, *1*(6), 1265-1281.

DOI: 10.14750/ME.2021.008

[34] Lum, W. C., Lee, S. H., Ahmad, Z., Halip, J. A., & Chin, K. L. (2019). Lignocellulosic nanomaterials for construction and building applications. *In Industrial Applications of Nanomaterials* (pp. 423-439). Elsevier.

[35] Dobele, G., Dizhbite, T., Gil, M. V., Volperts, A., & Centeno, T. A. (2012). Production of nanoporous carbons from wood processing wastes and their use in supercapacitors and CO2 capture. *Biomass and Bioenergy*, 46, 145-154.

[36] Rocha-Meneses, L., Raud, M., Orupõld, K., & Kikas, T. (2017). Second-generation bioethanol production: A review of strategies for waste valorisation. *Agronomy Research, 15*(3), 830-847.

[37] Xue, Y., Du, C., Wu, Z., & Zhang, L. (2018). Relationship of cellulose and lignin contents in biomass to the structure and RB-19 adsorption behavior of activated carbon. *New Journal of Chemistry, 42*(20), 16493-16502.

[38] Tiryaki, B., Yagmur, E., Banford, A., & Aktas, Z. (2014). Comparison of activated carbon produced from natural biomass and equivalent chemical compositions. *Journal of analytical and applied pyrolysis, 105*, 276-283.

[39] Daud, W. M. A. W., & Ali, W. S. W. (2004). Comparison on pore development of activated carbon produced from palm shell and coconut shell. *Bioresource technology, 93*(1), 63-69.

[40] Banerjee, S., Patti, A. F., Ranganathan, V., & Arora, A. (2019). Hemicellulose based biorefinery from pineapple peel waste: Xylan extraction and its conversion into xylooligosaccharides. *Food and Bioproducts Processing, 117*, 38-50.

[41] Jahirul, M. I., Rasul, M. G., Chowdhury, A. A., & Ashwath, N. (2012). Biofuels production through biomass pyrolysis—a technological review. *Energies, 5*(12), 4952-5001.

[42] Sun, Y., & Cheng, J. (2002). Hydrolysis of lignocellulosic materials for ethanol production: a review. *Bioresource technology, 83*(1), 1-11.

[43] Mood, S. H., Golfeshan, A. H., Tabatabaei, M., Jouzani, G. S., Najafi, G. H., Gholami, M., & Ardjmand, M. (2013). Lignocellulosic biomass to bioethanol, a comprehensive review with a focus on pretreatment. *Renewable and Sustainable Energy Reviews*, 27, 77-93.

[44] Alonso, D. M., Wettstein, S. G., & Dumesic, J. A. (2012). Bimetallic catalysts for upgrading of biomass to fuels and chemicals. *Chemical Society Reviews, 41*(24), 8075-8098.

[45] Patel, J. P., & Parsania, P. H. (2018). Characterization, testing, and reinforcing materials of biodegradable composites. In *Biodegradable and biocompatible polymer composites* (pp. 55-79). Woodhead Publishing United Kingdom.

[46] Sing, S. W., Everett, D. H., Haul, R. A. W. Moscou, L., Pieroti, R. A., Rouquerol, J., Siemieniewska, T. Sing, K. S. (1985). Reporting physisorption data for gas/solid systems with special reference to the determination of surface area and porosity (Recommendations 1984). *Pure and applied chemistry*, *57*(4), 603-619.

[47] Thommes, M., Kaneko, K., Neimark, A. V., Olivier, J. P., Rodriguez-Reinoso, F., Rouquerol, J., & Sing, K. S. (2015). Physisorption of gases, with special reference to the evaluation of surface area and pore size distribution (IUPAC Technical Report). *Pure and Applied Chemistry*, *87*(9-10), 1051-1069.

[48] Arenas, J. P., & Crocker, M. J. (2010). Recent trends in porous sound-absorbing materials. *Sound & vibration*, *44*(7), 12-18.

[49] Heidarinejad, Z., Dehghani, M. H., Heidari, M., Javedan, G., Ali, I., & Sillanpää, M. (2020). Methods for preparation and activation of activated carbon: a review. Environmental Chemistry Letters, 1-23.

[50] Laowachirasuwan, K. (2009). Preparation and characteristics of activated carbons from coffee residue by chemical activation method. University of the Thai Chamber of Commerce Journal.

[51] Boudrahem, F., Aissani-Benissad, F., & Aït-Amar, H. (2009). Batch sorption dynamics and equilibrium for the removal of lead ions from aqueous phase using activated carbon developed from coffee residue activated with zinc chloride. *Journal of environmental management*, *90*(10), 3031-3039.

[52] Depci, T., Kul, A. R., & Önal, Y. (2012). Competitive adsorption of lead and zinc from aqueous solution on activated carbon prepared from Van apple pulp: Study in single-and multi-solute systems. *Chemical engineering journal*, 200, 224-236.

[53] Huang, Y., Li, S., Chen, J., Zhang, X., & Chen, Y. (2014). Adsorption of Pb (II) on mesoporous activated carbons fabricated from water hyacinth using H3PO4 activation: adsorption capacity, kinetic and isotherm studies. *Applied Surface Science*, 293, 160-168.

[54] Mouni, L., Merabet, D., Bouzaza, A., & Belkhiri, L. (2011). Adsorption of Pb (II) from aqueous solutions using activated carbon developed from Apricot stone. *Desalination*, *276*(1-3), 148-153.

DOI: 10.14750/ME.2021.008

[55] Prahas, D., Kartika, Y., Indraswati, N., & Ismadji, S. J. C. E. J. (2008). Activated carbon from jackfruit peel waste by H_3PO_4 chemical activation: Pore structure and surface chemistry characterization. *Chemical Engineering Journal, 140*(1-3), 32-42.

[56] Demiral, İ., & Şamdan, C. A. (2016). Preparation and characterisation of activated carbon from pumpkin seed shell using H_3PO_4. *Anadolu Üniversitesi Bilim Ve Teknoloji Dergisi A-Uygulamalı Bilimler ve Mühendislik, 17*(1), 125-138.

[57] Tao, H. C., Zhang, H. R., Li, J. B., & Ding, W. Y. (2015). Biomass based activated carbon obtained from sludge and sugarcane bagasse for removing lead ion from wastewater. *Bioresource Technology*, 192, 611-617.

[58] Zhang, S., Zheng, M., Lin, Z., Li, N., Liu, Y., Zhao, B., Pang, H., Cao, J., He, P. & Shi, Y. (2014). Activated carbon with ultrahigh specific surface area synthesized from natural plant material for lithium–sulfur batteries. *Journal of Materials Chemistry A, 2*(38), 15889-15896.

[59] Mistar, E. M., Ahmad, S., Muslim, A., Alfatah, T., & Supardan, M. D. (2018, March). Preparation and characterization of a high surface area of activated carbon from Bambusa vulgaris—Effect of NaOH activation and pyrolysis temperature. *In IOP Conference Series: Materials Science and Engineering* (Vol. 334, No. 1, p. 012051). IOP Publishing.

[60] Raymundo-Pinero, E., Azaïs, P., Cacciaguerra, T., Cazorla-Amorós, D., Linares-Solano, A., & Béguin, F. (2005). KOH and NaOH activation mechanisms of multiwalled carbon nanotubes with different structural organisation. *Carbon, 43*(4), 786-795.

[61] Romanos, J., Beckner, M., Rash, T., Firlej, L., Kuchta, B., Yu, P., Suppes, G., Wexler, C. & Pfeifer, P. (2011). Nanospace engineering of KOH activated carbon. *Nanotechnology, 23*(1), 015401.

[62] Yahya, M. A., Ngah, C. Z. C., Hashim, M. A., & Al-Qodah, Z. (2016). Preparation of activated carbon from desiccated coconut residue by chemical activation with NaOH. *Journal of Materials Science Research, 5*(1), 24.

[63] Hu, Y., Wang, H., Yang, L., Liu, X., Zhang, B., Liu, Y., ... & Fu, H. (2013). Preparation of chitosan-based activated carbon and its electrochemical performance for EDLC. *Journal of the Electrochemical Society, 160*(6), H321.

[64] Sodtipinta, J., Ieosakulrat, C., Poonyayant, N., Kidkhunthod, P., Chanlek, N., Amornsakchai, T., & Pakawatpanurut, P. (2017). Interconnected open-channel carbon

nanosheets derived from pineapple leaf fiber as a sustainable active material for supercapacitors. *Industrial Crops and Products*, 104, 13-20.

[65] Shrivastava, I.H., Tieleman, D.P., Biggin, P.C. and Sansom, M.S., 2002. K+ versus Na+ ions in a K channel selectivity filter: a simulation study. *Biophysical journal, 83*(2), pp.633-645.

[66] Israelachvili, J. N. (2011). Interactions Involving Polar Molecules. *Intermolecular and Surface Forces*, 71-90.

[67] Kovtyukhova, N. I., Perea-López, N., Terrones, M., & Mallouk, T. E. (2017). Atomically thin layers of graphene and hexagonal boron nitride made by solvent exfoliation of their phosphoric acid intercalation compounds. *ACS nano, 11*(7), 6746-6754.

[68] Hong, X., & Chung, D. D. L. (2015). Exfoliated graphite with relative dielectric constant reaching 360, obtained by exfoliation of acid-intercalated graphite flakes without subsequent removal of the residual acidity. *Carbon, 91*, 1-10.

[69] Wei, T., Fan, Z., Luo, G., Zheng, C., & Xie, D. (2009). A rapid and efficient method to prepare exfoliated graphite by microwave irradiation. *Carbon, 47*(1), 337-339.

[70] Yan, Y., Kuila, T., Kim, N. H., & Lee, J. H. (2014). Effects of acid vapour mediated oxidization on the electrochemical performance of thermally exfoliated graphene. *Carbon, 74*, 195-206.

[71] Nicolosi, V., Chhowalla, M., Kanatzidis, M. G., Strano, M. S., & Coleman, J. N. (2013). Liquid exfoliation of layered materials. *Science*, *340*(6139).

[72] Fan, H., & Shen, W. (2015). Carbon nanosheets: synthesis and application. *ChemSusChem, 8*(12), 2004-2027.

[73] Reed, A. R., & Williams, P. T. (2004). Thermal processing of biomass natural fibre wastes by pyrolysis. *International Journal of Energy Research*, *28*(2), 131-145.

[74] Deng, J., Xiong, T., Wang, H., Zheng, A., & Wang, Y. (2016). Effects of cellulose, hemicellulose, and lignin on the structure and morphology of porous carbons. *ACS Sustainable Chemistry & Engineering*, *4*(7), 3750-3756.

[75] Hao, L., Li, X., & Zhi, L. (2013). Carbonaceous electrode materials for supercapacitors. *Advanced Materials, 25*(28), 3899-3904.

[76] Enock, T. K., King'ondu, C. K., Pogrebnoi, A., & Jande, Y. A. C. (2017). Status of biomass derived carbon materials for supercapacitor application. *International Journal of Electrochemistry*, 2017.

DOI: 10.14750/ME.2021.008

[77] Long, J. W., Bélanger, D., Brousse, T., Sugimoto, W., Sassin, M. B., & Crosnier, O. (2011). Asymmetric electrochemical capacitors-stretching the limits of aqueous electrolytes. Naval Research Lab Washington DC.

[78] Saha, S., & Kuila, T. (2019). Nanostructured Carbon-Based Electrodes for Supercapacitor Applications. *Nanomaterials for Electrochemical Energy Storage Device*s, 469.

[79] Redondo, E., Carretero-González, J., Goikolea, E., Ségalini, J., & Mysyk, R. (2015). Effect of pore texture on performance of activated carbon supercapacitor electrodes derived from olive pits. *Electrochimica Acta, 160*, 178-184.

[80] Roy, P., & Srivastava, S. K. (Eds.). (2019). *Nanomaterials for Electrochemical Energy Storage Devices*. Wiley-Scrivener.

[81] Zhang, X., Zhang, H., Li, C., Wang, K., Sun, X., & Ma, Y. (2014). Recent advances in porous graphene materials for supercapacitor applications. *Rsc Advances, 4*(86), 45862-45884.

[82] Mirzaeian, M., Abbas, Q., Ogwu, A., Hall, P., Goldin, M., Mirzaeian, M., & Jirandehi, H. F. (2017). Electrode and electrolyte materials for electrochemical capacitors. *International journal of hydrogen energy, 42*(40), 25565-25587.

[83] Hillier, N., Yong, S., & Beeby, S. (2020). The good, the bad and the porous: A review of carbonaceous materials for flexible supercapacitor applications The good, the bad and the porous: A review of carbonaceous materials for flexible supercapacitor applications. *Energy Reports, 6,* 148-156.

[84] Yang, P., & Mai, W. (2014). Flexible solid-state electrochemical supercapacitors. *Nano Energy*, *8,* 274-290.

[85] Rao, S. S., Kanaka Durga, I., Naresh, B., Jin-Soo, B., Krishna, T. N. V., In-Ho, C., Ahn, J.W. & Kim, H. J. (2018). One-pot hydrothermal synthesis of novel Cu-MnS with PVP cabbage-like nanostructures for high-performance supercapacitors. *Energies, 11*(6), 1590.

[86] Divyashree, A., & Hegde, G. (2015). Activated carbon nanospheres derived from bio-waste materials for supercapacitor applications–a review. *Rsc Advances, 5*(107), 88339-88352.

[87] Abioye, A. M., & Ani, F. N. (2015). Recent development in the production of activated carbon electrodes from agricultural waste biomass for supercapacitors: a review. *Renewable and sustainable energy reviews, 52,* 1282-1293.

DOI: 10.14750/ME.2021.008

[88] Faraji, S., & Ani, F. N. (2015). The development supercapacitor from activated carbon by electroless plating—A review. *Renewable and Sustainable Energy Reviews, 42,* 823-834.

[89] Saha, D., Li, Y., Bi, Z., Chen, J., Keum, J. K., Hensley, D. K., ... & Naskar, A. K. (2014). Studies on supercapacitor electrode material from activated lignin-derived mesoporous carbon. *Langmuir, 30*(3), 900-910.

[90] Gamby, J., Taberna, P. L., Simon, P., Fauvarque, J. F., & Chesneau, M. (2001). Studies and characterisations of various activated carbons used for carbon/carbon supercapacitors. *Journal of power sources, 101*(1), 109-116.

[91] Zhi, M., Yang, F., Meng, F., Li, M., Manivannan, A., & Wu, N. (2014). Effects of pore structure on performance of an activated-carbon supercapacitor electrode recycled from scrap waste tires. *ACS Sustainable Chemistry & Engineering, 2*(7), 1592-1598.

[92] Jain, A., Aravindan, V., Jayaraman, S., Kumar, P.S., Balasubramanian, R., Ramakrishna, S., Madhavi, S., Srinivasan, M.P. (2013). Activated carbons derived from coconut shells as high energy density cathode material for Li-ion capacitors. *Scientific reports, 3*(1), 1-6.

[93] Kim, M., Kim, K., Park, S. & Roh, K.C. (2016) Hierarchically structured activated carbon for ultracapacitors. *Scientific reports,* 6, 21182.

[94] Obreja, V. V., Dinescu, A., & Obreja, A. C. (2010). Activated carbon-based electrodes in commercial supercapacitors and their performance. *International Review of Electrical Engineering, 5*(1), 272-281.

[95] Nuilek, K., Simon, A., & Baumli, P. (2018). Carbonization of stinging nettle (Urtica dioica) by thermal and chemical processing. *International Journal of Advances in Science, Engineering and Technology (IJASEAT)* (Vol. 6, Issue 2, Spl. Iss-2 Jun, 2018), 6-10.

[96] Nuilek, K., Simon, A., & Baumli, P. (2019). Synthesis and Characterization of Carbon Nanosheets from Stinging Nettle (Urtica Dioica). In *IOP Conference Series: Materials Science and Engineering, 613*(1), 012017.

[97] Purkait, T., Singh, G., Singh, M., Kumar, D., & Dey, R. S. (2017). Large area few-layer graphene with scalable preparation from waste biomass for high-performance supercapacitor. *Scientific reports, 7*(1), 1-14.

[98] Sattayarut, V., Chanthad, C., Khemthong, P., Kuboon, S., Wanchaem, T., Phonyiem, M., Obata, M., Fujishige, M., Takeuchi, K., Wongwiriyapan, W. & Khanchaitit, P.

(2019). Preparation and electrochemical performance of nitrogen-enriched activated carbon derived from silkworm pupae waste. *RSC advances, 9*(18), 9878-9886.

[99] Metrohm AG: Swiss-quality products for chemical analysis. (2020). Retrieved 1 July 2020, from https://www.metrohm.com/en

[100] Smole, M., Hribernik, S., Stana, K. and Kreze, T. (2013). Advances in agrophysical research. Rijeka, Croatia: Intech.

[101] Zhang, S., Tao, L., Jiang, M., Gou, G., & Zhou, Z. (2015). Single-step synthesis of magnetic activated carbon from peanut shell. *Materials Letters, 157*, 281-284.

[102] Particle Model of Solids, Liquids and Gases. (2018). Retrieved from https://chemstuff.co.uk/academic-work/year-7/particle-model-of-solids-liquids-and-gases/

[103] Park, M. H., Kim, N. R., Yun, Y. S., Cho, S. Y., & Jin, H. J. (2016). Waste coffee grounds-derived nanoporous carbon nanosheets for supercapacitors. *Carbon Letters (Carbon Lett.), 1*9, 66-71.

[104] Hyun, K., & Saito, N. (2017). The solution plasma process for heteroatom-carbon nanosheets: the role of precursors. *Scientific reports, 7*(1), 1-9.

[105] Jacobsen, A. J., Mahoney, S., Carter, W. B., & Nutt, S. (2011). Vitreous carbon micro-lattice structures. *Carbon, 49*(3), 1025-1032.

[106] Güiza-Argüello, V., Bayona-Becerra, M., Cruz-Orellana, S., & Córdoba-Tuta, E. (2017, January). Development of highly open polyhedral networks from vitreous carbon for orthopaedic applications. In *Journal of Physics: Conference Series* (Vol. 786, No. 1, p. 012019). IOP Publishing.

[107] Cowlard, F. C., & Lewis, J. C. (1967). Vitreous carbon—a new form of carbon. *Journal of Materials Science, 2*(6), 507-512.

[108] Lillo-Ródenas, M. A., Cazorla-Amorós, D., & Linares-Solano, A. (2003). Understanding chemical reactions between carbons and NaOH and KOH: an insight into the chemical activation mechanism. *Carbon, 41*(2), 267-275.

[109] Cegla, R. N. R., Macha, I. J., Ben-Nissan, B., Grossin, D., Heness, G., & Chung, R. J. (2014). Comparative study of conversion of coral with ammonium dihydrogen phosphate and orthophosphoric acid to produce calcium phosphates. Journal of the Australian Ceramic Society.

[110] Wang, S., Wang, C., & Ji, X. (2017). Towards understanding the salt-intercalation exfoliation of graphite into graphene. *Rsc Advances, 7*(82), 52252-52260.

DOI: 10.14750/ME.2021.008

[111] Outokumpu HSC Chemistry for Windows, version 6.0; Outokumpu Research Oy: Pori, Finland, 2006.

[112] Ahmad, I., & Ullah, H. (2009). Influence of some intercalations on activation of pre-baked clay. *Journal of the Chilean Chemical Society*, *54*(3), 222-227.

[113] González, A., Goikolea, E., Barrena, J. A., & Mysyk, R. (2016). Review on supercapacitors: Technologies and materials. *Renewable and Sustainable Energy Reviews*, *58*, 1189-1206.

[114] Mishra, N., Shinde, S., Vishwakarma, R., Kadam, S., Sharon, M., & Sharon, M. (2013, June). MWCNTs synthesized from waste polypropylene plastics and its application in super-capacitors. In *AIP Conference Proceedings* (Vol. 1538, No. 1, pp. 228-236). American Institute of Physics.

[115] Wang, C. M., Wen, C. Y., Che, Y. C., Chang, J. Y., Ho, C. H., Kao, K. S., Shih, W.C., Chiu, C.M.& Shen, Y. A. (2015, March). The influence of specific surface area on the capacitance of the carbon electrodes supercapacitor. In *The Proceedings of the Second International Conference on Industrial Application Engineering* (pp. 439-442).

[116] Zhang, C. X., Zhang, R., Xing, B.L., Cheng, G., Xie, Y.B., Qiao, W.M., Liang, Z.H.A.N., Liang, X.Y. & Ling, L.C. (2010). Effect of pore structure on the electrochemical performance of coal-based activated carbons in non-aqueous electrolyte. *New Carbon Materials*, *25*(2), 129-133.

[117] Liu, W., Yao, Y., Fu, O., Jiang, S., Fang, Y., Wei, Y., & Lu, X. (2017). Lignin-derived carbon nanosheets for high-capacitance supercapacitors. *RSC advances*, *7*(77), 48537-48543.

[118] Rajamohan, T., & Archana, U. (2018). Nutrition and Health Aspects of Coconut. *In The Coconut Palm (Cocos nucifera L.)-Research and Development Perspectives* (pp. 757-777). Springer, Singapore.

[119] Li, X., Liu, Y., Hao, J., & Wang, W. (2018). Study of almond shell characteristics. *Materials*, *11*(9), 1782.

[120] Zhang, J., Chen, H., Ma, Z., Li, H., Dong, Y., Yang, H., Yang, L., Bai, L., Wei, D. & Wang, W. (2020). A lignin dissolution-precipitation strategy for porous biomass carbon materials derived from cherry stones with excellent capacitance. *Journal of Alloys and Compounds*, 155029.

[121] Olivares-Marín, M., Fernández, J. A., Lázaro, M. J., Fernández-González, C., Macías-García, A., Gómez-Serrano, V., Stoeckli, F. & Centeno, T. A. (2009). Cherry stones

as precursor of activated carbons for supercapacitors. *Materials Chemistry and Physics, 114*(1), 323-327.

[122] Juniar, L., Mulyati, S., Fathira, D., & Safitri, R. (2020, March). Preparation and Characterization of Activated Carbon from Gayo Coffee Shell as an Adsorbent for Removal of Lead (Pb) in Liquid Waste. *In Materials Science and Engineering Conference Series* (Vol. 796, No. 1, p. 012050).

[123] Schwietzke, S., Kim, Y., Ximenes, E., Mosier, N., & Ladisch, M. (2009). Ethanol production from maize. *In Molecular Genetic Approaches to Maize Improvement* (pp. 347-364). Springer, Berlin, Heidelberg.

[124] Ma'ruf, A., Pramudono, B., & Aryanti, N. (2017, March). Lignin isolation process from rice husk by alkaline hydrogen peroxide: Lignin and silica extracted. *In AIP Conference Proceedings* (Vol. 1823, No. 1, p. 020013). AIP Publishing LLC.

[125] Ortega, Z., Morón, M., Monzón, M. D., Badalló, P., & Paz, R. (2016). Production of banana fiber yarns for technical textile reinforced composites. *Materials, 9*(5), 370.

[126] Subramanian, V., Luo, C., Stephan, A. M., Nahm, K. S., Thomas, S., & Wei, B. (2007). Supercapacitors from activated carbon derived from banana fibers. The *Journal of Physical Chemistry C, 111*(20), 7527-7531.

[127] He, M. X., Li, Q., Liu, X. Y., Hu, Q. C., Hu, G. Q., Pan, K., Zhu, Q.L. & Wu, J. (2013). Bio-ethanol production from bamboo residues with lignocellulose fractionation technology (LFT) and separate hydrolysis fermentation (SHF) by Zymomonas mobilis. Am J Biomass Bioenergy, 1, 1-10.

[128] Han, J., Li, Q., Wang, J., Ye, J., Fu, G., Zhai, L., & Zhu, Y. (2018). Heteroatoms (O, N)-doped porous carbon derived from bamboo shoots shells for high performance supercapacitors. *Journal of Materials Science: Materials in Electronics, 29*(24), 20991-21001.

[129] Ukkakimapan, P., Sattayarut, V., Wanchaem, T., Yordsri, V., Phonyiem, M., Ichikawa, S., Obata, M., Fujishige, M., Takeuchi, K., Wongwiriyapan, W.& Endo, M. (2020). Preparation of activated carbon via acidic dehydration of durian husk for supercapacitor applications. *Diamond and Related Materials*, 107906.

[130] Lee, M. C., Koay, S. C., Chan, M. Y., Pang, M. M., Chou, P. M., & Tsai, K. Y. (2018). Preparation and characterization of durian husk fiber filled polylactic acid biocomposites. *In MATEC Web of Conferences* (Vol. 152, p. 02007). EDP Sciences.

[131] Wang, X., Zhou, X., Chen, W., Chen, M., & Liu, C. (2019). Enhancement of the electrochemical properties of commercial coconut shell-based activated carbon by H2O dielectric barrier discharge plasma. *Royal Society open science*, *6*(2), 180872.

[132] Azman, N. H. N., Mamat@ Mat Nazir, M. S., Ngee, L. H., & Sulaiman, Y. (2018). Graphene-based ternary composites for supercapacitors. *International Journal of Energy Research*, *42*(6), 2104-2116.

[133] Nuilek, K., Wongwiriyapan, W., Sattayarut, V., Simon, A., Koncz-Horváth, D., Ferenczi, T., Kristály, F. & Baumli, P. (2020). Comparison of acid exfoliators in carbon nanosheets synthesis from stinging nettle (Urtica dioica) for electrochemical applications. *Scientific Reports*, *10*(1), 1-12.

[134] Chen, X., Zhang, J., Zhang, B., Dong, S., Guo, X., Mu, X., & Fei, B. (2017). A novel hierarchical porous nitrogen-doped carbon derived from bamboo shoot for high performance supercapacitor. *Scientific reports*, *7*(1), 1-11.

[135] Li, Y., Yu, N., Yan, P., Li, Y., Zhou, X., Chen, S., Wang, G., Wei, T. & Fan, Z. (2015). Fabrication of manganese dioxide nanoplates anchoring on biomass-derived cross-linked carbon nanosheets for high-performance asymmetric supercapacitors. *Journal of Power Sources*, *300*, 309-317.

[136] Chen, L., Ji, T., Brisbin, L., & Zhu, J. (2015). Hierarchical porous and high surface area tubular carbon as dye adsorbent and capacitor electrode. *ACS applied materials & interfaces*, *7*(22), 12230-12237.

[137] Sivachidambaram, M., Vijaya, J.J., Kennedy, L.J., Jothiramalingam, R., Al-Lohedan, H.A., Munusamy, M.A., Elanthamilan, E. & Merlin, J.P., (2017). Preparation and characterization of activated carbon derived from the Borassus flabellifer flower as an electrode material for supercapacitor applications. *New Journal of Chemistry*, *41*(10), 3939-3949.

[138] Barzegar, F., Dangbegnon, J. K., Bello, A., Momodu, D. Y., Johnson Jr, A. C., & Manyala, N. (2015). Effect of conductive additives to gel electrolytes on activated carbon-based supercapacitors. *Aip Advances*, *5*(9), 097171.

[139] Lu, Y., Zhang, S., Yin, J., Bai, C., Zhang, J., Li, Y., Yang, Y., Ge, Z., Zhang, M., Wei, L. & Ma, M. (2018). Data on high performance supercapacitors based on mesoporous activated carbon materials with ultrahigh mesopore volume and effective specific surface area. *Data in brief*, 18, 1448-1456.

DOI: 10.14750/ME.2021.008

[140] Bhattacharjya, D., & Yu, J. S. (2014). Activated carbon made from cow dung as electrode material for electrochemical double layer capacitor. *Journal of Power Sources*, *262*, 224-231.

[141] Taer, E., Mustika, W. S., Agustino, F., Hidayu, N., & Taslim, R. (2017). The Flexible Carbon Activated Electrodes made from Coconut Shell Waste for Supercapacitor Application. In *IOP Conference Series: Earth and Environmental Science* (Vol. 58, No. 1, p. 012065). IOP Publishing.

[142] Kishore, B., Shanmughasundaram, D., Penki, T. R., & Munichandraiah, N. (2014). Coconut kernel-derived activated carbon as electrode material for electrical double-layer capacitors. *Journal of Applied Electrochemistry, 44*(8), 903-916.

[143] Meng, C., Gall, O. Z., & Irazoqui, P. P. (2013). A flexible super-capacitive solid-state power supply for miniature implantable medical devices. *Biomedical microdevices, 15*(6), 973-983.

DOI: 10.14750/ME.2021.008

9 Publications related to this thesis work

9.1 Journal papers

J1. Nuilek, K., Wongwiriyapan, W., Sattayarut, V., Simon, A., Koncz-Horváth, D., Ferenczi, T., Kristály, F. & Baumli, P. (2020). Comparison of acid exfoliators in carbon nanosheets synthesis from stinging nettle (Urtica dioica) for electrochemical applications. Scientific Reports, 10(1), 1-12. **(D1)**.

J2. Nuilek, K., Simon, A., Kurovics, E., Ibrahim, J. F. M., Varanasi, D., & Baumli, P. (2020). Effect of activation and exfoliation on the formation of carbon nanosheets derived from natural materials. In Journal of Physics: Conference Series (Vol. 1527, No. 1, p. 012036). IOP Publishing **(Q3)**.

J3. Nuilek, K., Simon, A., & Baumli, P. (2019, October). Synthesis and Characterization of Carbon Nanosheets from Stinging Nettle (Urtica Dioica). In IOP Conference Series: Materials Science and Engineering (Vol. 613, No. 1, p. 012017). IOP Publishing.

J4. Nuilek, K., Simon, A., & Baumli, P. (2018). Carbonization of stinging nettle (Urtica dioica) by thermal and chemical processing. International Journal of Advances in Science, Engineering and Technology (IJASEAT) (Vol. 6, Issue 2, Spl. Iss-2 Jun, 2018), 6-10.

J5. Nuilek, K., Simon, A., & Baumli, P. (2018). Influence of KOH on the carbon nanostructure of peanut shell. Resolution and Discovery, 3(2), 29-32.

9.2 Proceeding papers

P1. Nuilek, K., Simon, A., & Baumli, P. (2018). Carbonization of stinging nettle (Urtica dioica) by thermal and chemical processing., Proceeding of the ISER 120th International Conference, 14-15th April 2018, Krakow, Poland, ISBN 978-93-8 7703-91-9.

9.3 Oral and poster presentations

O1. Nuilek, K., Simon, A., & Baumli, P. Effect of activation and exfoliation on the formation of carbon nanosheets derived from natural materials, EC-SILICONF1, Hotel Palota in October 7-11th, 2019, Miskolc-Lillafüred Hungary. *(oral presentation)*

DOI: 10.14750/ME.2021.008

O2. Nuilek, K., Simon, A., & Baumli, P. Synthesis and characterization of carbon nanosheets from stinging nettle (Urtica dioica), IC-CMTP5, 8-12th October 2018, Miskolc-Lillafured, Hungary. *(oral presentation)*

O3. Nuilek, K., Simon, A., & Baumli, P. Influence of thermal treatment to the carbon nanostructure of natural waste materials, Spring Wind Conference 2018 (dosz), 4-6th May, 2018, Széchenyi University, Gyor, Hungary. *(oral presentation)*

O4. Nuilek, K., Simon, A., & Baumli, P. Carbonization of stinging nettle (Urtica dioica) by thermal and chemical processing, ISER 120th International Conference, 14-15th April 2018, Budapest, Krakow, Poland. *(oral presentation)*

O5. Nuilek, K., Simon, A., & Baumli, P. Synthesis of carbon nanostructure from natural waste materials, Doktoranduszok Fóruma, 16th November 2017, University of Miskolc, Hungary. *(oral presentation)*

O6. Nuilek, K., Varanasi, D., & Baumli, P. Wettability of graphite by molten KOH and NaOH. 9th International Conference on High Temperature Capillary, 19-25th June 2020 (webinar). *(poster)*

O7. Nuilek, K., Simon, A., & Baumli, P. Comparative of Potassium Hydroxide and Sodium Hydroxide Activation for preparing Carbon from natural Materials, CHEMIETAGE2019, 20-27th September 2019, Linz Austria. *(poster)*

O8. Nuilek, K., Simon, A., Koncz-Horvath, D., Ferenczi, T., Kristaly, Ferenc., and & Baumli, P. Investigation of the Surface Properties of the Chemical Preparation Carbon Nanosheet Materials, DIAM 2019, 8-12th September 2019, Seville, Spain. *(poster)*

O9. Nuilek, K., Simon, A., & Baumli, P. The Effect of Chemical Acids Exfoliation to Carbon Nanostructure of Peanut Shell, ANM 2019, 17-19th July 2019, University of Aveiro, Portugal. *(poster)*

O10. Nuilek, K., Simon, A., & Baumli, P. The effect of carbon nanosheet from natural waste materials on aluminium matrix composites, Junior Euro mat 2018, 8-12th July, 2018, Budapest, Hungary. *(poster)*

DOI: 10.14750/ME.2021.008

10 Appendix

10.1 ADF, NDF and ADL of raw materials

- Peanut shell

Cím:8500 Pápa
Jókai u.32.
Tel.:06-89-324-788
Fax:06-89-324-786
E-mail:labor@mezolabor.hu

"MEZŐLABOR"
Szolgáltató és Kereskedelmi Kft.
Laboratórium

Nyilv.szám:80/2014/Lab/NÉBIH

Web:www.mezolabor.hu

A NAH által NAH-1-1400/2016 számon akkreditált vizsgálólaboratórium.

Vizsgálati Jegyzőkönyv

Megrendelő neve: Miskolci Egyetem Kerámia- és Polimermérnöki Intézet
Címe: 3515 Miskolc-Egyetemváros

Mintavétel helye:
Helység: Miskolc
Vállalat:
Mintavétel ideje: 2018 június Minta beérk.ideje: 2019.03.28

Minta megnevezése: Mogyoróhéj

Küllem, szín, szag: Felezett héj darabok

Minta azonosító: 851 **Vizsgálatok kódja:**

Jegyzőkönyv azonosító: 851-2019

Kód	Megnevezés		Vizsgálati érték Eredetiben	Sz.a.-ban	Megengedett vizsgálati eltérés		Vizsgálati módszer
10/a	ADF	g/kg	699		±	35	MTK 1990.II.8.2. 7.3 szakasz
10/b	NDF	g/kg	783		±	39	MTK 1990.II.8.2. 7.2 szakasz
10/c	ADL	g/kg	272		±	14	MTK 1990.II.8.2. 7.6 szakasz

DOI: 10.14750/ME.2021.008

- Nettle stem

Cím:8500 Pápa
Jókai u.32.
Tel.:06-89-324-788
Fax:06-89-324-786
E-mail:labor@mezolabor.hu

"MEZŐLABOR"
Szolgáltató és Kereskedelmi Kft.
Laboratórium

Nyilv.szám:80/2014/Lab/NÉBIH
Web:www.mezolabor.hu

A NAH által NAH-1-1400/2016 számon akkreditált vizsgálólaboratórium.

Vizsgálati Jegyzőkönyv

Megrendelő neve: Miskolci Egyetem Kerámia- és Polimermérnöki Intézet
Címe: 3515 Miskolc-Egyetemváros

Mintavétel helye:
Helység: Miskolc
Vállalat:
Mintavétel ideje: 2018 június Minta beérk.ideje: 2019.03.28

Minta megnevezése: Csalánszár

Küllem, szín, szag: 5-10 cm hosszú vastag szárrész

Minta azonosító: 850 **Vizsgálatok kódja:**

Jegyzőkönyv azonosító: 850-2019

Kód	Megnevezés		Vizsgálati érték Eredetiben	Sz.a.-ban	Megengedett vizsgálati eltérés		Vizsgálati módszer
10/a	ADF	g/kg	617		±	31	MTK 1990.II.8.2. 7.3 szakasz
10/b	NDF	g/kg	770		±	39	MTK 1990.II.8.2. 7.2 szakasz
10/c	ADL	g/kg	119		±	6	MTK 1990.II.8.2. 7.6 szakasz

DOI: 10.14750/ME.2021.008

- Nettle leaf

Cím:8500 Pápa
Jókai u.32.
Tel.:06-89-324-788
Fax:06-89-324-786
E-mail:labor@mezolabor.hu

"MEZŐLABOR"
Szolgáltató és Kereskedelmi Kft.
Laboratórium

Nyilv.szám:80/2014/Lab/NÉBIH
Web:www.mezolabor.hu

A NAH által NAH-1-1400/2016 számon akkreditált vizsgálólaboratórium.

Vizsgálati Jegyzőkönyv

Megrendelő neve: Miskolci Egyetem Kerámia- és Polimermérnöki Intézet
Címe: 3515 Miskolc-Egyetemváros

Mintavétel helye:
Helység: Miskolc
Vállalat:
Mintavétel ideje: 2018 június Minta beérk.ideje: 2019.03.28

Minta megnevezése: Csalánlevél
Küllem, szín, szag: Szárított, morzsázott levél
Minta azonosító: 849 **Vizsgálatok kódja:**
Jegyzőkönyv azonosító: 849-2019

Kód	Megnevezés		Vizsgálati érték Eredetiben	Sz.a.-ban	Megengedett vizsgálati eltérés		Vizsgálati módszer
10/a	ADF	g/kg	183		±	9	MTK 1990.II.8.2. 7.3 szakasz
10/b	NDF	g/kg	308		±	15	MTK 1990.II.8.2. 7.2 szakasz
10/c	ADL	g/kg	22		±	5	MTK 1990.II.8.2. 7.6 szakasz

DOI: 10.14750/ME.2021.008

10.2 Chemical composition (EDS results)

Table 10.1 Chemical composition of raw materials (EDS results).

Dried materials	Chemical composition (wt.%)							
	C	O	Si	Zn	K	Ca	S	Mg
Nettle stem	50.80	36.03	2.45	-	6.97	3.07	0.42	0.26
Nettle leaf	41.86	37.14	6.33	-	3.96	8.30	1.83	0.58
Peanut shell	61.55	37.69	0.04	0.72	-	-	-	-

Table 10.2 Chemical composition of the nettle stem (EDS results).

Samples		Chemical composition (wt.%)					
Activation	Exfoliation	C	O	K	Si	S	Others
KOH (solid) activation (1hour)		87.35	10.78	0.30	0.12	-	1.45
KOH (solid) activation (2hours)		88.00	8.83	3.17	-	-	-
KOH (solute) activation (1hour)		87.56	8.99	1.95	0.68	-	0.82
KOH (solute) activation (2hours)		93.84	4.78	1.38	-	-	-
NaOH (solute) activation (2hours)		91.60	5.20	-	1.56	-	1.64
KOH	HNO_3	88.15	10.52	0.33	0.80	0.21	-
NaOH		89.30	10.32	-	-	-	0.38
KOH	H_2SO_4	88.71	9.38	-	0.76	1.15	-
NaOH		91.75	7.93	-	-	-	0.32
KOH	H_3PO_4	90.96	7.70	0.32	0.67	0.36	-
NaOH		89.52	10.09	-	-	-	0.39

Table 10.3 Chemical composition of the peanut shell (EDS results).

Samples		Chemical composition (wt.%)					
Activation	Exfoliation	C	O	K	Si	S	Others
KOH (solid) activation (1hour)		51.86	31.79	15.73	-	-	0.62
KOH (solid) activation (2hours)		85.42	7.69	5.97	0.92	-	-
KOH (solute) activation (1hour)		85.57	9.87	2.55	2.01	-	-
KOH (solute) activation (2hours)		81.71	10.93	5.81	1.55	-	-
NaOH (solute) activation (2hours)		89.91	9.65	-	0.44	-	-
KOH	HNO_3	88.98	9.9	0.18	0.71	0.24	-
NaOH		90.12	8.81	-	1.07	-	-
KOH	H_2SO_4	89.37	8.97	0.27	0.48	0.91	-
NaOH		90.37	8.61	-	1.02	-	-
KOH	H_3PO_4	90.19	8.63	0.28	0.6	0.3	-
NaOH		88.20	10.06	-	1.74	-	-